UNIVERSIDAD DE CONCEPCION
Dirección de Postgrado
Facultad de Ingeniería
Magíster en Ciencias de la Ingeniería con mención en Ingeniería Química

# SÍNTESIS Y CARACTERIZACIÓN DE AEROGELES BASADOS EN ÓXIDO DE GRAFENO Y GELATINA CON CARGA DE EXTRACTOS DE UVA PAÍS COMO POTENCIAL AGENTE HEMOSTÁTICO.

Tesis para optar al grado de Magíster en Ciencias de la Ingeniería mención Ingeniería Química

SEBASTIÁN IGNACIO GUAJARDO DE CELIS
CONCEPCIÓN - CHILE
AGOSTO, 2020.

Profesor Guía: Katherina Fernández Elgueta.
Dpto. de Ingeniería Química, Facultad de Ingeniería
Universidad de Concepción.

*“La actividad más importante que un ser humano puede lograr es aprender para entender, porque entender es ser libre”*

*-Baruch Spinoza*

**Agradecimientos**

Agradezco profundamente a todas las personas que me acompañaron durante este proceso, su apoyo y comprensión han sido de gran importancia para mí.

Agradezco a mi familia, en especial a mis padres Silvia De Celis y Patricio Guajardo, por su infinito cariño y apoyo en todo momento. Donde estoy hoy es gracias a su esfuerzo y sacrificio.

Agradezco también a mis amigos, en especial a Camilo Torres y Toribio Figueroa. Su amistad, compañía, y apoyo en todo este tiempo fueron de gran importancia para mí. No tengo dudas, no hubiese sido lo mismo sin ustedes.

Agradezco a los profesores que me han guiado y enseñado en este proceso, en especial a Katherina Fernández y Alfredo Gordon. Su apoyo, guía, y consejos, no sólo en el programa sino en proyectos personales, han sido de gran valor para mí.

Agradezco a mis compañeros y profesionales de laboratorio, en especial a Verónica Sanhueza. Su ayuda y apoyo, tanto dentro como fuera del laboratorio, fue de gran importancia en todo el proceso.

Y en general, a todo quien me acompañó en este camino y creyó en mí en todo momento, tanto en lo académico como en lo personal, estoy agradecido de corazón.

**Resumen**

La hemorragia es una de las principales causas de muerte por traumas, incluso en su tratamiento, debido al sangramiento continuo y coagulopatías. Por lo cual, el desarrollo de nuevos materiales hemostáticos, es de vital importancia para procedimientos óptimos en el tratamiento de traumas y control de hemorragias.

El objetivo de este estudio fue desarrollar y caracterizar un aerogel en base a óxido de grafeno (OG) y gelatina (G) para su uso en aplicaciones hemostáticas, mediante métodos de interacción covalentes y no covalentes, evaluando la influencia de la proporción OG:G y el pH de la suspensión de OG, en las propiedades fisicoquímicas del material. Además, se sintetizaron aerogeles OG-G con la incorporación de proantocianidinas (PAs), evaluando la influencia de su concentración en las principales propiedades funcionales del material.

La actividad hemostática *in-vitro* de los aerogeles fue evaluada, a través de ensayos de coagulación dinámica, estimación de tiempos de protrombina y de tromboplastina parcialmente activada, y cuantificación de P-selectina soluble. Finalmente, la citotoxicidad de los aerogeles fue determinada en cultivos de fibroblastos de piel humana.

Los aerogeles OG-G se sintetizaron mediante métodos covalentes y no covalentes, y la naturaleza de su interacción fue confirmada mediante FTIR y XPS. Comparativamente, bajas proporciones OG:G en condiciones alcalinas de la suspensión de OG, promovieron interacciones covalentes, presentando un módulo elástico de 4.44±0.18 kPa. Por el contrario, altas proporciones OG:G, bajo condiciones ácidas de la suspensión de OG promovieron las interacciones no covalentes, presentando un módulo elástico de 3.85±0.15 kPa. La microscopía electrónica de barrido (SEM) mostró estructuras heterogéneas con tamaños de poro de 53.26±25.53 µm y 25.31±10.38 µm para aerogeles covalentes y no covalentes, respectivamente. El método de síntesis no tuvo influencia en la carga superficial; sin embargo, se presentaron diferencias que dependieron de la proporción OG:G y el pH de la suspensión de OG en la síntesis. Los aerogeles no covalentes presentaron mayor capacidad de absorción de solución buffer fosfato-salino (PBS), con razones

de absorción entre 35.5±2.4 $g_{PBS}/g_{aerogel}$ y 49.6±3.8 $g_{PBS}/g_{aerogel,}$ que los aerogeles covalentes, con razones de absorción entre 24.9±1.7 $g_{PBS}/g_{aerogel}$ y 36.2±3.1 $g_{PBS}/g_{aerogel}$.

La incorporación de PAs en los aerogeles no tuvo influencia en la carga superficial de los aerogeles, obteniendose valores entre 17.81±2.71 mV y -16.97±2.30 mV. Sólo se produjo una mejora en la capacidad de absorción de PBS para aerogeles covalentes, con una razón de 43.92±4.33 $g_{PBS}/g_{aerogel}$, valor menor a la capacidad de absorción de aerogeles no covalentes sin carga de extracto. Debido a estos resultados, sólo se evaluó el desempeño hemostático *in-vitro* en aerogeles OG-G no covalentes.

Los aerogeles OG-G de carga superficial negativa presentaron un alto rendimiento hemostático, coagulando cerca de un 95.6% de sangre, acelerando el proceso de coagulación, y promoviendo la formación del coágulo, mediante mecanismos de soporte alternativos fuera de los comúnmente propuestos y entregando una estructura adecuada para el proceso. Además, estos aerogeles mostraron promover la proliferación de fibroblastos, debido al alto contenido de amino ácidos en la matriz y la estructura generada en el material, otorgando mayor cito-compatibilidad.

Los aerogeles OG-G no covalentes con carga superficial positiva inhibieron la formación del coágulo, coagulando un 8.1% de la sangre, y mostrando tiempos de tromboplastina parcialmente activada mayores al plasma sanguíneo.

De este modo, en base a los resultados obtenidos, los aerogeles OG-G no covalentes de carga superficial negativa, son potenciales dispositivos hemostáticos para uso como apósitos en el tratamiento de heridas y traumas.

**Índice de figuras**

**Índice de tablas.**

**Nomenclaturas**

| | |
|---|---|
| **aPTT** | Tiempo de tromboplastina parcialmente activada |
| **BMIMAc** | Acetato de 1-butil-3-metilimidazolio |
| **CaCl2** | Cloruro de calcio |
| **DMSO** | Dimetíl sulfóxido |
| **DTG** | Termogravimetría derivada |
| **EMIMAc** | Acetato de 1-etil-3-metilimidazolio |
| **FTIR** | Espectroscopía infrarroja por transformada de Fourier |
| **G** | Gelatina |
| **Gly** | Glicina |
| **GMIA** | Gelatin Manufacturers Institute of America |
| **GO** | Graphene Oxide |
| **$H_2SO_4$** | Ácido sulfúrico |
| **$H_3O^+$** | Ion hidronio |
| **$H_3PO_4$** | Ácido fosfórico |
| **HCl** | Ácido clorhídrico |
| **HDF** | Fibroblástos de piel humana |
| **$HSO_4^-$** | Sulfato ácido |
| **$K^+$** | Potasio |
| **KOH** | Hidróxido de potasio |
| **$KMnO_4$** | Permanganato de potasio |
| **$Mn_2O_7$** | Heptaóxido de manganeso |
| **$MnO_3^+$** | Ion permanganilo |
| **$MnO_4^-$** | Ion permanganato |
| **$N_2O_4$** | Tetraóxido de dinitrógeno |
| **NaNO3** | Nitrato de sodio |
| **$NO_2$** | Dióxido de nitrógeno |
| **$NO_x$** | Óxidos de nitrógeno |
| **OG** | Óxido de grafeno |
| **PAAm** | Poliacrilamida |
| **PAs** | Proantocianidinas |

| | |
|---|---|
| **PBS** | Solución salina buffer-fosfato |
| **pH** | Índice del grado de acidez |
| **PPP** | Plasma pobre en plaquetas |
| **PRP** | Plasma rico en plaquetas |
| **Pro** | Prolina |
| **PT** | Tiempo de protrombina |
| **PVA** | Alcohol polivinílico |
| **rGO** | Reduced graphene oxide |
| **sP-Selectin** | P-selectina soluble |
| **SEM** | Microscopía electrónica de barrido |
| **TGA** | Análisis termogravimétrico |
| **Tris-HCl** | tris(hidroximetil)aminometano ajusto por ácido clorhídrico |
| **XPS** | Espectroscopía de fotoelectrones emitidos por rayos X |
| **XRD** | Difracción de rayos X |

**Tabla de contenidos**

## 1. Introducción

El impacto en la salud humana de lesiones traumáticas no puede ser subestimado, ya que la hemorragia es una de las principales causas de muerte por este tipo de lesiones. La reducción de los volúmenes de sangre circulante luego de una hemorragia severa conduce a una deficiencia de oxígeno en los tejidos, y complicaciones como la hipotermia, coagulopatía y acidosis, que están asociadas con el aumento en la morbilidad y mortalidad. Existen varias técnicas hemostáticas convencionales para minimizar la pérdida de sangre, entre ellas la presión manual, ligaduras y la aplicación de torniquetes. El sellado de vasos en sangramiento también se puede realizar mediante métodos térmicos como la cauterización. Sin embargo, estos métodos pueden resultar de un esfuerzo mayor y ralentizar el procedimiento operativo, como también crear áreas carbonizadas y tejido necrótico, incrementando la probabilidad de infecciones y daño en las paredes de la herida. Además, los métodos convencionales son menos efectivos en el control del sangramiento en heridas complejas y su acceso al área de sangramiento resulta de mayor dificultad; por lo que el desarrollo de agentes hemostáticos de uso tópico puede ser de particular ayuda en tales situaciones (Kauvar et al 2006; Seyednejad et al, 2008; Chan et al, 2016).

Intentando dar respuesta a esta necesidad, diferentes tipos de materiales se han desarrollado para promover la coagulación y detener el sangramiento en diferentes traumas. Algunos ejemplos de esto son las esponjas de colágeno reforzadas con quitosano y pirofosfato de calcio (Lan et al, 2015; Yan et al, 2017), y las esponjas de grafeno reticulado (Quan et al, 2015).

En línea con el ejemplo anterior, distintos materiales basados en óxido de grafeno (OG) se han desarrollado para uso biomédico debido a sus distintas propiedades relevantes para aplicaciones biológicas tales como su buena dispersión en agua, su sensibilidad a cambios de pH, propiedades ópticas y superficiales únicas, y su alta área superficial (Kiew et al, 2016; McCallion et al, 2016). Sin embargo, su uso en dispositivos hemostáticos ha sido escasamente estudiado.

Su funcionalización con polímeros o proteínas resulta necesaria para aumentar su biocompatibilidad y reducir su citotoxicidad debido a su tendencia a la agregación en soluciones biológicas y su tamaño poco uniforme. (Krishnamoorthy et al, 2013; Kiew et al, 2016)

Un buen candidato para esto es la gelatina (G). Sus propiedades, tales como biodegradabilidad y biocompatibilidad, han hecho de esta un buen material para el desarrollo de dispositivos de uso médico. Además, su desempeño como portador de fármacos y sus propiedades como agente hemostático pasivo hacen de este un buen material para liberación local de drogas, tratamiento de heridas y de sangramiento profuso (Young et al, 2005; Seyednejad et al, 2008; GMIA, 2012).

En base a lo anterior, distintos autores han desarrollado aerogeles en base a OG y G para su uso en la biomedicina, particularmente en el transporte y liberación de fármacos. Sin embargo, su estudio como dispositivo hemostático es escaso. (An et al, 2013; Chen et al, 2014; Piao & Chen, 2016)

La incorporación de proantocianidinas (PAs) a la superficie del material es capaz de mejorar sus propiedades biológicas, aumentando la adhesión y actividad celular (Reitzer et al, 2018). Además, son capaces de disminuir los triglicéridos en la sangre y la presión arterial mediante la inhibición de la enzima convertidora de la Angiotensina I (Godoy et al, 2012). Este tipo de compuestos puede ser extraído desde vegetales y frutas, particularmente en esta investigación se trabaja con los componentes extraídos desde semillas de la uva País, los que poseen actividad en la función endotelial, en la agregación plaquetaria, y como agente antioxidante (Fernández et al, 2015).

Considerando lo anterior, el proyecto plantea el desarrollo de aerogeles en base a óxido de grafeno y gelatina, mediante síntesis covalente y no covalente, considerando la incorporación de PAs para uso en aplicaciones hemostáticas y/o cicatrizantes. Los aerogeles serán caracterizados química, física y morfológicamente, y se evaluará su capacidad de absorción de PBS, como también su capacidad de coagulación *in vitro*. Esto con el fin de generar un nuevo material que detenga el sangramiento profuso y promueva la coagulación.

## 2. Antecedentes generales

A continuación, se definen distintos conceptos asociados a la química y física de los distintos compuestos utilizados en este estudio, técnicas de síntesis y caracterización del GO y el aerogel, entre otros.

### 2.1 Química del carbono, grafito y grafeno

El carbono es uno de los elementos químicos más abundantes y el más importante en el estudio de los compuestos orgánicos. El carbono puede compartir electrones con muchos átomos diferentes, como también puede compartir electrones con otros átomos de carbono. De esta manera, es capaz de formar una gran cantidad de compuestos estables con un amplio rango de propiedades químicas simplemente por compartir electrones.

Según Erwin Shrödinger, en el año 1926, el comportamiento de cada electrón en un átomo o molécula puede ser descrito mediante una ecuación de onda. La solución a esta es llamada orbital. Estos muestran la energía de un electrón y el volumen de espacio alrededor del núcleo donde un electrón es más probable de encontrar. La distribución de estos electrones, tanto en sus orbitales como en sus distintas capas, se muestra en la Tabla 1.

Tabla 1: Distribución de electrones en las primeras cuatro capas que envuelven el núcleo de un átomo.

| | Primera capa | Segunda Capa | Tercera Capa | Cuarta capa |
|---|---|---|---|---|
| Orbital atómico | s | s, p | s, p, d | s, p, d, f |
| Nº de orbitales atómicos | 1 | 1, 3 | 1, 3, 5 | 1, 3, 5, 7 |
| Nº máximo de electrones | 2 | 8 | 18 | 32 |

De acuerdo a la mecánica cuántica, los electrones en un átomo pueden verse como habitantes de un grupo de capas concéntricas que envuelven el núcleo. Es importante mencionar que mientras más cercano al núcleo se ubica la capa, menor es su energía.

La configuración electrónica de un átomo describe el orbital ocupado por los electrones del átomo cuando ellos están dispuestos en los orbitales con menor energía. La configuración electrónica para el carbono en su estado fundamental corresponde a

$$1s^2\ 2s^2\ 2p^2$$

Sin embargo, el carbono busca promover un electrón desde su orbital 2s a su orbital 2p, ya que la formación de enlaces es más ventajosa energéticamente, por lo que el carbono tiende a ser tetravalente. Así, tomando en cuenta la regla de Hund, su configuración será

$$1s^2\ 2s^1\ 2p_x^1\ 2p_y^1\ 2_z^1$$

Por otro lado, un detalle importante en la química del carbono es que puede combinar estos orbitales produciendo orbitales híbridos. Si el orbital s y los tres orbitales p de la segunda capa se combinan, cada orbital resultante será una parte s y tres partes p. Este tipo de combinación de orbitales es llamada orbital $sp^3$ y es usual en enlace del carbono a cuatro átomos distintos.

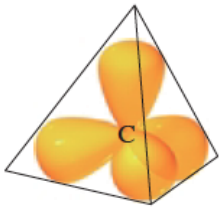

Estructura tetrahédrica

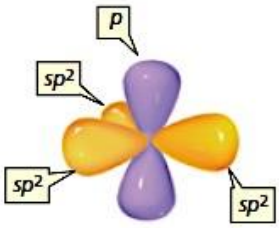

Estructura tetrahédrica (Yurkanis P., 2003)

Para enlazar con tres átomos, el átomo de carbono hibrida tres orbitales atómicos. Este tipo de combinación es llamada $sp^2$, debido a que un orbital s y dos orbitales p son hibridados. Después de la hibridación, el átomo de carbono posee tres orbitales $sp^2$ degenerados y un orbital p.

Cuando un átomo de carbono se enlaza a otros dos átomos, solo un orbital s y uno p son hibridados dando como resultado dos orbitales sp degenerados. De esta manera, el átomo de carbono posee dos orbitales sp y dos orbitales p sin hibridar.

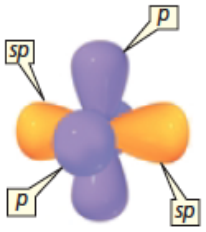

Estructura tetrahédrica (Yurkanis P., 2003)

Además, es importante mencionar los tipos de enlace sigma (σ) y pi (π), esquematizados en la Figura 1. Un enlace en el que los orbitales se traslapan a lo largo de una línea que conecta a los átomos, el eje internuclear, se llama enlace sigma. Por otro lado, un enlace en el que los orbitales, perpendiculares al eje internuclear, se traslapan de manera paralela se denomina enlace π.

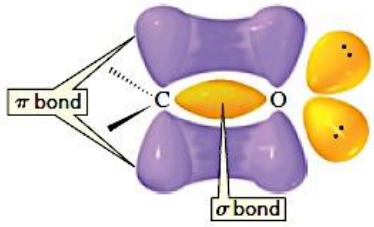


Figura 1: Esquema de enlace carbonilo (Yurkanis P., 2003)

Los electrones en un enlace π se llaman electrones π y la probabilidad de encontrar uno de estos electrones es mayor en la región por encima y por debajo del plano de la molécula. Este corresponde a un plano nodal, donde la probabilidad de encontrar un electrón π es cero. Estos se pueden encontrar, por ejemplo, en un enlace doble carbono-carbono, el cual se puede ver como la suma de un enlace σ y un enlace π.

El alótropo más común del carbono es el grafito, el cual consiste en capas atómicas de carbonos hibridados $sp^2$ los cuales se encuentran unidos entre sí por débiles fuerzas de van der Waals. Tal como se observa en la Figura 2, en cada plano el carbono se enlaza a otros tres átomos, formando una serie de hexágonos continuos en lo que se puede considerar una molécula infinita bidimensional llamada grafeno.

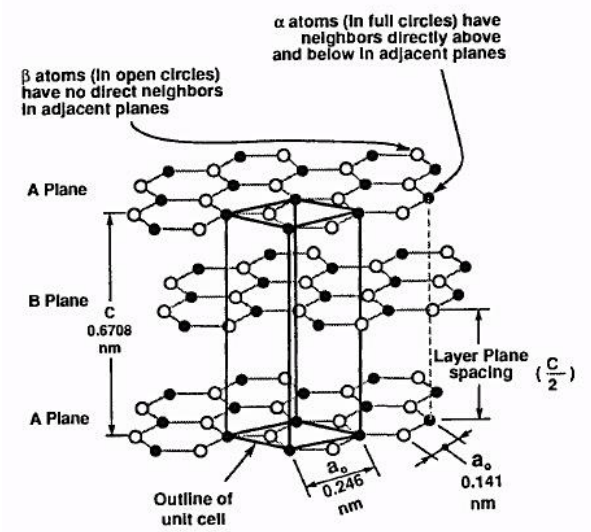


Figura 2: Estructura cristalina del grafito y celda unitaria (Pierson H., 1993)

El espacio entre las placas es relativamente largo (0.335 nm) o más de dos veces el espacio entre átomos del plano basal y aproximadamente dos veces el radio de van der Waals del carbono. (Pierson H., 1993)

El grafeno ha mostrado tener distintas propiedades tales como alta conductividad térmica y eléctrica en sentido paralelo al plano y bajas conductividades en sentido perpendicular al plano influenciado por las interacciones interfaciales, defectos atómicos y fallas superficiales. Esta ambivalencia lo transforma en un material útil para dispositivos de disipación de calor o aplicaciones termoeléctricas (Pop et al, 2012; Pierson H., 1993). Es uno de los materiales más delgados que se conocen y el más fuerte, ha mostrado gran rigidez, es impermeable a los gases y tiene una buena proporción entre fragilidad y ductilidad. Además, reacciones han sido ampliamente utilizadas en grafeno para la producción de dispersiones estables, estas reacciones proporcionan una variedad de derivaciones orgánicas que tienen distintas aplicaciones como en compósitos poliméricos, biotecnología, dispositivos nanoeléctricos, liberación de drogas y celdas solares (Georgakilas V., 2014).

## 2.2 Óxido de grafeno

### 2.2.1 Aspectos generales del óxido de grafeno

El OG, derivado soluble en agua del grafeno, es una forma altamente oxidada del grafeno modificado químicamente, el cual posee carbonos de hibridación $sp^2$ en la red aromática y carbonos de hibridación $sp^3$ con grupos hidroxilo (-OH) y epóxido (-O-) en el plano basal, y ácidos carboxílicos (-COOH) en sus bordes (Shim et al, 2016). Su estructura química ha estado sujeta a gran discusión. Existen muchas razones por las cuales no se ha encontrado un modelo que no entregue ambigüedad, pero el principal contribuidor es la complejidad del material debido a sus deformaciones, su composición atómica no estequiométrica, y la ausencia de técnicas analíticas precisas para la caracterización de este tipo de material. No obstante, se han realizado esfuerzos considerables para entender la estructura del OG, la Figura 3 muestra el resumen de algunos de estos modelos (Dreyer et al, 2009).

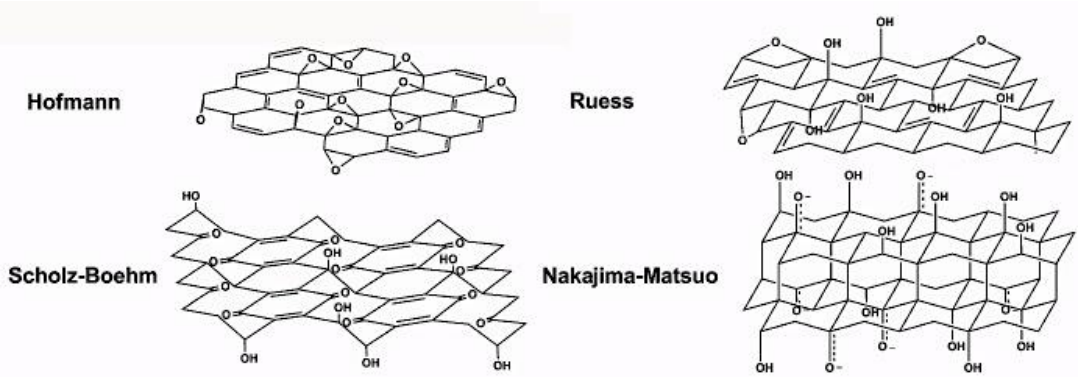


Figura 3: Resumen de algunos modelos estructurales del OG (Dreyer et al, 2009).

Sin embargo, las características químicas del óxido de grafeno son comúnmente descritas por el modelo Larf-Klinowski, que considera comprender al OG como una típica malla plana tipo panal de enlaces $sp^2$ con defectos ocasionales, interrumpida por enlaces $sp^3$ que permiten proyectar epóxidos y alcoholes desde el plano superficial, mientras que los bordes están poblados de grupos carboxilos como muestra la Figura 4 (McCallion et al, 2016).

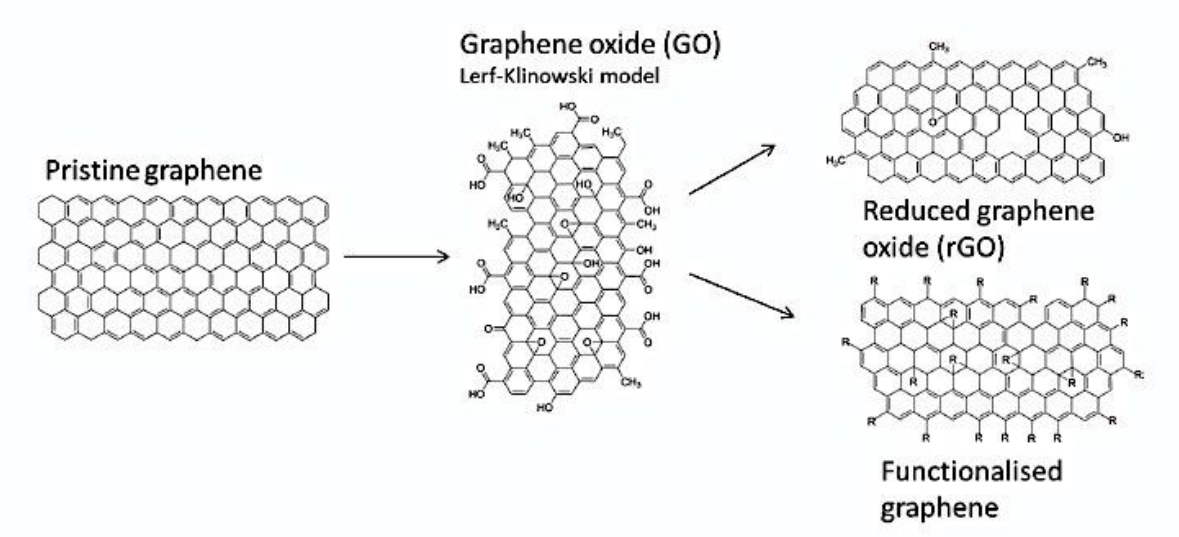


Figura 4: Modelos de formas comunes del grafeno (McCallion et al, 2016).

El área no modificada de grafeno en el OG contiene electrones π libres que son hidrófobos y capaces de realizar modificaciones no covalentes en la superficie mediante acoplamiento de electrones π-π e interacciones hidrófobas. Los grupos epóxido, hidroxilo y ácido carboxílico del OG son polares, a pesar de no poseer carga, permitiendo débiles interacciones, puentes de hidrógeno y otras reacciones superficiales (Lin et al, 2016).

El proceso de oxidación resulta en un rompimiento parcial de la estructura $sp^2$ del grafito aumentando la distancia entre las láminas de carbono. Este rompimiento de la estructura conjugada entrega electrones π, resultando en un descenso general de sus propiedades mecánicas, eléctricas y térmicas en comparación con el grafeno o el óxido de grafeno reducido. Sin embargo, las zonas remanentes $sp^2$ con grupos hidrófilos adheridos durante el proceso de oxidación, como se observa en la Figura 5, hacen que el OG exhiba propiedades únicas, como su afinidad por anillos aromáticos y su habilidad de desactivación fluorescente, mientras que mantiene alta dispersión en solventes acuosos y carga negativa pH-dependiente en su superficie derivadas de sus grupos carboxílicos periféricos (Lee et al, 2016; Zhang et al, 2015).

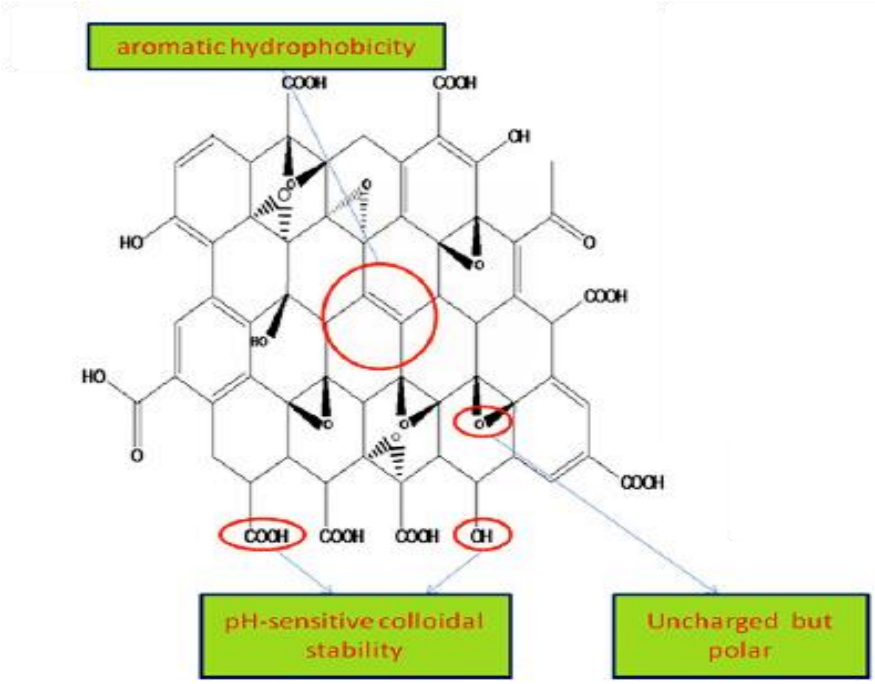


Figura 5: Estructura del OG y sus propiedades de funcionales (Zhang et al, 2015).

De esta manera, el OG posee aplicaciones únicas en diferentes campos como la optoelectrónica, supercapacitores, dispositivos de memoria, materiales compósitos, fotocatálisis y agente portador de fármacos. La naturaleza hidrófila generada por el contenido de grupos funcionales oxigenados entrega biocompatibilidad y una buena dispersión en agua, características importantes en bioaplicaciones (Krishnamoorthy et al, 2013). Sin embargo, el óxido de grafeno posee ciertas limitaciones para este tipo de aplicaciones, tales como su agregación en soluciones biológicas, su tamaño

no uniforme, y el poco conocimiento del comportamiento del OG *in vivo* (Kiew et al, 2016). De este modo, su funcionalización con polímeros o proteínas resulta necesaria para reducir su citotoxicidad debido a su tendencia a la agregación en soluciones biológicas y su tamaño poco uniforme (Krishnamoorthy et al, 2013; Kiew et al, 2016).

Por lo anterior, dado su potencial uso en aplicaciones biomédicas y la necesidad de reducción de su citotoxicidad, se describe a continuación la síntesis del OG y sus métodos de funcionalización.

### 2.2.2 Síntesis del óxido de grafeno

En términos de su sintesis, el OG es comúnmente producido mediante los métodos Brodie, Staudenmaier, y Hummers, o métodos con modificaciones menores de estos. Generalmente se obtiene mediante la oxidación del grafito en una mezcla de ácidos fuertes y agentes oxidantes. (Lee et al, 2016).

El ácido nítrico es un agente oxidante común, conocido por reaccionar fuertemente con superficies de carbono aromáticas. La reacción resulta en la formación de varias especies con contenido de óxido incluyendo carboxilos, lactonas, y quetonas. Las reacciones de oxidación con ácido nítrico liberan compuestos gaseosos como $NO_2$ y/o $N_2O_4$. Igualmente, el clorato de potasio es un agente oxidante fuerte, fuente típica de dioxígeno *in situ*, el cual actúa como especie reactiva.

El método de Hummers, uno de los métodos más utilizados, combina permanganato de potasio y ácido sulfúrico. A pesar de que comúnmente se utiliza el permanganato como agente oxidante el compuesto activo es el anhídrido permangánico resultado de la reacción del $KMnO_4$ en presencia de un ácido fuerte (Dreyer et al, 2009).

$$KMnO_4 + 3\,H_2SO_4 \rightarrow K^+ + MnO_3^+ + H_3O^+ + 3\,HSO_4^-$$

$$MnO_3^+ + MnO_4^- \rightarrow Mn_2O_7$$

Se ha demostrado que el $Mn_2O_7$ posee la habilidad de oxidar selectivamente doble enlaces alifáticos por sobre doble enlaces aromáticos, lo cual puede llegar a ser relevante por la estructura del grafito y los mecanismos de reacción que ocurren durante la oxidación. De hecho, el $Mn_2O_7$ tiene la capacidad de epoxidar grupos

oxigenados insaturados formados en el grafito durante la reacción de oxidación teniendo como resultado el aumento de grupos O-C-O en el óxido de grafeno (Dreyer et al, 2009; Krishnamoorty et al, 2013).

Marcano y colaboradores proponen una modificación al método de Hummers, como se plantea en la Figura 6, dada la evidencia de nanobandas de óxido de grafito con más planos basales intactos mediante la adición de ácido fosfórico.

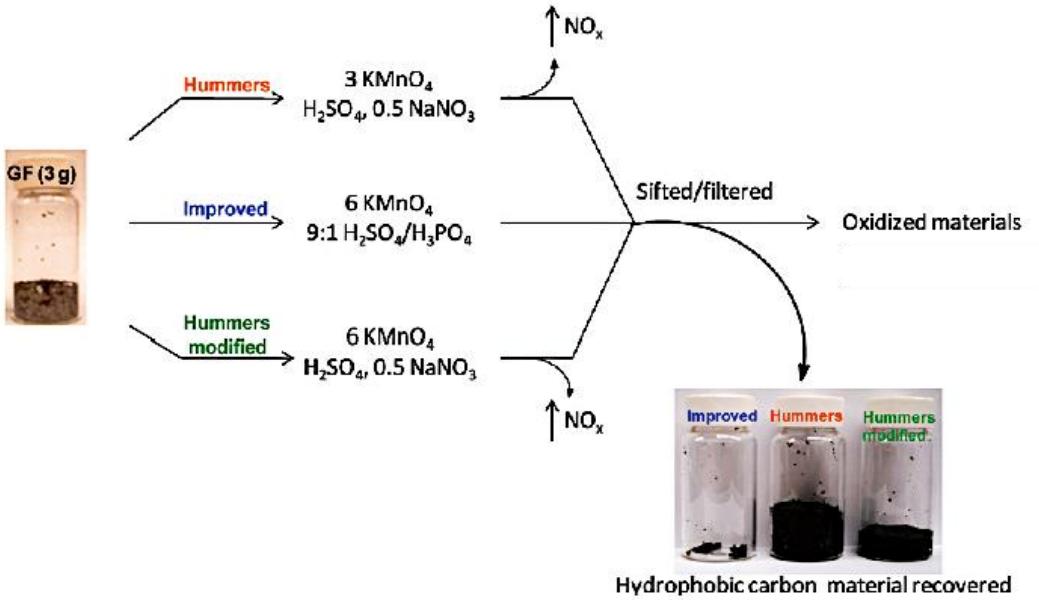


Figura 6: Metodologías utilizadas por Marcano y colaboradores (Marcano et al, 2010).

El método de Hummers modificado por Marcano y colaboradores, en el año 2010, muestra ventajas significativas con respecto a el método de Hummers convencional. El protocolo de reacción no involucra cantidades exotérmicas importantes y no produce gases tóxicos como los $NO_x$. Además, esta modificación del método produce una mayor fracción de material carbonoso hidrófilo correctamente oxidado (Marcano et al, 2010).

Así, de las diversas opciones de síntesis de OG, en este trabajo se utilizó el método de Hummers modificado por Marcano y colaboradores para realizar un proceso menos tóxico y de mayor grado de oxidación. Además, se modificaron los tiempos utilizados dado que solo 1 hora de reacción genera un alto grado de oxidación lo que reduce los tiempos utilizados en los métodos comunes de síntesis de OG.

### 2.2.3 Funcionalización del óxido de grafeno

#### 2.2.3.1 Funcionalización covalente

El óxido de grafeno contiene oxígenos funcionales químicamente reactivos tales como ácidos carboxílicos, grupos que se encuentran en los bordes según el modelo Lerf-Klinowski, y grupos epoxi e hidroxilo en el plano basal. Un acercamiento ideal a la modificación química del OG se encuentra en utilizar reacciones ortogonales de estos grupos para funcionalizar selectivamente algunos sitios sobre otros (Dreyer et al, 2009).

Los métodos de funcionalización covalente pueden ser clasificados en dos grandes grupos, los métodos de “injerto a” y los métodos de “injerto desde”. En general para los métodos de “injerto a” las cadenas del polímero son previamente sintetizadas y finalmente estos polímeros pre-sintetizados son enlazados con los grupos funcionales del OG o con su superficie aromática. La base de las técnicas involucradas es el enlace covalente directo de los grupos funcionales del polímero en la superficie del OG usando esterificación, amidación, química “click”, nitración, adición de radical, entre otros (Layek & Nandi, 2013).

Un amplio rango de reacciones utilizando ácidos carboxílicos han sido desarrolladas en el curso del desarrollo de la química orgánica, y muchas de estas reacciones pueden ser, y han sido, utilizadas en el óxido de grafeno. Estas usualmente requieren la activación del grupo ácido seguido de la adición nucleofílica de especies como aminos o hidroxilos, produciendo grupos funcionales enlazados covalentemente al óxido de grafeno mediante la formación de amidas o ésteres. Por otro lado, los grupos epoxi pueden ser modificados mediante reacciones de apertura del anillo bajo varias condiciones. Un mecanismo probable para esta reacción involucra el ataque nucleofílico de la amina al α-carbono (Dreyer et al, 2009).

Esta reacción del grupo epoxi puede ocurrir junto a la reacción del grupo carboxílico simultáneamente produciendo reacciones de amidación en ambos grupos funcionales. Además de las reacciones de amidación y esterificación, otras reacciones originadas por la reactividad química del grupo hidroxilo han sido desarrolladas. Una de las reacciones características del grupo hidroxilo del OG es

la silanización, reacción que ocurre entre un grupo hidroxilo y un silano etoxi-sustituido (Georgakilas V., 2014).

Por otro lado, las técnicas de “injerto desde” son asociadas con la polimerización de monómeros desde los microiniciadores derivados desde la superficie del OG. Estos iniciadores son directamente enlazados, de manera covalente, en grupos hidroxilos o carboxilos, o implantando pequeñas moléculas en un principio para entregar la funcionalidad necesaria seguida por el enlazado del iniciador. (Layek & Nandi, 2013)

En este estudio, se utilizaron técnicas de “injerto a” debido a que los grupos oxigenados presentes en el OG fueron funcionalizados a través de amidaciones de los grupos carboxi- y epoxi- con los grupos amino presentes en las cadenas poliméricas.

En nuestro estudio se plantea la funcionalización covalente del OG a través de la reacción de amidación entre los grupos amino presentes en las cadenas de G y distintos grupos oxigenados presentes en las láminas de OG.

#### 2.2.3.2 Funcionalización no covalente

Es la interacción no-covalente del OG y el polímero mediante solapamiento π-π, catión-π o fuerzas de van der Waals en la estructura $sp^2$ que no ha sido oxidada o enlaces del tipo puente de hidrógeno (Dreyer et al, 2009). Este tipo de funcionalización posee ventajas significativas sobre la funcionalización covalente dado que aumenta la solubilidad del material sin la alteración de la amplia configuración π de las láminas de grafeno dado que en la funcionalización covalente se crean defectos $sp^3$ en los anillos (Layek & Nandi, 2013).

Mientras que la adsorción en el grafeno puro es mayormente controlada por el solapamiento de electrones π y la hidrofobicidad, la adsorción de moléculas en la superficie del OG también puede ser asistida por puentes de hidrógeno e interacciones electroestáticas, por lo que el OG es una plataforma útil para adsorción y transporte de drogas aromáticas insolubles en agua. Una larga variedad de conjugados del grafeno se ha desarrollado mediante interacciones no-covalentes debido a que este tipo de funcionalización ofrece la posibilidad de re-adsorber

moléculas en la superficie del grafeno sin alterar la estructura electrónica (Georgakilas V., 2014).

Sin embargo, existen algunas desventajas en comparación a la funcionalización covalente. Por un lado, las interacciones no-covalentes no son tan fuertes como las interacciones covalentes y son vulnerables a la variación según el ambiente externo, disminuyendo la estabilidad de la distribución de fármacos *in vitro* e *in vivo* en interacción con el sistema biológico. Por otro lado, la capacidad de carga del grafeno funcionalizado no-covalentemente es menor debido a las áreas conjugadas del grafeno que están parcialmente ocupadas por el recubrimiento polimérico (Zhang et al, 2015).

### 2.3 Gelatina

La gelatina es un polímero biocompatible y posee una abundancia de grupos amino en sus cadenas que la hace susceptible a la funcionalización, además de ser un material de fácil acceso en el mercado, por lo que se utiliza en este proyecto como biopolímero natural para la interacción con el OG y así mejorar sus propiedades biológicas. Por otro lado, polímeros naturales como la gelatina o el colágeno han sido considerados para la liberación de fármacos a nivel local, con cortos tiempos de aplicación, gracias a que poseen relativamente cortos tiempos de degradación (Siepmann et al, 2012).

#### 2.3.1 Química de la gelatina

La gelatina, forma desnaturalizada del colágeno, es un polímero natural modificado formado mediante la hidrólisis del colágeno insoluble. Es típicamente aislada desde la piel o huesos de bovinos o porcinos mediante hidrólisis parcial ácida (Tipo A) o alcalina (Tipo B). Este procedimiento rompe el colágeno tripolipéptidico, generando cadenas singulares de polipéptidos (Siepmann et al, 2012). La representación $(Gly - X - Pro)_n$ es responsable de su estructura (Figura 7), donde X representa a los aminoácidos nombrados anteriormente.

La gelatina puede ser tratada químicamente para obtener cambios significativos en sus propiedades químicas y físicas. Estos cambios son el resultado de modificaciones estructurales o reacciones que típicamente incluyen la acetilación, esterificación, desaminación, reticulación y polimerización, como también reacciones simples con ácidos y bases (GMIA, 2012).

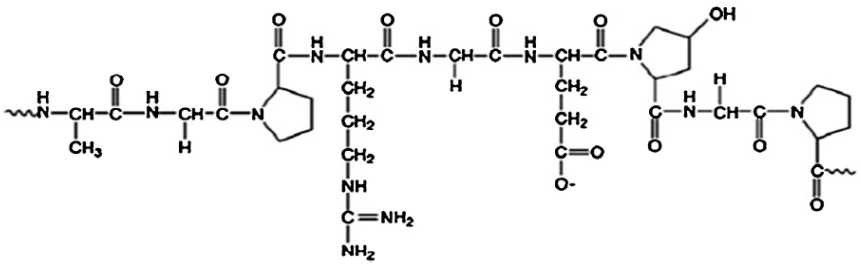

Figura 7: Estructura química básica de gelatina (Elzoghby A., 2013)

Una molécula de gelatina contiene aproximadamente 13% de su naturaleza cargada positivamente, por la presencia de lisina y arginina, un 12% de carga negativa, debido a los ácidos glutámico y aspártico, y un 11% de la cadena hidrofóbica que comprende los aminoácidos Leucina, Isoleucina, Metionina y Valina. Glicina, Prolina e Hidroxiprolina forman el resto de la cadena (Elzoghby A., 2013). Esto le entrega un carácter anfótero, capaz de actuar como ácido o base, dependiendo del carácter de la solución. En soluciones ácidas, la gelatina estará cargada positivamente en cambio en una solución alcalina estará cargada negativamente, el punto donde la carga neta es cero y no ocurre movimiento es conocido como punto isoeléctrico. La gelatina de tipo A posee un punto isoeléctrico en el rango de pH de 7-9, en cambio gelatina del tipo B posee su punto isoeléctrico en un rango de 4.7-5.4 (GMIA, 2012).

### 2.3.2 Reticulado y estructura tridimensional de la gelatina

La gelatina es capaz de formar geles físicos en solventes compatibles con la formación de puentes de hidrógeno a una concentración mayor a ~ 2% w/v. La solución de gelatina entra en una transición de gelificado termo-reversible de primer orden a temperaturas menores a ~ 30ºC, durante este proceso las moléculas de gelatina experimentan una transición mediada de asociación conformacional desde un enrollado azaroso a la triple-hélice. La solución posee entramados azarosos polidispersos de moléculas de gelatina y agregados, los cuales en estado de gel

son propensos a la estabilización de triple-hélices mediante la formación de puentes de hidrógeno intermoleculares formando una estructura tridimensional (Mohanty & Bohidar, 2005).

Este tipo de comportamiento se puede observar de mejor manera en hidrogeles no covalentes, donde priman las interacciones físicas en el sistema y las cadenas de gelatina tienen un mayor grado de renaturalización manteniendo las propiedades originales.

El reticulado es más que solo puentes de hidrógeno al azar entre cadenas de polímeros adyacentes, ya que también se puede obtener a través de enlaces químicos. Este reticulado puede ser inducido por radiación o reacción química. En particular, en el primer caso, las reacciones de radiación incluyen haz de electrones, rayos-γ, rayos-X, o luz ultra-violeta. En el segundo caso de reticulado químico, la reacción puede ocurrir entre agentes reticuladores de bajo peso molecular y una cadena del polímero. El agente reticulador enlaza dos cadenas a través de dos o más de sus grupos funcionales, o una reacción de reticulación-copolimerización puede llevarse a cabo entre los monómeros y monómeros multifuncionales que se encuentran presentes en bajas cantidades (Barbucci R., 2009).

En este proyecto, el OG actúa como agente reticulador formando enlaces del tipo covalente entre sus grupos oxigenados, epoxi- y carboxi-, con los grupos amino de la cadena de gelatina. Los grupos residuales suelen formar complejos de interacción física entre ellos complementando la reticulación del sistema formando, en solventes compatibles, estructuras poliméricas llamadas hidrogeles.

El hidrogel, que corresponde a una estructura polimérica física o químicamente reticulada hinchada con grandes cantidades de agua, debido a su naturaleza no se disuelve en medios acuosos, debido a sus importantes cantidades de moléculas de agua solvatada en la matriz de cadenas poliméricas (Kikuchi & Okano, 2005). Cuando el poro líquido del hidrogel es reemplazado por aire sin una alteración significativa de la red estructural o el volumen del cuerpo del gel se obtiene un aerogel. (Hüsing & Schubert, 1998)

Su producción, acompañada de un arreglo de orden-desorden en el cual las cadenas recobran parcialmente la estructura de triple-hélice, conlleva la formación de la gelatina renaturalizada con importantes regiones amorfas de cadenas de gelatina enrolladas azarosamente interconectadas con zonas de microcristales espacialmente ordenados, estabilizados por puentes de hidrógeno entre la glicina y la prolina. La estabilización de la conformación molecular y las interacciones inter-hélices son consecuencia de la existencia de capas de hidratación con agua, altamente ordenada, uniendo mediante puentes de hidrógeno dos grupos entre la misma o diferentes cadenas de gelatina (Gorgieva & Kokol, 2011).

Los hidrogeles son generalmente caracterizados por su capacidad de absorción y la cinética de esta, como también sus propiedades mecánicas en humedad o hidratados. Estas propiedades se ven afectadas por distintos factores donde los más importantes corresponden a la densidad de reticulado y la integridad estructural comprendiendo la porosidad, el tamaño del poro y su distribución (Siepmann et al, 2012).

Se ha reportado el desarrollo de hidrogeles basados en óxido de grafeno y gelatina para su uso en distintos ámbitos como en la remoción de colorantes (Liu et al, 2017), mineralización biomimética de minerales como la hidroxiapatita (Liu et al, 2014), mejoras en el desempeño de ánodos Ion-Li (Lee et al, 2016) y para su uso en la biomedicina, en el transporte y liberación de drogas e ingeniería de tejidos (An et al, 2013; Chen et al, 2014; Piao & Chen, 2016).

La caracterización de este tipo de hidrogeles es común para la mayoría de las publicaciones. Se caracteriza químicamente mediante espectros FTIR, Raman y XRD, además de evaluar su estabilidad térmica mediante técnicas termogravimétricas. Además, se evalúan distintas propiedades donde usualmente se encuentra su comportamiento mecánico, su capacidad de absorción de agua, y propiedades estructurales como la porosidad, el tamaño de poro y la distribución de estos, entre otros.

### 2.3.3 Caracterización química e interacción covalente OG-G

Existe una vasta gama de técnicas que permiten evaluar las características cualitativas de un material. Entre ellas las técnicas espectroscópicas, como la espectroscopía de infrarrojo con transformada de Fourier (FT-IR) y la espectroscopía Raman, que son utilizadas para la identificación de estructura química en la superficie del material. Además, es común el uso de la difracción de rayos X (XRD) para análisis del estado cristalino del material. Estas técnicas suelen ser aplicadas para la caracterización química de materiales basados en OG, aportando evidencia cualitativa para la determinación de su funcionalización (Krishnamoorthy et al, 2012; Layek & Nandi, 2013). A continuación, se presenta una breve descripción de estas técnicas y algunos de los resultados reportados para este tipo de material.

Espectroscopía de infrarrojo con transformada de Fourier (FTIR): Técnica que se fundamenta en la absorción de radiación infrarroja por las moléculas, para las cuales existen pequeñas diferencias de energía entre los distintos estados vibracionales y rotacionales. Una molécula absorberá la energía de un haz de luz infrarroja cuando dicha energía incidente sea igual a la necesaria para que se dé una transición vibracional de la molécula. Es decir, la molécula comienza a vibrar de una determinada manera gracias a la energía que se le suministra mediante luz infrarroja (Skoog, 2008). Estos espectros entregan información cualitativa y permiten determinar la presencia de los grupos funcionales presentes en una muestra. Materiales OG-G covalentes, y no covalentes , reportan que el espectro de OG muestra la presencia de diferentes tipos de grupos funcionales oxigenados a través de sus bandas relacionadas a la vibración de sus enlaces, como la banda entre 3200 y 3400 $cm^{-1}$ relacionada al enlace O-H, la banda a 1729 $cm^{-1}$ relacionada con el enlace C-O del grupo carbonilo, la banda a 1361 $cm^{-1}$ relacionada al enlace C-OH, la banda a 1225 $cm^{-1}$ relacionada al enlace C-O-C del grupo epoxi, y la banda a 1046 $cm^{-1}$ del enlace C-O del grupo alcoxi, como también se observa una banda a 1621 $cm^{-1}$ relacionada al enlace C=C de los dominios de la estructura aromática. Por otro lado, se reportan las bandas características de la gelatina como la banda Amida I a los 1627 $cm^{-1}$ relacionada al enlace C=O del grupo amida, la banda Amida

II a los 1521 $cm^{-1}$ relacionada al enlace N-H del grupo amida, la banda Amida III a los 1238 $cm^{-1}$, y la banda relacionada al enlace N-H a los 3262 $cm^{-1}$ (Piao & Chen, 2015; Piao & Chen, 2016; Liu et al, 2017). Además, se ha reportado un debilitamiento de la banda relacionada al enlace C-O-C del grupo epoxi y la desaparición de la banda asociada al enlace C=O en la interacción OG-G covalente, resultados que advierten son evidencia de las reacciones de amidación entre los grupos oxigenados de las láminas de OG y los grupos amina de las cadenas de gelatina (Piao & Chen, 2016).

Espectroscopía Raman: Esta técnica proporciona información química y estructural de compuestos orgánicas e inorgánicos. Los espectros Raman se obtienen al irradiar una muestra con una fuente de rayos láser de radiación monocromática visible o infrarroja. Durante el proceso se registra el espectro de la radiación dispersa a un cierto ángulo, habitualmente 90°, con ayuda de un espectrómetro apropiado (Skoog, 2008). La principal ventaja de esta técnica es que es no destructiva y se realiza directamente sobre el material sin necesidad de preparar la muestra. El espectro de OG se caracteriza por dos bandas prominentes, la banda G a ~1588 $cm^{-1}$ y la banda D ~1350 $cm^{-1}$, correspondientes a los átomos de carbono de hibridación $sp^2$ en la estructura aromática y a los átomos de hibridación $sp^3$ en los defectos de la estructura, respectivamente (An et al, 2013; Liu et al, 2017). Además, se ha reportado que una variación en la razón intensidad entre la banda D y G ($I_{D/G}$), como en la posición de la banda G, evidencian la reducción y funcionalización del OG (Makharza et al, 2015; Piao & Chen, 2016; Liu et al, 2017).

Difracción de rayos X (XRD): Es un método para análisis de materiales, que utiliza la difracción de radiación, un fenómeno físico que se produce en la interacción de un haz de rayos X, de longitud de onda conocida, con un material cristalino. Esta técnica se basa en la dispersión coherente del haz en el material y en la interferencia constructiva de las ondas que están en fase y que dispersan en determinadas direcciones del espacio (Skoog, 2008). En la aplicación de esta técnica a materiales OG-G, se ha reportado un pico alrededor de los 10°, debido a la cristalinidad producto de la aglomeración de las láminas de OG. Luego de la reducción del OG con las cadenas de gelatina, no se observa un pico significativo, demostrando la

dispersión lograda mediante la funcionalización del OG (An et al, 2013; Liu et al, 2011). Mismo comportamiento se reporta en funcionalización física del OG, mostrando que ambos métodos son capaces de dispersar las láminas de OG disminuyendo su cristalinidad (Wan et al, 2011; Piao & Chen, 2014).

Distintas técnicas se han utilizado para confirmar la interacción covalente entre el OG y distintos polímeros, de manera complementaria a la evidencia entregada por las técnicas anteriormente descritas. Entre las más importantes se encuentra la resonancia magnética nuclear (NMR), la cual provee evidencia directa de enlaces covalentes entre el OG y el componente utilizado para su reducción. Ejemplos de esto han sido los resultados reportados en la funcionalización por sulfuro del OG, y la reducción química del OG por aminas primarias alifáticas y amino ácidos (Bourlinos et al, 2003; Thomas et al, 2014). Sin embargo, dada la complejidad de la técnica para materiales OG-G y su disponibilidad, se han reportado técnicas alternativas para la confirmación de la reducción química del OG mediante como la espectroscopía UV-Visible y la espectroscopía de fotoelectrones emitidos por rayos X (XPS). La confirmación mediante espectroscopía UV-Visible evidencia la reducción química durante la formación del hidrogel OG-G por el desplazamiento del espectro del material, asociado a la restauración parcial de la red de átomos de carbono de hibridación $sp^2$ en la estructura aromática (An et al, 2013; Piao & Chen, 2016). Por otro lado, el análisis XPS entrega información cualitativa sobre los enlaces asociados a un elemento químico a través de sus estados de oxidación. La deconvolución del espectro obtenido, para un elemento en específico, entrega información de los enlaces asociados a este, y una estimación del porcentaje atómico relativo al tipo de enlace. De este modo, es posible confirmar la formación de enlaces covalentes mediante comparación directa de los espectros y sus respectivos porcentajes atómicos. Este método ha sido utilizado para confirmación de la funcionalización química del OG con distintos agentes como el quitosano, L-cisteína, tioacetato de potasio, entre otros (Rana et al, 2011; Muralikrishna et al, 2014; Thomas et al, 2014).

Así, en este estudio se utilizó el análisis XPS para determinar la formación de enlaces amida en la interacción OG-G, tal como se ha reportado para la formación

de enlaces amida en nano-láminas de OG-quitosano (Rana et a, 2011). De este modo, al diferenciar el tipo de interacción OG-G presente en los materiales mediante análisis químico, se podrá evaluar la influencia de estas interacciones en las propiedades macroscópicas de los aerogeles, mediante comparación entre estos.

## 2.4 Proantocianidinas y extractos de uva

### 2.4.1 Aspectos generales de las proantocianidinas

Los taninos o proantocianidinas (PAs), son polifenoles solubles en agua que están ampliamente distribuidos en el mundo vegetal, incluidos los alimentos de grano y frutas. Estos se categorizan en cuatro grupos: galotaninos, elagitaninos, complejos, y condensados, teniendo como elementos estructurales más comunes una o más unidades de polialcoholes y una o más unidades de polifenoles.

Estos compuestos han llamado la atención en el área de la salud por sus propiedades antioxidantes, antimicrobianas, anti-inflamatorias, antialérgicas y actividad inhibitoria de enzimas. La disminución del colesterol a través de compuestos bioactivos presentes en las legumbres o la acción antioxidante de polifenoles presentes en el té verde son algunos ejemplos. (Erdelyi et al, 2005; Asgary et al, 2018; Shavandi et al, 2018).

Otra fuente rica en PAs es la uva, particularmente su piel y semillas, los que se obtienen comúnmente mediante la extracción por solventes y extracción enzimática. Los principales monómeros presentes en estas PAs, compuestas por subunidades de flavan-3-ol, son la (+)-catequina, (-)-epicatequina, (-)-epicatequin galato, y la (-)-epigalocatequina, cuyas estructuras se presentan en la Figura 8.

Las PAs poseen actividad en la función endotelial, como antioxidante, y en la agregación plaquetaria. Además, son capaces de reducir los triglicéridos presentes en la sangre y disminuir la presión arterial a través de la inhibición de la enzima convertidora de la Angiotensina I (Godoy et al, 2012; Asgary et al, 2018).

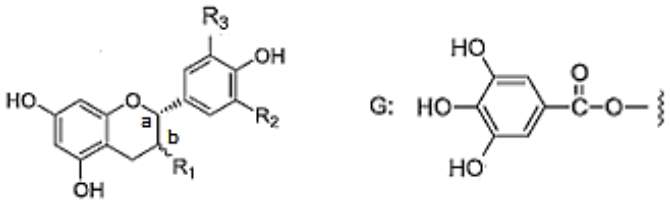


| Monómero de PAs | $R_1$ | $R_2$ | $R_3$ |
|---|---|---|---|
| (+)-catequina | OH | OH | H |
| (-)-epicatequina | OH | H | OH |
| (-)-epigalocatequina | OH | OH | OH |
| (-)epicatequin galato | G | H | OH |

(-): (a,b - cis), (+): (a,b - trans)

Figura 8: Estructura de monómeros presentes en proantocianidinas de uva (Liu et al, 2003; Chung et al, 1998; Guerrero et al, 2012).

De este modo, la incorporación de proantocianididinas en biomateriales modifica sus propiedades biológicas a través de la interacción con la matriz, su estructura y su superficie. Ejemplos de esto son las esponjas de colágeno, colágeno-ácido hialurónico, y colágeno-ácido hialurónico-quitosano diseñadas para el tratamiento de heridas y el estudio de la influencia de la catequina, epigalocatequina galato, y ácido gálico provenientes del té en el comportamiento de estos materiales, mostrando una variación poco significativa con respecto a las esponjas sin polifenoles en la viabilidad celular de fibroblastos, promoviendo además la proliferación de estas células. (Francesko et al, 2013). Mismo comportamiento se ha reportado en el tratamiento de matrices basadas en colágeno con ácido tánico, indicando que no existe variación significativa en la viabilidad celular de los fibroblastos en este tipo de material (Natarajan et al, 2012). Por lo anterior, los extractos no tendrían efecto citotóxico sobre los tejidos de la piel.

### 2.4.2 Interacción con polímeros e interfaces

Las propiedades biológicas de los extractos naturales han sido comúnmente preservadas a través de su inmovilización en interfaces (Reitzer et al, 2018). Esta aplicación en dispositivos biomédicos se puede clasificar en dos categorías,

biomateriales que liberan polifenoles en su alrededor permitiendo su difusión en los tejidos contiguos y biomateriales que no liberan algún compuesto activo.

Esta última categoría puede ser dividida en la inmovilización vía enlace covalente del polifenol o su incorporación para la modificación de la superficie con el fin de adquirir propiedades biológicas como la adhesión y actividad celular (Reitzer et al, 2018).

### 2.4.2.1 Interacción polímero-polifenol

Los compuestos polifenólicos son excelentes donadores de hidrógenos que pueden formar puentes con grupos carboxílicos de proteínas en una interacción reversible. De esta manera son capaces de reticular con polímeros, como el colágeno, a través de la formación de múltiples puentes de hidrógeno con los grupos funcionales laterales de la cadena asociados a aminoácidos polares, como se muestra en la figura 9.

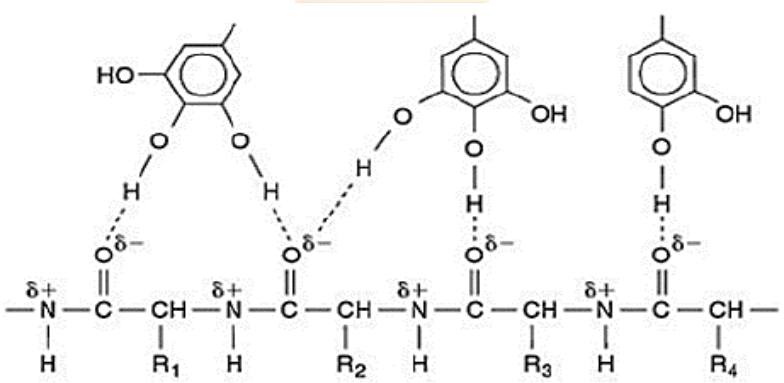

Figura 9: Modelo propuesto para la formación de puentes de hidrógeno entre el polifenol y el péptido. (Albu et al, 2015)

Debido a que estos oligofenoles contienen una cantidad importante de grupos hidroxilo y carbonilo, estos pueden formar puentes de hidrógeno en múltiples puntos, otorgando mayor estabilidad a la matriz polimérica (Albu et al, 2015; Buitimea-Cantúa et al, 2017).

Otro tipo de interacción reversible, como la formada entre ácidos fenólicos y α-lactalbumina, se produce por interacciones electrostáticas y condiciones neutras entre los ácidos fenólicos en su forma deprotonada (Buitimea-Cantúa et al, 2017).

En el caso de las proantocianidinas de extracto de uva, Poncet-Legrand y colaboradores (2007) indican que existe una diferencia entre ellos en la capacidad de interactuar y formar agregados coloidales con proteínas, como también en su estabilidad en el sistema. Se reporta que epicatequinas y epigalocatequinas no forman agregados con poli(L-prolina), a diferencia de catequinas y epicatequin galatos que si son capaces de formarlos. Cuando estos complejos se forman, su estabilidad depende de la razón entre monómero y proteína, y en la concentración inicial de esta.

Por otro lado, los compuestos polifenólicos pueden reaccionar covalentemente con proteínas, ya sea como un radical fenólico o luego de ser transformado en un radical quinona o semiquinona, esta última producida por un mecanismo de reacción de oxidación de ácidos fenólicos simples. Este tipo de interacción además puede producir cambios en estructuras de proteínas secundarias y terciarias como la gelatina (Buitimea-Cantúa et al, 2017).

#### 2.4.2.2 Modificación estructural de la matriz por incorporación de PAs

Muchos estudios se han llevado a cabo evaluando los efectos provocados por la adición de diferentes sustancias, como reticuladores, agentes reforzantes, plastificadores o aditivos con actividades antimicrobiales o antioxidantes en distintos tipos de materiales, como los aerogeles, para mejorar sus propiedades funcionales. Estructuralmente, esta mejora ocurre cuando las fuerzas intermoleculares de las cadenas de proteína son reducidas mediante la acción de estructuras moleculares modificando su carácter hidrofílico o promoviendo la formación de enlaces covalentes en la red proteica.

Se ha demostrado la viabilidad de utilizar extractos naturales como nuevos reticuladores naturales mediante la formación de puentes de hidrógeno entre el agua y grupos hidroxilo libres en grupos amino o polifenoles produciendo un aumento en la dureza de la proteína en el material comparada con esta sin tratar (Ramos et al, 2016).

Más aún, diversos investigadores han reportado que la adición de polifenoles, como el ácido tánico, mejoran sus propiedades mecánicas significativamente basadas en

la interacción de estos con el polímero. Se ha reportado una fuerte resistencia mecánica, gran elongación, excelente rigidez y dureza, entre otras propiedades mecánicas, en hidrogeles tratados con ácido tánico en comparación a los hidrogeles originales basados en alcohol polivinílico (PVA) y poliacrilamida (PAAm). El abundante enlazado mediante puentes de hidrógeno, el fácil rompimiento de estos, y su estructura amorfa, proveen a la red de un mecanismo disipación de energía que otorga mayor dureza y elongación. Resultados similares se han observado en la adición de extractos de cáscara de coco en láminas de gelatina que, debido a la alta interacción entre los grupos funcionales de la gelatina y los compuestos fenólicos, mostraron una mejora en sus propiedades mecánicas mayores que las láminas sin tratar. (Chen et al, 2016; Ramos et al, 2016; Fan et al, 2018).

En base a lo anterior, se espera que la adición de extractos polifenólicos provenientes de la uva País modifique la estructura del aerogel, mejorando sus propiedades mecánicas, como su dureza y rigidez.

#### 2.4.2.3 Modificación superficial de la matriz por incorporación de PAs

La modificación de las propiedades superficiales de los materiales, entre ellas propiedades químicas, mojabilidad, composición y morfología del dominio, han demostrado tener influencia en la adsorción de proteínas, en su posterior respuesta celular y de tejido, y en la liberación de fármacos, entre otros. Por ejemplo, la adhesión plaquetaria y la activación en superficies de biomateriales es influenciada por las propiedades superficiales como la energía, carga y composición de esta.

En particular, una hidrofilicidad alta y buena lubricación son características esenciales para dispositivos médicos utilizados en vasos sanguíneos, conductos corporales, entre otros. En general, el aumento de la hidrofilicidad es una manera eficiente de mejorar la biocompatibilidad y las propiedades antibacterianas, por lo que las propiedades superficiales es uno de los parámetros más importantes en el diseño de biomateriales o dispositivos de implante. (Thevenot et al, 2008; Zhou et al, 2010; Xu et al, 2014).

Muchos compuestos fenólicos naturales han sido identificados como alternativas para la modificación superficial. Polifenoles provenientes de plantas y polifenoles

como el ácido tánico, pirogalol, y la epigalocatequina galato se enlazan a superficies orgánicas e inorgánicas y proveen capas reactivas. Estos polifenoles interactúan entre sí vía enlaces covalentes y no covalentes para formar oligomeros, depósitos en superficies sólidas, y alojadas en moléculas tiol- o amino-terminales (Abouelmagd et al, 2016).

Como resultado de esta modificación el material sufre un cambio en su carga superficial debido al carácter negativo de los compuestos polifenólicos. Un ejemplo de esto es el ácido tánico el cual presenta carga negativa en rangos de pH cercanos a 3,5 aumentando su carácter negativo al incrementar el pH (Oćwieja et al, 2014). Así, la presencia de taninos en el material produce un descenso en la carga superficial del material el cual dependerá del pH en solución del tanino y la concentración de esta, y es responsable del aumento en la interacción electroestática con iones positivos (Wang et al 2009; Wang et al, 2018). De esta manera, se espera que la incorporación de los compuestos fenólicos modifique la carga superficial del aerogel.

### 2.5 Biomateriales como dispositivos hemostáticos

Los biomateriales han sido utilizados frecuentemente en distintos campos de la medicina y cirugía con amplio rango de aplicaciones médicas desde vendas de corto plazo a implantes de largo plazo, jugando un rol importante en el tratamiento de enfermedades. Una etapa crucial en los tratamientos de emergencia es la detención del sangrado, especialmente en casos de traumas sin control en accidentes de tráfico mayores, desastres naturales, entre otros.

La hemorragia normalmente no puede ser controlada por el mecanismo hemostático natural del cuerpo humano por lo que una serie de materiales hemostáticos han sido desarrollados para su tratamiento. En particular, debido a su bioactividad y funciones bioquímicas únicas en el cuerpo humano, materiales y polímeros naturales como la gelatina y el quitosano han sido de particular atractivo en el desarrollo de este tipo de dispositivos por sobre polímeros sintéticos y materiales inorgánicos. El mecanismo de acción de estos dispositivos y algunos ejemplos de estos se detallan a continuación.

### 2.5.1 Mecanismo hemostático externo o de contacto

La sangre es comúnmente el primer fluido corporal que entra en contacto con dispositivos de contacto. La interacción sangre-material desencadena una compleja serie de eventos que incluye la adsorción de proteínas, adhesión y activación plaquetaria, coagulación, y formación del trombo (Xu et al, 2014). Una rápida adsorción de las proteínas del plasma es el primer evento ocurriendo en la superficie del biomaterial durante la interacción sangre-material, y permite la activación de proteínas adsorbidas que pueden catalizar, mediar o moderar las respuestas biológicas posteriores en el biomaterial.

En particular, la fase inicial de la activación en el sistema trombogénico de contacto con materiales externos requiere sitios cargados negativamente y compromete cuatro proteínas distintas, promoviendo la interacción entre estas. Se ha reportado que los tejidos internos del sistema vascular intactos están cargados negativamente con respecto a las que se desarrollan en lugares no habituales pero un trauma en el vaso está relacionada a la generación de cargas positivas locales por lo que se estima que superficies cargadas positivamente en materiales en contacto con sangre induzcan la formación de los primeros aglomerados de plaquetas (Mao et al, 2004). Luego de la activación, las plaquetas pasan a una morfología dendrítica y posteriormente, desarrollan signos de retroalimentación positiva para plaquetas adicionales para proliferación sobre la superficie del biomaterial. Este ciclo de retroalimentación positiva de degranulado y proliferación, promueven la adhesión de plaquetas adicionales para formar capas de interacción plaqueta-plaqueta, agregación y formación del trombo. (Werner et al, 1999; Nanda et al, 2018). De esta manera, se espera que la modificación de la carga superficial en el aerogel, mediante la incorporación de los extractos polifenólicos, genere mejores condiciones para la absorción de sangre y formación del coágulo.

### 2.5.2 Dispositivos hemostáticos

Actualmente diversos tipos de materiales hemostáticos han sido desarrollados, como las zeolitas, sílice porosa, granulosa y quitosano. En el caso de materiales inorgánicos micro- o meso-porosos, estos promueven la hemostasia en base a la

absorción rápida del fluido y la proliferación de células sanguíneas y plaquetas (Liang et al, 2018).

Un ejemplo de esto son gazas de quitosano modificada con polímeros sintéticos, desarrollada por Chan y colaboradores (2016), cuya superficie cargada positivamente detiene el sangrado de heridas mediante interacción electrostática con las membranas celulares cargadas negativamente de eritrocitos para causar su aglutinación y el sellado de la herida mediante la adhesión tisular. Yan y colaboradores (2017) proponen un nuevo material tipo esponja basado en colágeno reforzado con quitosano y nanoflores de pirofosfato de calcio, el cual en la composición óptima es capaz de activar el procedimiento intrínseco de la cascada de coagulación, induciendo la adherencia de hemocitos y plaquetas, promoviendo la coagulación de la sangre logrando el control de la hemorragia *in vitro* e *in vivo*. Del mismo modo se han desarrollado hidrogeles para actividad hemostática, Behrens y colaboradores (2013) han desarrollado partículas de hidrogel sintético con N-(3-aminopropil) metacrilamida mostrando un rápido hinchamiento debido a la absorción de sangre causando agregación local, mientras se retarda la coagulación en el seno del fluido, evitando el riesgo de la formación de trombos distales. Esto debido a la superfiecie altamente positiva y una baja densidad de reticulado. Todos ellos coinciden en la importancia de la modificación superficial para la mejora de sus propiedades y su posterior agregación plaquetaria iniciando la coagulación.

Otro tipo de material con gran potencial para el tratamiento de traumas son las esponjas de grafeno reticulado (Quan et al, 2015). Estas absorben el plasma rápidamente acelerando la coagulación. Sin embargo, cuando entra en contacto con la sangre, este no puede estimular los hemocitos para promover el control del sangrado por lo que la formación de nuevos compósitos con un nuevo mecanismo de activación es necesario para lograr un alto desempeño en la hemostasia. En base a esto, se han desarrollado distintos tipos de esponjas de grafeno reticuladas con aditivos externos como trombina o kaolita mostrando mejores desempeños hemostáticos que sus materiales originales debido al aumento en la capacidad de absorción de plasma y aglomeración de células sanguíneas, y la posterior activación de los factores de coagulación (Li et al, 2018; Liang et al, 2018).

Tal como los materiales antes mencionados, se plantea el desarrollo de una estructura polimérica, basada en G y OG, que propicie la absorción de sangre y formación del coágulo. Sin embargo, la interacción del material con el extracto de uva generará cambios en la estructura y en sus propiedades que favorecerán su uso como dispositivo hemostático, lo cual será verificado por análisis SEM.

## 2.6 Referencias


- Abouelmagd, S. A., Meng, F., Kim, B. K., Hyun, H., & Yeo, Y. (2016). Tannic acid-mediated surface functionalization of polymeric nanoparticles. *ACS biomaterials science & engineering*, *2*(12), 2294-2303.
- Albu, M. G., Deselnicu, V., Ioannidis, I., Deselnicu, D., & Chelaru, C. (2015). Chemical functionalization and stabilization of type I collagen with organic tanning agents. *Korean Journal of Chemical Engineering*, *32*(2), 354-361.
- An, J., Gou, Y., Yang, C., Hu, F., & Wang, C. (2013). Synthesis of a biocompatible gelatin functionalized graphene nanosheets and its application for drug delivery. *Materials Science and Engineering: C*, *33*(5), 2827-2837.
- Asgary, S., Rastqar, A., & Keshvari, M. (2018). Functional Food and Cardiovascular Disease Prevention and Treatment: A Review. *Journal of the American College of Nutrition*, 1-27.
- Barbucci, R. (Ed.). (2010). *Hydrogels: Biological properties and applications*. Springer Science & Business Media.
- Behrens, A. M., Sikorski, M. J., Li, T., Wu, Z. J., Griffith, B. P., & Kofinas, P. (2014). Blood-aggregating hydrogel particles for use as a hemostatic agent. *Acta biomaterialia*, *10*(2), 701-708.
- Bourlinos, A. B., Gournis, D., Petridis, D., Szabó, T., Szeri, A., & Dékány, I. (2003). Graphite oxide: chemical reduction to graphite and surface modification with primary aliphatic amines and amino acids. Langmuir, 19(15), 6050-6055.
- Buitimea-Cantúa, N. E., Gutiérrez-Uribe, J. A., & Serna-Saldivar, S. O. (2018). Phenolic–protein interactions: Effects on food properties and health benefits. *Journal of medicinal food*, *21*(2), 188-198.
- Chan, L. W., Kim, C. H., Wang, X., Pun, S. H., White, N. J., & Kim, T. H. (2016). PolySTAT-modified chitosan gauzes for improved hemostasis in external hemorrhage. *Acta biomaterialia*, *31*, 178-185.
- Chen, G., Qiao, C., Wang, Y., & Yao, J. (2014). Synthesis of Biocompatible Gelatin-functionalised graphene nanosheets for drug delivery applications. *Australian Journal of Chemistry*, *67*(10), 1532-1537.

- Chen, Y. N., Peng, L., Liu, T., Wang, Y., Shi, S., & Wang, H. (2016). Poly (vinyl alcohol)–tannic acid hydrogels with excellent mechanical properties and shape memory behaviors. *ACS applied materials & interfaces*, *8*(40), 27199-27206.
- Chung, K. T., Wong, T. Y., Wei, C. I., Huang, Y. W., & Lin, Y. (1998). Tannins and human health: a review. *Critical reviews in food science and nutrition*, *38*(6), 421-464.
- Dreyer, D., Park, S., Bielawski, Ch., Ruoff, R. (2010). The chemistry of graphene oxide. Chemical Society Reviews, 39, 228-240.
- Elzoghby, A. O. (2013). Gelatin-based nanoparticles as drug and gene delivery systems: reviewing three decades of research. *Journal of Controlled Release*, *172*(3), 1075-1091.
- Erdelyi, K., Kiss, A., Bakondi, E., Bai, P., Szabo, C., Gergely, P., ... & Virag, L. (2005). Gallotannin inhibits the expression of chemokines and inflammatory cytokines in A549 cells. *Molecular pharmacology*.
- Fan, H., Wang, J., & Jin, Z. (2018). Tough, Swelling-Resistant, Self-Healing, and Adhesive Dual-Cross-Linked Hydrogels Based on Polymer–Tannic Acid Multiple Hydrogen Bonds. *Macromolecules*, *51*(5), 1696-1705.
- Fernández, K., Vega, M., & Aspé, E. (2015). An enzymatic extraction of proanthocyanidins from País grape seeds and skins. *Food chemistry*, *168*, 7-13.
- Francesko, A., da Costa, D. S., Reis, R. L., Pashkuleva, I., & Tzanov, T. (2013). Functional biopolymer-based matrices for modulation of chronic wound enzyme activities. *Acta biomaterialia*, *9*(2), 5216-5225.
- Georgakilas, V. (Ed.). (2014). *Functionalization of graphene*. John Wiley & Sons.
- Godoy, S., Roeckel, M., & Fernández, K. (2012). Influence of the structure and composition of the País grape proanthocyanidins on the inhibition of angiotensin I-converting enzyme (ACE). *Food chemistry*, *134*(1), 346-350.
- Gorgieva, S., & Kokol, V. (2011). Collagen-vs. gelatine-based biomaterials and their biocompatibility: review and perspectives. In *Biomaterials applications for nanomedicine*. InTech.

- Guerrero, L., Castillo, J., Quiñones, M., Garcia-Vallvé, S., Arola, L., Pujadas, G., & Muguerza, B. (2012). Inhibition of angiotensin-converting enzyme activity by flavonoids: structure-activity relationship studies. *PloS one*, *7*(11), e49493.
- Handbook, G. G. (2012). Gelatin Manufacturers Institute of America. New York, NY, USA.
- Hüsing, N., & Schubert, U. (1998). Aerogels—airy materials: chemistry, structure, and properties. *Angewandte Chemie International Edition*, *37*(1-2), 22-45.
- Kauvar, D. S., Lefering, R., & Wade, C. E. (2006). Impact of hemorrhage on trauma outcome: an overview of epidemiology, clinical presentations, and therapeutic considerations. *Journal of Trauma and Acute Care Surgery*, *60*(6), S3-S11.
- Kiew, S. F., Kiew, L. V., Lee, H. B., Imae, T., & Chung, L. Y. (2016). Assessing biocompatibility of graphene oxide-based nanocarriers: a review. *Journal of Controlled Release*, *226*, 217-228.
- Kikuchi, A., Okano, T. (2005). Hydrogels: Stimuli-Sensitive Hydrogels. En Kwon, S. (2005). Polymeric Drug Delivery Systems. Florida, USA. Taylor & Francis Group.
- Krishnamoorthy, K., Veerapandian, M., Yun, K., & Kim, S. J. (2013). The chemical and structural analysis of graphene oxide with different degrees of oxidation. *Carbon*, *53*, 38-49.
- Lan, G., Lu, B., Wang, T., Wang, L., Chen, J., Yu, K., Liu, J., Dai, F., & Wu, D. (2015). Chitosan/gelatin composite sponge is an absorbable surgical hemostatic agent. *Colloids and surfaces B: Biointerfaces*, *136*, 1026-1034.
- Layek, R. K., & Nandi, A. K. (2013). A review on synthesis and properties of polymer functionalized graphene. *Polymer*, *54*(19), 5087-5103.
- Lee, J. H., Lee, Y., Shin, Y. C., Kim, M. J., Park, J. H., Hong, S. W., Kim, B., Oh, J. W., Park, K. D., & Han, D. W. (2016). In situ forming gelatin/graphene oxide hydrogels for facilitated C2C12 myoblast differentiation. *Applied Spectroscopy Reviews*, *51*(7-9), 527-539.

- Lee, J., Kim, J., Kim, S., & Min, D. H. (2016). Biosensors based on graphene oxide and its biomedical application. *Advanced drug delivery reviews*, *105*, 275-287.
- Li, G., Quan, K., Xu, C., Deng, B., & Wang, X. (2018). Synergy in thrombin-graphene sponge for improved hemostatic efficacy and facile utilization. *Colloids and Surfaces B: Biointerfaces*, *161*, 27-34.
- Liang, Y., Xu, C., Li, G., Liu, T., Liang, J. F., & Wang, X. (2018). Graphene-kaolin composite sponge for rapid and riskless hemostasis. *Colloids and Surfaces B: Biointerfaces*, *169*, 168-175.
- Lin, J., Chen, X., Huang, P. (2016). Graphene-based nanomaterials for bioimaging. Advancerd Drug Delivery Reviews, 105, 242-254.
- Liu, C., Liu, H., Xu, A., Tang, K., Huang, Y., & Lu, C. (2017). In situ reduced and assembled three-dimensional graphene aerogel for efficient dye removal. *Journal of alloys and compounds*, *714*, 522-529.
- Liu, H., Cheng, J., Chen, F., Bai, D., Shao, C., Wang, J., Xi, P., & Zeng, Z. (2014). Gelatin functionalized graphene oxide for mineralization of hydroxyapatite: biomimetic and in vitro evaluation. *Nanoscale*, *6*(10), 5315-5322.
- Liu, K., Zhang, J. J., Cheng, F. F., Zheng, T. T., Wang, C., & Zhu, J. J. (2011). Green and facile synthesis of highly biocompatible graphene nanosheets and its application for cellular imaging and drug delivery. Journal of Materials Chemistry, 21(32), 12034-12040.
- Liu, J. C., Hsu, F. L., Tsai, J. C., Chan, P., Liu, J. Y. H., Thomas, G. N., Tomlinson, B., Lo, M. Y., & Lin, J. Y. (2003). Antihypertensive effects of tannins isolated from traditional Chinese herbs as non-specific inhibitors of angiontensin converting enzyme. *Life sciences*, *73*(12), 1543-1555.
- Makharza, S., Vittorio, O., Cirillo, G., Oswald, S., Hinde, E., Kavallaris, M., Büchner, B., Mertig, M., & Hampel, S. (2015). Graphene oxide-gelatin nanohybrids as functional tools for enhanced carboplatin activity in neuroblastoma cells. Pharmaceutical research, 32(6), 2132-2143.

- Mao, C., Qiu, Y., Sang, H., Mei, H., Zhu, A., Shen, J., & Lin, S. (2004). Various approaches to modify biomaterial surfaces for improving hemocompatibility. *Advances in colloid and interface science*, *110*(1-2), 5-17.
- Marcano, D. C., Kosynkin, D. V., Berlin, J. M., Sinitskii, A., Sun, Z., Slesarev, A., Alemany, L. B., Lu, W., & Tour, J. M. (2010). Improved synthesis of graphene oxide. *ACS nano*, *4*(8), 4806-4814.
- McCallion, C., Burthem, J., Rees-Unwin, K., Golovanov, A., & Pluen, A. (2016). Graphene in therapeutics delivery: problems, solutions and future opportunities. *European Journal of Pharmaceutics and Biopharmaceutics*, *104*, 235-250.
- Mohanty, B., & Bohidar, H. B. (2005). Microscopic structure of gelatin coacervates. *International journal of biological macromolecules*, *36*(1-2), 39-46.
- Muralikrishna, S., Sureshkumar, K., Varley, T. S., Nagaraju, D. H., & Ramakrishnappa, T. (2014). In situ reduction and functionalization of graphene oxide with L-cysteine for simultaneous electrochemical determination of cadmium (II), lead (II), copper (II), and mercury (II) ions. Analytical Methods, 6(21), 8698-8705.
- Nanda, H. S., Shah, A. H., Wicaksono, G., Pokholenko, O., Gao, F., Djordjevic, I., & Steele, T. W. (2018). Nonthrombogenic hydrogel coatings with carbene-cross-linking bioadhesives. *Biomacromolecules*, *19*(5), 1425-1434.
- Natarajan, V., Krithica, N., Madhan, B., & Sehgal, P. K. (2013). Preparation and properties of tannic acid cross-linked collagen scaffold and its application in wound healing. *Journal of Biomedical Materials Research Part B: Applied Biomaterials*, *101*(4), 560-567.
- Oćwieja, M., Adamczyk, Z., & Morga, M. (2015). Adsorption of tannic acid on polyelectrolyte monolayers determined in situ by streaming potential measurements. Journal of colloid and interface science, 438, 249-258.
- Piao, Y., & Chen, B. (2015). Self-assembled graphene oxide–gelatin nanocomposite hydrogels: Characterization, formation mechanisms, and pH-

sensitive drug release behavior. Journal of Polymer Science Part B: Polymer Physics, 53(5), 356-367.

- Piao, Y., & Chen, B. (2016). One-pot synthesis and characterization of reduced graphene oxide–gelatin nanocomposite hydrogels. *RSC Advances*, *6*(8), 6171-6181.
- Pierson, H. O. (1993). Handbook of Carbon. *Graphite, Diamond and Fullerenes*, 106.
- Poncet-Legrand, C., Gautier, C., Cheynier, V., & Imberty, A. (2007). Interactions between flavan-3-ols and poly (L-proline) studied by isothermal titration calorimetry: effect of the tannin structure. *Journal of agricultural and food chemistry*, *55*(22), 9235-9240.
- Pop, E., Varshney, V., & Roy, A. K. (2012). Thermal properties of graphene: Fundamentals and applications. *MRS bulletin*, *37*(12), 1273-1281.
- Quan, K., Li, G., Luan, D., Yuan, Q., Tao, L., & Wang, X. (2015). Black hemostatic sponge based on facile prepared cross-linked graphene. *Colloids and Surfaces B: Biointerfaces*, *132*, 27-33.
- Ramos, M., Valdés, A., Beltrán, A., & Garrigós, M. C. (2016). Gelatin-based films and coatings for food packaging applications. *Coatings*, *6*(4), 41.
- Rana, V. K., Choi, M. C., Kong, J. Y., Kim, G. Y., Kim, M. J., Kim, S. H., Mishra, S., Singh, R. P., & Ha, C. S. (2011). Synthesis and drug-delivery behavior of chitosan-functionalized graphene oxide hybrid nanosheets. Macromolecular Materials and Engineering, 296(2), 131-140.
- Reitzer, F., Allais, M., Ball, V., & Meyer, F. (2018). Polyphenols at interfaces. *Advances in Colloid and Interface Science*.
- Seyednejad, H., Imani, M., Jamieson, T., & Seifalian, A. M. (2008). Topical haemostatic agents. *British Journal of Surgery*, *95*(10), 1197-1225.
- Shavandi, A., Bekhit, A. E. D. A., Saeedi, P., Izadifar, Z., Bekhit, A. A., & Khademhosseini, A. (2018). Polyphenol uses in biomaterials engineering. *Biomaterials*, *167*, 91-106.

- Shim, G., Kim, M. G., Park, J. Y., & Oh, Y. K. (2016). Graphene-based nanosheets for delivery of chemotherapeutics and biological drugs. *Advanced drug delivery reviews*, *105*, 205-227.
- Siepmann, J., Siegel, R., Rathbone, M. (2012). Fundamentals and Applications of Controlled Release Drug Delivery. New York, USA. Springer.
- Skoog, D., Holler, F., Crouch, S., & Skoog, D. (2008). Principios de análisis instrumental. 6e. México, México: Cengage Learning Editores S.A. de C.V.
- Thevenot, P., Hu, W., & Tang, L. & (2008). Surface chemistry influences implant biocompatibility. *Current topics in medicinal chemistry*, *8*(4), 270-280.
- Thomas, H. R., Marsden, A. J., Walker, M., Wilson, N. R., & Rourke, J. P. (2014). Sulfur-Functionalized Graphene Oxide by Epoxide Ring-Opening. Angewandte Chemie International Edition, 53(29), 7613-7618.
- Wan, C., Frydrych, M., & Chen, B. (2011). Strong and bioactive gelatin–graphene oxide nanocomposites. Soft Matter, 7(13), 6159-6166.Liu, C., Liu, H., Xu, A., Tang, K., Huang, Y., & Lu, C. (2017). In situ reduced and assembled three-dimensional graphene aerogel for efficient dye removal. *Journal of Alloys and Compounds*, *714*, 522-529.
- Wang, J., Li, A., Xu, L., & Zhou, Y. (2009). Adsorption of tannic and gallic acids on a new polymeric adsorbent and the effect of Cu (II) on their removal. Journal of Hazardous Materials, 169(1-3), 794-800.
- Wang, R. H., Zhu, X. F., Qian, W., Tang, H. Y., Jiang, J., Yu, Y. C., & Xu, R. K. (2018). Effect of tea polyphenols on copper adsorption and manganese release in two variable-charge soils. Journal of Geochemical Exploration, 190, 374-380.
- Werner, C., König, U., Augsburg, A., Arnhold, C., Körber, H., Zimmermann, R., & Jacobasch, H. J. (1999). Electrokinetic surface characterization of biomedical polymers—a survey. *Colloids and Surfaces A: Physicochemical and Engineering Aspects*, *159*(2-3), 519-529.

- Xu, L. C., Bauer, J. W., & Siedlecki, C. A. (2014). Proteins, platelets, and blood coagulation at biomaterial interfaces. *Colloids and Surfaces B: Biointerfaces*, *124*, 49-68.
- Yan, T., Cheng, F., Wei, X., Huang, Y., & He, J. (2017). Biodegradable collagen sponge reinforced with chitosan/calcium pyrophosphate nanoflowers for rapid hemostasis. *Carbohydrate polymers*, *170*, 271-280.
- Young, S., Wong, M., Tabata, Y., & Mikos, A. G. (2005). Gelatin as a delivery vehicle for the controlled release of bioactive molecules. *Journal of controlled release*, *109*(1-3), 256-274.
- Yurkanis P. (2003). Organic Chemistry, 4th edition. New Jersey, USA. Prentice Hall.
- Zhang, B., Wang, Y., & Zhai, G. (2016). Biomedical applications of the graphene-based materials. *Materials Science and Engineering: C*, *61*, 953-964.
- Zhou, X., Zhang, T., Jiang, X., & Gu, N. (2010). The surface modification of medical polyurethane to improve the hydrophilicity and lubricity: The effect of pretreatment. *Journal of applied polymer science*, *116*(3), 1284-1290.

## 3. Hipótesis

Aerogeles formulados en base a OG y G, con carga de PAs en su matriz, serán capaces de absorber sangre, y de acelerar la formación del coágulo, al otorgar la estructura porosa y la carga superficial necesaria para la adsorción y activación de los factores de coagulación.

## 4. Objetivos

### 4.1 Objetivo general

Desarrollar y caracterizar un aerogel en base a óxido de grafeno (OG) y gelatina (G), el cual considera la incorporación de PAs para su uso en aplicaciones hemostáticas.

### 4.2 Objetivos específicos

- Desarrollar y caracterizar morfológica, mecánica, física y químicamente los aerogeles sintetizados mediante unión covalente y no covalente, evaluando la influencia de la proporción OG:G y el pH de la suspensión de OG, en sus propiedades.
- Formular aerogeles OG-G con incorporación de PAs, evaluando la influencia de su concentración en las propiedades funcionales del material.
- Determinar la citotoxicidad y la capacidad de coagulación *in vitro* de los aerogeles desarrollados en los puntos anteriores, evaluando su comportamiento frente a sangre humana.

## 5. A Comparative Study of Graphene Oxide-Gelatin Aerogel Syntheses: Chemical Characterization, Morphologies and Functional Properties

*Sebastián Guajardo, Toribio Figueroa, Jessica Borges, Manuel Meléndrez, Katherina Fernández**

S. Guajardo, T. Figueroa, J. Borges, Dr. K. Fernández.

Laboratory of Biomaterials, Department of Chemical Engineering, Faculty of Engineering, University of Concepcion, P.O. Box 160-C, Concepcion 4030000, Chile.

E-mail: kfernandeze@udec.cl

Dr. M. Meléndrez.

Department of Materials Engineering, Faculty of Engineering, University of Concepcion, Concepcion 4030000, Chile

**Keywords:** synthesis, gels, matrix, biomaterials, structure-property relations

## 5.1 Abstract

Graphene oxide (GO)-gelatin (G) aerogels were synthesized by covalent and noncovalent methods, changing on the synthesis the GO:G ratio and the pH of the GO suspension, evaluating the physical, chemical and functional properties of these materials. Comparatively, low GO:G ratios with alkali GO suspension promoted GO-G interactions for covalent aerogels. In contrast, high GO:G ratios under acidic conditions promoted noncovalent interactions. Scanning electron microscopy (SEM) showed heterogeneous structures with pore sizes of 53.26±25.53 μm and 25.31±10.38 μm for covalent and noncovalent aerogels, respectively. The synthesis method did not influence the surface charge; however, differences were depending on the GO content and their chemical activation, shifting from 15.63±0.55 mV to -20.53±1.07 mV. Noncovalent aerogels presented higher absorption ratios in phosphate-buffered saline (PBS) solution (35.5±2.4 $g_{PBS}/g_{aerogel}$ - 49.6±3.8 $g_{PBS}/g_{aerogel}$) than covalent aerogels. Therefore, due to these properties, noncovalent aerogels could be more useful than covalent aerogels for absorption potential applications, as biomedicine or water-treatment, where the promotion of surface interactions and high absorption capability is desired.

## 5.2 Introduction

Aerogels are porous structures obtained by removing the liquid from a polymeric network and replacing it with a gas; the above is completed without decisively altering the overall configuration. These materials are synthesized using inorganic (e.g., silica, alumina), organic (e.g., resorcinol-formaldehyde, melamine-formaldehyde), carbon derivatives (e.g., using nanotubes, graphene oxide) and natural-based sources (e.g., cellulose, polysaccharides) [1,2]. Aerogels have low density (0.0003-0.5 g/cm$^3$), high surface area (50-1200 m$^2$/g) and high porosity (70.0-99.8%), and their interesting properties make them useful for applications in diverse fields such as packaging production, food development, and biomedical uses [3].

In particular, gelatin (G) aerogels are highlighted due to their nontoxicity, lack of immunogenicity, low price, and high sensitivity.[4,5] G produces random polydispersed frameworks, which tend to stabilize a triple helix through intermolecular H-bonding, producing tridimensional structures[6,7]. These matrices are not stable for a long period in a neutral medium; therefore, cross-linking agents are usually added to increase their strength and enzyme resistance and/or to maintain their stability and shape[6,8].

Graphene oxide (GO) can act as a cross-linking agent for G. GO is a highly oxidized form of graphene. It has carbons with sp$^2$ hybridization in the aromatic network and sp$^3$ hybridized carbons with hydroxyl and epoxy groups in their basal plane and carboxylic acids at their edges. GO can interact in covalent and noncovalent modes with G through chemical bonds and physical complexes between the oxygenated groups of GO and the amine groups of G chains [9,10]. As a result of these interactions, GO-G aerogels have been developed to improve the performance of Li-ion anodes [11], dye removal methods [12], and drug delivery systems[13–15]; furthermore, they have potential use in the mineralization of hydroxyapatite [16] and a variety of other applications.

Nevertheless, despite GO-G aerogels had been studied before, previous reports had a lack of their surface charge analysis. Moreover, the influence of covalent and

noncovalent GO-G synthesis on the material functional properties has been poorly studied; therefore, their comparison is scarce. The synthesis method, as well as the amount of GO incorporated and their chemical activation, could mediate the GO-G aerogel properties such as their stiffness, absorption, and surface charge.

It is interesting to note that there is no clear evidence that confirms the formation of amide bonds between GO-G in a covalent synthesis since the chemical characterization is mainly made by FT-IR analysis and the same spectra have been previously reported for covalent and noncovalent material synthesis[15,17]. Thus, the influence of the nature of interaction within covalent and noncovalent aerogels needs to be understood to improve the performance of the materials in future applications for different fields where aerogels are used.

Therefore, this study aims to develop GO-G aerogels by means of covalent and noncovalent interactions; then, the physical and chemical properties of these materials are compared by changing the GO:G ratio and the pH of the GO suspension in both syntheses.

## 5.3 Experimental section

### 5.3.1 GO-G aerogel preparation

A GO precursor was synthesized from natural graphite powder using a modified Hummers' method [18]. GO-G aerogels were prepared using two different methods reported by Piao & Chen in 2015 and 2016, with some modifications[15,17]. In a typical synthesis of GO-G aerogels, a desired amount of G was dissolved in 150 mL of Milli-Q water at 60°C with constant stirring for 1 h. Additionally, a GO suspension of 2 mg $mL^{-1}$ was prepared and sonicated for 30 min. Then, 50 mL of the GO suspension was dropwise added to the G solution with constant stirring. The materials were classified as covalent or noncovalent depending on the interaction promoted between the GO sheets and the G chains in each synthesis. The nature of these interactions will be confirmed by chemical characterization. For noncovalent aerogels, the suspension was stirred for 2 min at 37°C to promote physical interactions. For covalent aerogels, the suspension was stirred for 24 h at 70°C to

promote chemical interactions. The final suspension was stored at 4°C for 12 h to obtain a three-dimensional network and frozen at -86°C (BIOBASE Ultra Freezer, China). Finally, the samples were freeze-dried (LABCONCO Freeze Dryers, USA) to obtain the final aerogels. To study the effect of GO incorporation and chemical activation, the amount of G and the pH of the GO suspension were modified to obtain different GO:G ratios (1:10, 2:25, 1:15) and pH values (3, 7, 11); to apply response surface methodology described at the end of this section.

### 5.3.2 GO-G aerogel characterization and measurements

X-ray diffraction (XRD) patterns of GO and the powdered aerogel samples were obtained using an X-ray diffractometer (Bruker AXS, D4 Endeavor, USA) with Cu Kα radiation (λ=1.541841 Å; 2.2 kW) as the reference target, a voltage of 40 kV, and a current of 20 mA. The samples were measured from 2° to 50° (2θ) with steps of 0.02° and a measuring time of 141 seconds per step.

Fourier transform infrared (FT-IR) spectroscopy (Perkin Elmer UATR Two FT-IR Spectrometer, USA) was used to characterize GO and the powdered aerogel samples at wavenumbers ranging from 500 $cm^{-1}$ to 4000 $cm^{-1}$.

Raman spectroscopy was used to characterize and compare the covalent and noncovalent GO and GO-G aerogels. A vibrational analysis was acquired through a high-resolution confocal microscope (Horiba LabRam HR Evolution, Japan) with a 633 nm excitation laser line, a power of 13.3 mW, and 1.96 eV. The laser spot was centered on the sample using a lens (Olympus 100x VIS and a NUV camera B/S UV 50/50 + Lens F125 D25). The intensity of the laser remained constant to minimize any damage to the sample. The samples were measured using an object holder at room temperature (~22°C); none of the samples were characterized in solution.

X-ray photoelectron spectroscopy (XPS) was used to analyze and compare the oxidation state of the principal elements of the GO and GO-G aerogels. The measurement was performed in a Surface Analysis Station 1 (STAIB model RQ300/2, USA) in ultravacuum ($<10^{-9}$ bar) equipped with a hemispherical electron analyzer (SPEC PHOIBOS 100, Germany). The photoelectrons were excited with

non-monochromatic radiation Mg Kα (1486.6 eV) and analyzed with a constant energy step of 1 eV. The X-ray source was used with a strength of 300 Watts.

Thermogravimetric analysis (TGA) was used to study the thermal stability of the samples. The analysis was performed with a simultaneous thermal analysis instrument (NETZSCH STA 409 PC/PG, Germany) at a heating ratio of 10°C $min^{-1}$ from room temperature to 800°C under a nitrogen atmosphere (100 mL $min^{-1}$).

Scanning electron microscopy (SEM) was performed using a (JEOL JSM-6380LV, Japan) microscope at 10 kV. The samples were coated using a gold sputter coater, and the surfaces were observed at different resolutions for comparison. Additionally, the images were processed with Digital Gatan Microscopy 3.0 software to analyze the pore size distribution.

Regard to the above descriptions, it should be mentioned that all these analyses were applied in GO-G aerogels synthesized with a GO:G ratio of 1:10.

Aerogel porosities were measured by submerging an approximately 10 mm x 10 mm x 7 mm aerogel sample on a pycnometer that had a total volume ($V_m$) of 50 mL and is full of absolute ethanol with a density ($\rho_e$) of approximately 0.789 g $cm^{-3}$. The mass of the pycnometer ($W_0$), the pycnometer with the sample ($W_m$), the full ethanol pycnometer ($W_e$), and the pycnometer with the submerged sample ($W_w$) was measured, and the porosity of the sample was calculated as follows:

$$Porosity\ (\%) = 100 \times \left(1 - \frac{(W_e - W_0) - (W_w - W_m)}{\rho_e \times V_m}\right) \quad (1)$$

Dynamic light scattering (DLS) analysis was used to determine the response contour of the surface charge (ʒ-potential) using a nanoparticle analyzer (SZ-100 Horiba Scientific, Japan) where the samples (approximately 1 $cm^3$) were suspended in 30 mL of Milli-Q water, vigorously shaken and then sonicated for 30 min before being measured. The pH of the suspension was adjusted to 7.4 in all the samples, previous the measurement

The elastic modulus (E) was measured with a uniaxial compression test in which a cylindrical sample (diameter ~ 4.5 cm, height ~ 1 cm) was compressed until reaching

a constant compressive stress of 480 kN in a universal testing system (Instron Model 4468, USA) with a loading capacity 0.001 ~ 500 kN, at a constant loading speed of 1 mm $min^{-1}$. The samples were freeze-dried in a Petri dish (90 mm diameter) to obtain a regular cylindrical form. The compressive modulus was calculated in the first linear region, 10% - 40%, of the strain axis.

The absorption of phosphate-buffered saline (PBS) solution at equilibrium was measured by submerging a 10 mm x 10 mm x 7 mm aerogel sample in 3 mL of PBS in a Petri dish. Then, excess PBS was extracted from the dish at different times (15, 30, and 45 min). The mass of the sample before ($S_0$) and after ($S_{PBS}$) every immersion was measured, and the ratio was calculated as follows:

$$PBS\ Absorption\ Ratio = \frac{(S_{PBS} - S_0)}{S_0} \quad (2)$$

Response surface methodology was used to study the effects of the GO:G ratio and the pH of the GO suspension. A $2^2$ design with a central point was used. All combinations were measured in triplicate. The results were expressed as arithmetic means with a standard deviation. Paired tests, ANOVA, and response surface methodology were performed using Statgraphics Centurion XVI software with a significant average p-value ≤ 0.05. Additionally, OriginPro8 software was used to plot the results.

## 5.4 Results and discussion

### 5.4.1 Chemical characterization

XRD patterns of the G, GO, and GO-G aerogels are shown in **Figure 5.1a**. The spectrum of G presented a broad peak at 21°, which was related to its crystalline structure that originates from an α-helix and its triple-helical structure. The GO spectrum showed a peak at 10° related to the agglomeration of their sheets. This peak, in the aerogels synthesized by covalent and noncovalent interactions, tended to disappear, suggesting good dispersion of the GO sheets due to the formation of chemical bonds or physical complexes[13,17].

To study the GO-G chemical interaction, the FT-IR spectra of the samples are presented in **Figure 5.1b**. The GO spectrum showed different oxygenated functional groups: O-H stretching bonds at 3200-3400 $cm^{-1}$, C=O stretching at 1731 $cm^{-1}$ from carboxylic groups, a C-OH stretching vibration at 1396 $cm^{-1}$, C-O-C epoxy groups at 1218 $cm^{-1}$, and C-O alkoxy groups at 1056 $cm^{-1}$, as well as C=C vibrations from aromatic structures at 1621 $cm^{-1}$. The G spectrum showed the characteristic bond vibrations at 1631 $cm^{-1}$ from amide I in relation to the stretching of the C=O bond from an amide group, the amide II signal at 1519 $cm^{-1}$ is from the bending of N-H, the amide III at 1237 $cm^{-1}$ represents the stretching of the C-N bond of the amide, and the stretching of the N-H bond at 3261 $cm^{-1}$ is of the primary amine.[12,17]

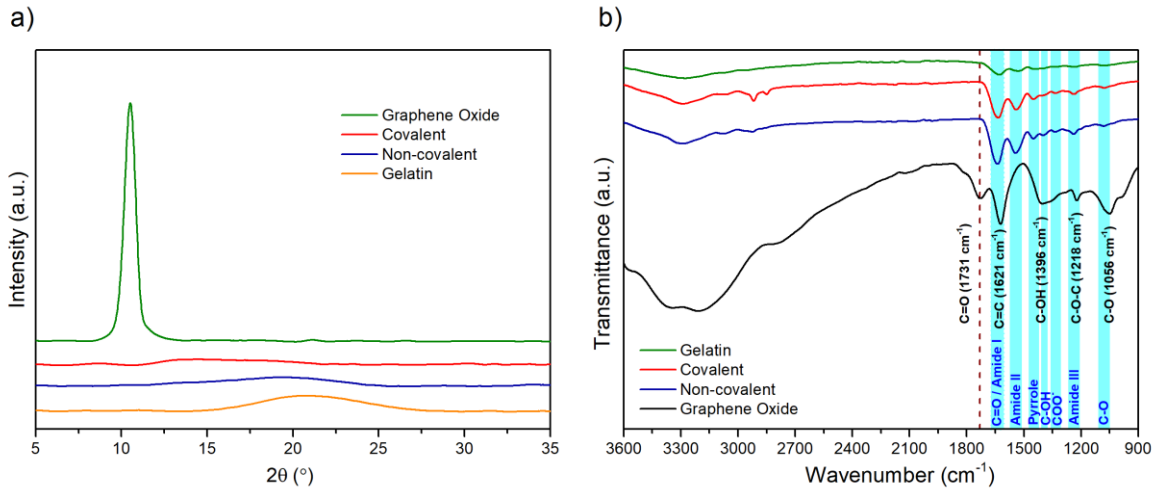


Figure 5.1: Chemical characterization of G, GO, and GO-G aerogels with XRD patterns (a) and FT-IR spectra (b).

GO-G aerogel spectra presented the same bands mentioned before for G and GO, but with a complete reduction of the C=O peak at 1731 $cm^{-1}$ for covalent aerogels, which is caused by the formation of amide bonds. Furthermore, under the same synthesis conditions and comparing covalent and noncovalent GO-G aerogels, the deconvolution of the spectra in the 1000-1800 $cm^{-1}$ range showed differences in the peaks related to the epoxy and hydroxyl groups; the above groups are associated with the ring-opening reaction in the GO reduction to form covalent bonds with the amines of G chains. In the noncovalent spectrum, the C=O peak at 1731 $cm^{-1}$ tends

to disappear as a consequence of forming a physical complex, which produces a shift in the C=O peak close to the wavenumber related to amide I at 1631 $cm^{-1}$.

Thus, in general, GO-G aerogels showed the same chemical behavior with differences in their epoxy groups due to the ring-opening reduction and interactions between the carboxylic groups at the edge of the GO sheets with the amine groups of the G chains. These interactions have been previously reported for covalent[12,17] and noncovalent[15] GO-G hydrogels, and other polymers forming physical complexes.[19,20]

Nonetheless, as the GO-G aerogels showed similar FT-IR spectra for covalent and noncovalent chemical interactions, due to the complexity of the structures, the analysis was complemented with Raman and XPS spectra. Moreover, these results could be expressed in different properties whose behavior was mediated by the chemical environment.

Raman spectra of GO and GO-G aerogels are shown in **Figure 5.2a**. In the figure, the characteristic D band at 1340 $cm^{-1}$ was induced by structural disorder and defects on the GO sheets, and the G band at 1594 $cm^{-1}$ was related to the in-phase vibration of the graphitic lattice. The comparable intensity between these bands is the result of the high content of defects present in the crystal, which can be associated with the oxygenated groups [12,21].

The $I_D/I_G$ ratio was evaluated, which is a comparative index of $sp^2$ over $sp^3$ hybridization. Covalent aerogels showed an $I_D/I_G$ ratio of 2.48, a higher value than the noncovalent aerogels, which had an $I_D/I_G$ ratio of 2.25. The high value in the covalent interaction suggested the presence of unrepaired defects on the GO sheets after the removal of large amounts of oxygenated groups by their reduction through amide formation [22].

The G band of the noncovalent aerogels showed the same Raman shift as the GO sample. Meanwhile, the covalent spectra showed a blueshift to 1598 $cm^{-1}$, which was a response to the graphitic autocorrection of the $sp^2$ domain through the formation of covalent bonds.[23,24]

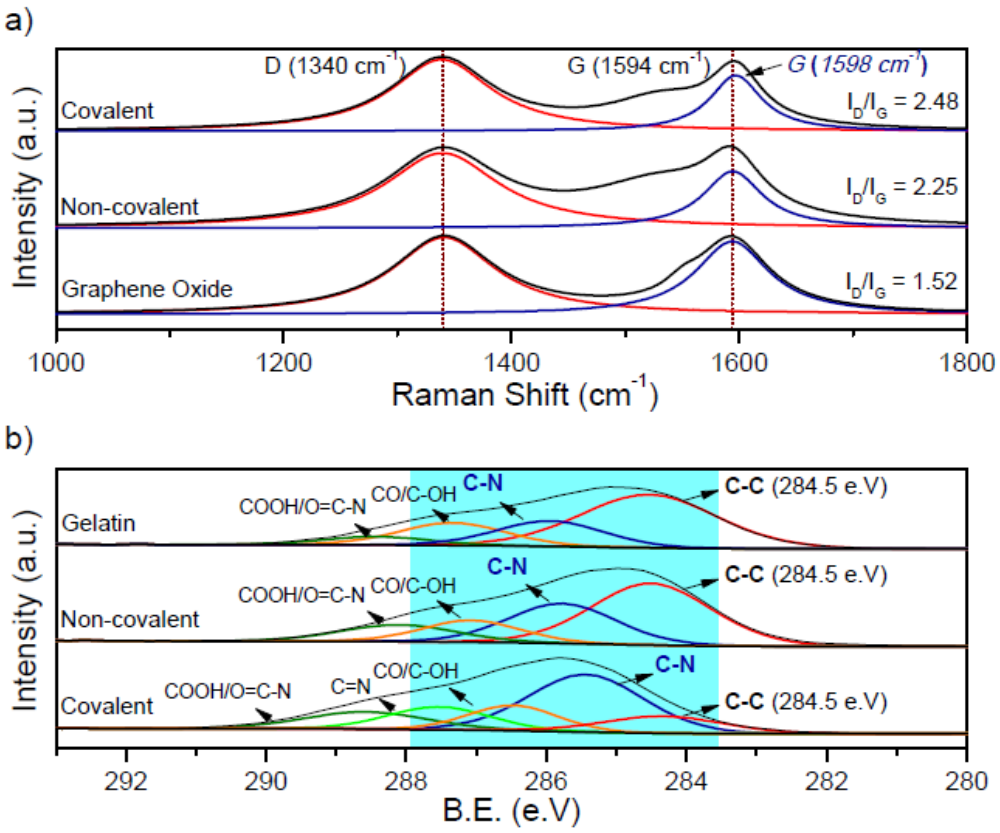


Figure 5.2: Analysis of the chemical interaction of GO-G aerogels with Raman spectroscopy (a) and XPS spectra of C 1s (b).

The elemental oxidation states present on the samples were evaluated by XPS, and the carbon spectra were deconvoluted, as shown in **Figure 5.2b**. The peaks related to the carbon of G appeared at 284.5 mV for $sp^2/sp^3$ hybrids as C-C/C=C, the C-N bond of the amide groups was at 285.9 mV, C=O was at 287.3 mV and COOH was at 288.4 mV [25,26]. The noncovalent aerogels showed similar oxidation states of their carbons to those previously discussed for G, with small contributions of hydroxyl and epoxy groups, which indicated physical interactions among their compounds without significant changes in their chemical structure. Covalent spectra of the aerogels showed an increase in the peak related to C-N bonds, with a shift to 285.4 mV and a new peak at 287.5 mV. These differences were the result of amide formation between the carboxylic groups and amines of the G chain and the formation of C=N bonds through a secondary reaction catalyzed by GO [27,28]. Therefore, the XPS and Raman results confirmed the different nature of the covalent and noncovalent aerogels.

All the samples evaluated by a TGA analysis (**Figure 5.3a**) showed a mass loss before 100°C, which corresponded to the evaporation of moisture present on the material. The covalent and noncovalent GO and GO-G aerogels start to lose mass at approximately 140°C, and G starts at 242°C. At 600°C, GO-G aerogels lose approximately 61% of their mass, whereas G aerogels lose approximately 66% and GO aerogels lose approximately 32% of their mass.

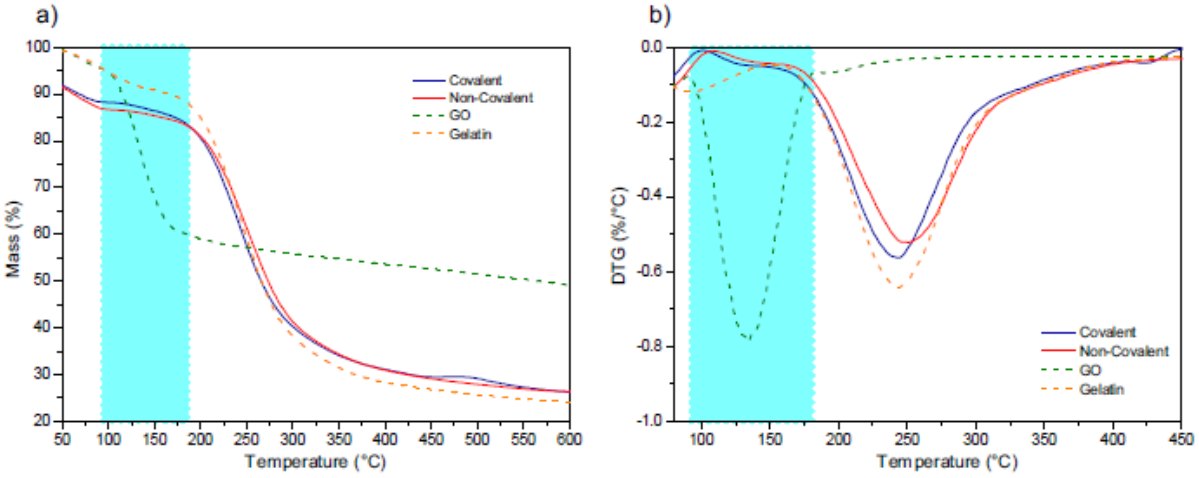


Figure 5.3: Thermal degradation of the G, GO, and GO-G aerogels with thermogravimetric analyses (a) and derived thermogravimetric patterns (b).

According to these results, a DTG analysis (**Figure 5.3b**) suggests that the decomposition of GO-G aerogels occurred in two main steps. Initially, the GO-G aerogels suffered a mass loss at 140°C for the decomposition of the oxygenated groups and then exhibited a mass loss related to the pyrolysis of the G chains.

The thermal degradation was almost the same for both synthesis pathways with a difference being demonstrated in the G decomposition temperature; the above suggested that noncovalent aerogels had more thermal resistance than covalent aerogels. This fact could be caused by the thermal denaturalization of the G chains, which is a product of the high temperature during the covalent synthesis treatment.

The above results agreed with the thermal stability previously reported for similar GO-G materials, where authors reported mass losses of less than 70% of their total mass [29,30], while a total mass loss value close to 61% was obtained with our GO-G aerogels in the same steps.

### 5.4.2 Aerogel surface charge

The response contour of the surface charge (ʒ-potential) for the aerogels is shown in **Figure 5.4**. When the surface charge was compared among the different syntheses, for a given pH value and GO:G ratio, the ʒ-potential values were similar (p-value > 0.05), which suggested that the nature of the GO-G interaction had no influence on the GO-G surface charge.

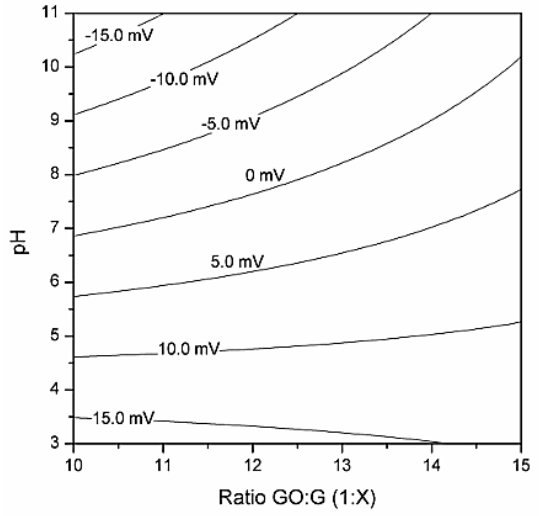


Figure 5.4: ʒ-potential response contours of the GO-G aerogels (σ = 3.07 mV, $R^2$ = 0.9611) under different synthesis conditions (GO:G ratio and pH of GO suspension).

Since the ʒ-potential could be mediated by the interaction of the functional groups present on the material surface and their activation based on pH changes, this result could be an expression of the similar chemical environment between covalent and noncovalent aerogels observed in the analysis of the infrared spectra discussed previously.

Regarding the synthesis conditions, the surface charge was dependent on the pH of the GO suspension and the GO:G ratio, with the pH effect (F-ratio = 426.8) being more influential than the effect of the GO:G ratio (F-ratio = 32.02). Therefore, when the pH of the GO suspension goes from acidic to alkali conditions, aerogels had ʒ-potential values between 13.47±1.42 mV and -2.30±1.22 mV at the highest ratio. For the lowest ratio, the values were between 15.63±0.55 mV and -20.53±1.07 mV.

GO in a water suspension had a negative ʒ-potential at pH values above its isoelectric point (IP ~ 2.0) [31–33]. When the GO suspension was near pH 3, the GO-G aerogel charge was similar to that of pure G under acidic conditions, as reported previously for G nanoparticles.[34] At high pH, the GO-G samples were more negative due to the chemical activation of the oxygenated groups present on GO. Thus, chemical activation of the oxygenated groups of GO through pH modifications in alkali conditions enhanced the influence of GO on the aerogel surface charge, which was caused by an increase in the negativity of the suspension.

### 5.4.3 Morphological analysis

Under the same synthesis conditions, SEM images of the aerogels (**Figure 5.5**) showed a highly heterogeneous microporous structure, with larger pore sizes in the covalent aerogels (53.26±25.53 µm, Figure 5.5a) than in the noncovalent aerogels (25.31±10.38 µm, Figure 5.5b); additionally, the covalent aerogels have a finer network than the noncovalent aerogels. These differences could be caused by the damage induced on the G chains by the long exposure to thermal stress during synthesis. Heterogeneous structures are expected for protein-based materials[11,35,36], with a microporous nature that has been reported for similar GO-G materials with comparable pore size scales. For example, G aerogels with reduced GO presented pore sizes of approximately several and tens of micrometers [12], GO-G covalent hydrogels reported sizes between 2.3±1.1 µm and 7.7±5.4 µm[17], and GO-G hydrogels with polyacrylic acid reported sizes between 70 µm and 300 µm [37].

The GO-G aerogels had apparent porosities with an average value of 98.04±1.31% (homogeneous groups in Table 1), with no significant differences associated with the synthesis methods (p-value > 0.05). However, the lowest GO:G ratios (samples with high GO content) produced lower porosities, 93.2±3.5% for covalent aerogels at pH 3 and 94.1±2.5% for noncovalent aerogels at pH 11. These results indicated that low GO:G ratios could retain a high porosity in the aerogel, which was caused by the effect of the pH in the GO suspension; the above pH conditions promoted the

interaction of each aerogel based on its chemical nature (covalent or noncovalent). Otherwise, the increase in GO content could produce a decrease in aerogel porosity.

Table 5.1: Aerogel porosities for both synthesis methods under different conditions

| Sample | ratio GO:G | pH | Porosity (%) |
|---|---|---|---|
| Non-Covalent | 1:10 | 3 | 96.7 ± 1.3 $^{\alpha\,\beta}$ |
| | | 11 | 94.1 ± 2.5 $^{\alpha}$ |
| | 2:25 | 7 | 97.0 ± 3.0 $^{\beta}$ |
| | 1:15 | 3 | 97.5 ± 0.9 $^{\alpha\,\beta}$ |
| | | 11 | 97.4 ± 1.7 $^{\alpha\,\beta}$ |
| Covalent | 1:10 | 3 | 93.2 ± 3.5 |
| | | 11 | 96.2 ± 3.2 $^{\gamma}$ |
| | 2:25 | 7 | 97.9 ± 1.4 $^{\gamma\,\delta}$ |
| | 1:15 | 3 | 97.0 ± 3.0 $^{\gamma\,\delta}$ |
| | | 11 | 99.1 ± 0.6 $^{\delta}$ |

α, β, γ, δ homogeneous groups

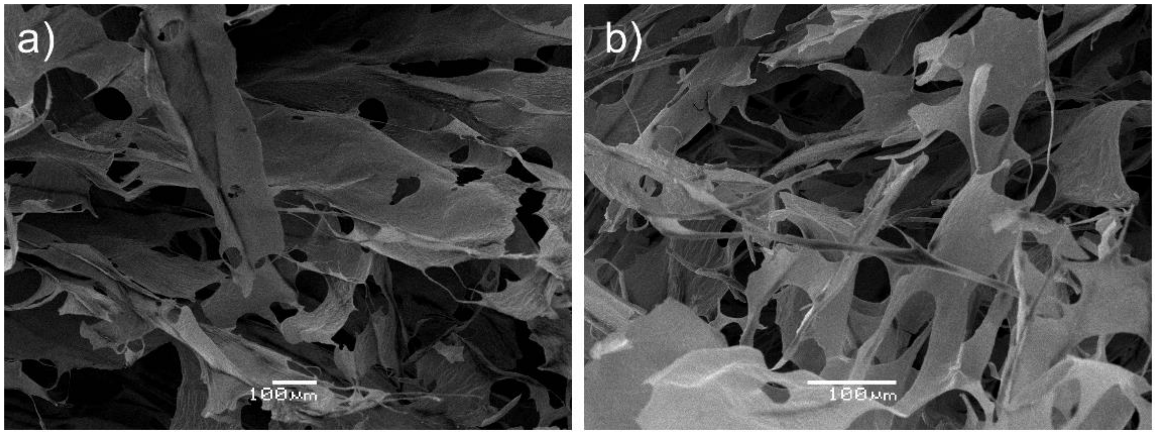


Figure 5.5: SEM images of the covalent (a) and noncovalent (b) GO-G aerogels under the same synthesis conditions.

Thus, high porosities in low GO:G ratios were connected with the capacity of the GO to interact with the G chains, which depended on their chemical activation. As mentioned, the IP of the GO suspension was under pH 2.0. Hence, when the GO suspension was in alkali conditions, the oxygenated groups of the GO were activated and predisposed to form covalent bonds. In contrast, acidic conditions promoted H-bonds to form noncovalent interactions.

The obtaining of high porosity, and its decrease with a decreasing GO:G ratio, had been previously reported to be similar to hydrogel materials based on reduced GO and methacryloyl G or lyophilized G-GO, which were activated with KOH.[38,39]

### 5.4.4 Stiffness and absorption capacity

The elastic modulus (E) is an indicator of the material stiffness, and the values for both syntheses are shown in **Figure 5.6**. In covalent aerogels (**Figure 5.6a**), when the GO:G ratio decreased and the pH of the GO suspension increased, the aerogels were stiffer, with E values between 0.82±0.02 kPa and 4.44±0.18 kPa. In contrast, the noncovalent aerogels (**Figure 5.6b**) were stiffer with a high GO:G ratio and low pH in the GO suspension, with E values between 0.64±0.01 kPa and 3.85±0.15 kPa.

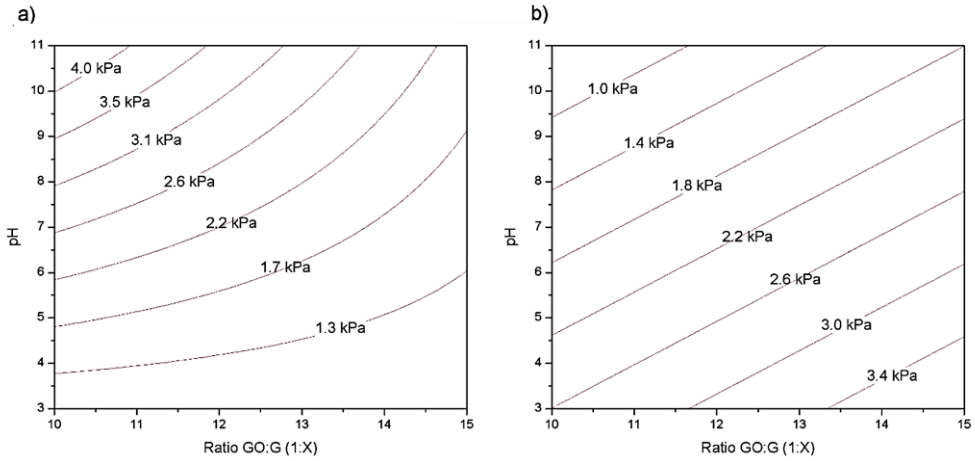


Figure 5.6: Elastic modulus contour plots for covalent (a) and noncovalent (b) aerogels, with $R^2$ = 0.9904 and $R^2$ = 0.9376, respectively.

These results were the product of the chemical activation of the oxygenated groups in the GO sheets under high pH conditions, which promoted the covalent interactions as previously discussed. Additionally, GO could act as a cross-linking agent contributing to increasing the stiffness. Moreover, the activation of GO led to a decrease in the number of free chemical groups that could form physical interactions, such as H-bonds, which suggested that GO sheets could hinder network formation in noncovalent aerogels at low GO concentration ranges and high pH values in the GO suspension.

The E values found were comparable in orders of magnitude with other similar materials based on GO (or their reduced form) and gelatin methacryloyl or peroxide-reactive gelatin, which confirmed the stiffer characteristics of materials with a decreasing GO:G ratio [39–41].

Focusing on potential applications, PBS was employed to measure the absorption capacity of aerogels for their similarity with mammalian extracellular fluids. The PBS absorption at equilibrium (**Figure 5.7**) for covalent aerogels (24.9±1.7 gPBS/gaerogel to 36.2±3.1 gPBS/gaerogel) was lower than that for noncovalent aerogels (35.5±2.4 gPBS/gaerogel to 49.6±3.8 gPBS/gaerogel).

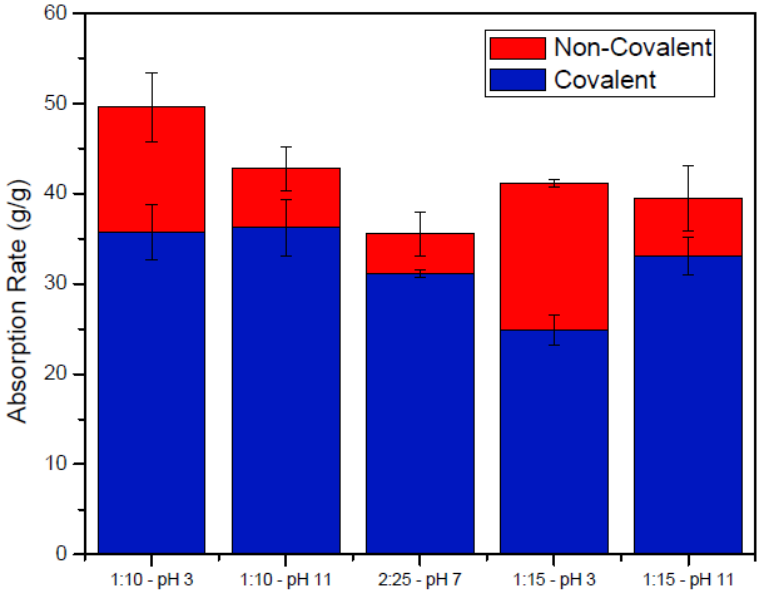


Figure 5.7: PBS absorption rates at equilibrium under different synthesis conditions.

Covalent aerogels presented fewer oxygenated groups; the above was caused by their reduction during amide formation, which generated an attenuation of the structural hydrophilicity and inhibited the absorption capacity due to a GO cross-linking effect. In contrast, the noncovalent aerogels formed more H-bonds, which were promoted in the synthesis method and helped to increase the hydrophilicity and structural stability when the material was in an aqueous media.

The decrease of hydrophilicity in the covalent aerogels had been reported for other reduced GO materials, such as glutaraldehyde grafted GO-G hydrogels and reduced GO-G composite films, where the GO content and their increase had a negative

effect on this property.[29,42] Likewise, the hydrophilicity, which was guided by H-bond interactions, had been widely reported for several materials, including G; in the above scenario, a decrease in the pH might lead to an increase in the interaction of the hydrophilic segments of the chain, thus making the hydration network more extensive and stronger.[34,43]

In comparison with other aerogels developed for biomedical applications (**Table 5.2**), GO-G aerogels had better performance as an absorbent material than aerogels based on Xanthan, Guar Gum or β-glucans [44,45] showing shorter times to reach the maximum absorption of PBS (7.4) and more than 3 times those equilibrium rates. The same result was obtained when were compared with other aerogels based in alginate [46,47] or chitosan [48] tested with different solvents such as Tris-HCl buffer or water, making GO-G aerogels a potential absorbent material for biomedical applications.

Table 5.2: Compared swelling rates of aerogels for biomedical applications

| Aerogel material | Solvent | Time | Absorption rates at maximum/equilibrium ($g/g_{aerogel}$) | Ref. |
|---|---|---|---|---|
| GO-G | PBS | < 1 h | 49.6 ± 3.8 | This Work |
| Xanthan Gum | PBS | 3 h | ~ 14.9 | 44 |
| | | 2 d | ~ 58.4 | |
| Guar Gum | PBS | 3 h | ~ 7.2 | 44 |
| | | 2 d | ~ 26.3 | |
| β-glucans | PBS | > 1 d | ~ 6.2 - 13.9 | 45 |
| Alginate-Starch | Tris-HCl Buffer | > 3 d | 14.54 | 46 |
| Alginate-Lignin | Tris-HCl Buffer | > 3 d | 16.13 | 47 |
| Chitosan-BMIMAc | Water | < 1 h | 6.43 | 48 |
| Chitosan-EMIMAc | Water | < 1 h | 3.79 | 48 |

~: Estimated values by graphical interpolation.

## 5.5 Conclusions

Chemical characterization of the synthesized materials allowed us to confirm the covalent and noncovalent nature of the aerogels, where the main interactions were amide bond formation and physical complex generation, respectively.

Synthesis conditions that promoted GO-G interactions for covalent aerogels were a low GO:G ratio at alkali conditions in the GO suspension. In contrast, noncovalent aerogels promoted GO-G interactions in high GO:G ratios under acidic conditions in the GO suspension. These conditions improved the morphology of the aerogels, which allowed them to retain a high porosity and made them stiffer. Comparatively, GO incorporation into the matrix was only favorable for covalent aerogels, as long as their conditions promoted a cross-linking process. Nevertheless, the cross-linking improvement had a contrary effect on PBS absorption, so covalent aerogels showed low absorption rates, especially at low pH values in the GO suspension. Thus, noncovalent aerogels were more stable in aqueous media, having a high PBS absorption capacity.

Since the surface charge presented the same behavior for both covalent and noncovalent aerogels and considering the trend of PBS absorption capacity, noncovalent aerogels with a low GO:G ratio could be more practical to their application in different fields, as biomedicine or water-treatment, where the promotion of surface interactions and high absorption capability is desired.

## 5.6 References


[1] N. Hsing, U. Schubert, Aerogels-Airy Materials: Chemistry, Structure, and Properties, Angew. Chem. Int. Ed. (1998) 24.

[2] S.K. H. Gulrez, S. Al-Assaf, G. O, Hydrogels: Methods of Preparation, Characterisation and Applications, in: A. Carpi (Ed.), Progress in Molecular and Environmental Bioengineering - From Analysis and Modeling to Technology Applications, InTech, 2011. https://doi.org/10.5772/24553.

[3] S. Plazzotta, S. Calligaris, L. Manzocco, Innovative bioaerogel-like materials from fresh-cut salad waste via supercritical-CO 2 -drying, Innovative Food Science & Emerging Technologies. 47 (2018) 485–492. https://doi.org/10.1016/j.ifset.2018.04.022.

[4] J. Siepmann, R.A. Siegel, M.J. Rathbone, Controlled Release Society, eds., Fundamentals and applications of controlled release drug delivery, Springer : Controlled Release Society, New York, 2012.

[5] H. Nassira, A. Sánchez-Ferrer, J. Adamcik, S. Handschin, H. Mahdavi, N. Taheri Qazvini, R. Mezzenga, Gelatin-Graphene Nanocomposites with Ultralow Electrical Percolation Threshold, Adv. Mater. 28 (2016) 6914–6920. https://doi.org/10.1002/adma.201601115.

[6] S. Gorgieva, V. Kokol, Collagen- vs. Gelatine-Based Biomaterials and Their Biocompatibility: Review and Perspectives, in: R. Pignatello (Ed.), Biomaterials Applications for Nanomedicine, InTech, 2011. https://doi.org/10.5772/24118.

[7] B. Mohanty, H.B. Bohidar, Microscopic structure of gelatin coacervates, International Journal of Biological Macromolecules. 36 (2005) 39–46. https://doi.org/10.1016/j.ijbiomac.2005.03.012.

[8] L. Baldino, S. Concilio, S. Cardea, E. Reverchon, Interpenetration of Natural Polymer Aerogels by Supercritical Drying, Polymers. 8 (2016) 106. https://doi.org/10.3390/polym8040106.

[9] G. Shim, M.-G. Kim, J.Y. Park, Y.-K. Oh, Graphene-based nanosheets for delivery of chemotherapeutics and biological drugs, Advanced Drug Delivery Reviews. 105 (2016) 205–227. https://doi.org/10.1016/j.addr.2016.04.004.

[10] J. Lin, X. Chen, P. Huang, Graphene-based nanomaterials for bioimaging, Advanced Drug Delivery Reviews. 105 (2016) 242–254. https://doi.org/10.1016/j.addr.2016.05.013.

[11] S.-H. Lee, M. Kotal, J.-H. Oh, P. Sennu, S.-H. Park, Y.-S. Lee, I.-K. Oh, Nanohole-structured, iron oxide-decorated and gelatin-functionalized graphene for high rate and high capacity Li-Ion anode, Carbon. 119 (2017) 355–364. https://doi.org/10.1016/j.carbon.2017.04.031.

[12] C. Liu, H. Liu, A. Xu, K. Tang, Y. Huang, C. Lu, In situ reduced and assembled three-dimensional graphene aerogel for efficient dye removal, Journal of Alloys and Compounds. 714 (2017) 522–529. https://doi.org/10.1016/j.jallcom.2017.04.245.

[13] J. An, Y. Gou, C. Yang, F. Hu, C. Wang, Synthesis of a biocompatible gelatin functionalized graphene nanosheets and its application for drug delivery, Materials Science and Engineering: C. 33 (2013) 2827–2837. https://doi.org/10.1016/j.msec.2013.03.008.

[14] G. Chen, C. Qiao, Y. Wang, J. Yao, Synthesis of Biocompatible Gelatin-functionalised Graphene Nanosheets For Drug Delivery Applications, Australian Journal of Chemistry. 67 (2014) 1532. https://doi.org/10.1071/CH13678.

[15] Y. Piao, B. Chen, Self-assembled graphene oxide-gelatin nanocomposite hydrogels: Characterization, formation mechanisms, and pH-sensitive drug release behavior, Journal of Polymer Science Part B: Polymer Physics. 53 (2015) 356–367. https://doi.org/10.1002/polb.23636.

[16] H. Liu, J. Cheng, F. Chen, D. Bai, C. Shao, J. Wang, P. Xi, Z. Zeng, Gelatin functionalized graphene oxide for mineralization of hydroxyapatite: biomimetic and in vitro evaluation, Nanoscale. 6 (2014) 5315. https://doi.org/10.1039/c4nr00355a.

[17] Y. Piao, B. Chen, One-pot synthesis and characterization of reduced graphene oxide–gelatin nanocomposite hydrogels, RSC Advances. 6 (2016) 6171–6181. https://doi.org/10.1039/C5RA20674J.

[18] D.C. Marcano, D.V. Kosynkin, J.M. Berlin, A. Sinitskii, Z. Sun, A. Slesarev, L.B. Alemany, W. Lu, J.M. Tour, Improved Synthesis of Graphene Oxide, ACS Nano. 4 (2010) 4806–4814. https://doi.org/10.1021/nn1006368.

[19] B. Boeckx, G. Maes, Experimental and Theoretical Observation of Different Intramolecular H-bonds in Lysine Conformations, J. Phys. Chem. B. 116 (2012) 12441–12449. https://doi.org/10.1021/jp306916e.

[20] E. Garand, M.Z. Kamrath, P.A. Jordan, A.B. Wolk, C.M. Leavitt, A.B. McCoy, S.J. Miller, M.A. Johnson, Determination of Noncovalent Docking by Infrared Spectroscopy of Cold Gas-Phase Complexes, Science. 335 (2012) 694–698. https://doi.org/10.1126/science.1214948.

[21] N.A. Kumar, H.-J. Choi, Y.R. Shin, D.W. Chang, L. Dai, J.-B. Baek, Polyaniline-Grafted Reduced Graphene Oxide for Efficient Electrochemical Supercapacitors, ACS Nano. 6 (2012) 1715–1723. https://doi.org/10.1021/nn204688c.

[22] S. Bose, T. Kuila, Md.E. Uddin, N.H. Kim, A.K.T. Lau, J.H. Lee, In-situ synthesis and characterization of electrically conductive polypyrrole/graphene nanocomposites, Polymer. 51 (2010) 5921–5928. https://doi.org/10.1016/j.polymer.2010.10.014.

[23] K.N. Kudin, B. Ozbas, H.C. Schniepp, R.K. Prud'homme, I.A. Aksay, R. Car, Raman Spectra of Graphite Oxide and Functionalized Graphene Sheets, Nano Letters. 8 (2008) 36–41. https://doi.org/10.1021/nl071822y.

[24] V.K. Rana, M.-C. Choi, J.-Y. Kong, G.Y. Kim, M.J. Kim, S.-H. Kim, S. Mishra, R.P. Singh, C.-S. Ha, Synthesis and Drug-Delivery Behavior of Chitosan-Functionalized Graphene Oxide Hybrid Nanosheets, Macromolecular Materials and Engineering. 296 (2011) 131–140. https://doi.org/10.1002/mame.201000307.

[25] S. Makharza, O. Vittorio, G. Cirillo, S. Oswald, E. Hinde, M. Kavallaris, B. Büchner, M. Mertig, S. Hampel, Graphene Oxide - Gelatin Nanohybrids as Functional Tools for Enhanced Carboplatin Activity in Neuroblastoma Cells, Pharmaceutical Research. 32 (2015) 2132–2143. https://doi.org/10.1007/s11095-014-1604-z.

[26] C. Wan, M. Frydrych, B. Chen, Strong and bioactive gelatin–graphene oxide nanocomposites, Soft Matter. 7 (2011) 6159. https://doi.org/10.1039/c1sm05321c.

[27] C. Su, M. Acik, K. Takai, J. Lu, S. Hao, Y. Zheng, P. Wu, Q. Bao, T. Enoki, Y.J. Chabal, K. Ping Loh, Probing the catalytic activity of porous graphene oxide and the origin of this behaviour, Nat Commun. 3 (2012) 1298. https://doi.org/10.1038/ncomms2315.

[28] B. Chen, L. Wang, S. Gao, Recent Advances in Aerobic Oxidation of Alcohols and Amines to Imines, ACS Catal. 5 (2015) 5851–5876. https://doi.org/10.1021/acscatal.5b01479.

[29] W. Wang, Z. Wang, Y. Liu, N. Li, W. Wang, J. Gao, Preparation of reduced graphene oxide/gelatin composite films with reinforced mechanical strength, Materials Research Bulletin. 47 (2012) 2245–2251. https://doi.org/10.1016/j.materresbull.2012.05.060.

[30] E.M. Zadeh, A. Yu, L. Fu, M. Dehghan, I. Sbarski, I. Harding, Physical and thermal characterization of graphene oxide modified gelatin-based thin films, Polymer Composites. 35 (2014) 2043–2049. https://doi.org/10.1002/pc.22865.

[31] K. Min, T.H. Han, J. Kim, J. Jung, C. Jung, S.M. Hong, C.M. Koo, A facile route to fabricate stable reduced graphene oxide dispersions in various media and their transparent conductive thin films, Journal of Colloid and Interface Science. 383 (2012) 36–42. https://doi.org/10.1016/j.jcis.2012.06.021.

[32] Z. Lei, N. Christov, X.S. Zhao, Intercalation of mesoporous carbon spheres between reduced graphene oxide sheets for preparing high-rate supercapacitor

electrodes, Energy & Environmental Science. 4 (2011) 1866. https://doi.org/10.1039/c1ee01094h.

[33] K. Krishnamoorthy, M. Veerapandian, K. Yun, S.-J. Kim, The chemical and structural analysis of graphene oxide with different degrees of oxidation, Carbon. 53 (2013) 38–49. https://doi.org/10.1016/j.carbon.2012.10.013.

[34] S.M. Ahsan, C.M. Rao, The role of surface charge in the desolvation process of gelatin: implications in nanoparticle synthesis and modulation of drug release, International Journal of Nanomedicine. Volume 12 (2017) 795–808. https://doi.org/10.2147/IJN.S124938.

[35] C. Bastioli, Rapra Technology Limited, eds., Handbook of biodegradable polymers, Rapra Technology, Shrewsbury, 2005.

[36] M. Ramos, A. Valdés, A. Beltrán, M. Garrigós, Gelatin-Based Films and Coatings for Food Packaging Applications, Coatings. 6 (2016) 41. https://doi.org/10.3390/coatings6040041.

[37] S. Mohammadi, H. Keshvari, M. Eskandari, S. Faghihi, Graphene oxide–enriched double network hydrogel with tunable physico-mechanical properties and performance, Reactive and Functional Polymers. 106 (2016) 120–131. https://doi.org/10.1016/j.reactfunctpolym.2016.07.015.

[38] H. Fan, W. Shen, Gelatin-Based Microporous Carbon Nanosheets as High Performance Supercapacitor Electrodes, ACS Sustainable Chem. Eng. 4 (2016) 1328–1337. https://doi.org/10.1021/acssuschemeng.5b01354.

[39] S.R. Shin, C. Zihlmann, M. Akbari, P. Assawes, L. Cheung, K. Zhang, V. Manoharan, Y.S. Zhang, M. Yüksekkaya, K. Wan, M. Nikkhah, M.R. Dokmeci, X.S. Tang, A. Khademhosseini, Reduced Graphene Oxide-GelMA Hybrid Hydrogels as Scaffolds for Cardiac Tissue Engineering, Small. 12 (2016) 3677–3689. https://doi.org/10.1002/smll.201600178.

[40] C. Cha, S.R. Shin, X. Gao, N. Annabi, M.R. Dokmeci, X.S. Tang, A. Khademhosseini, Controlling Mechanical Properties of Cell-Laden Hydrogels by

Covalent Incorporation of Graphene Oxide, Small. 10 (2014) 514–523. https://doi.org/10.1002/smll.201302182.

[41] J.H. Lee, Y. Lee, Y.C. Shin, M.J. Kim, J.H. Park, S.W. Hong, B. Kim, J.-W. Oh, K.D. Park, D.-W. Han, *In situ* forming gelatin/graphene oxide hydrogels for facilitated C2C12 myoblast differentiation, Applied Spectroscopy Reviews. 51 (2016) 527–539. https://doi.org/10.1080/05704928.2016.1165686.

[42] Y. Piao, B. Chen, Synthesis and mechanical properties of double cross-linked gelatin-graphene oxide hydrogels, International Journal of Biological Macromolecules. 101 (2017) 791–798. https://doi.org/10.1016/j.ijbiomac.2017.03.155.

[43] E.-P. Ng, S. Mintova, Nanoporous materials with enhanced hydrophilicity and high water sorption capacity, Microporous and Mesoporous Materials. 114 (2008) 1–26. https://doi.org/10.1016/j.micromeso.2007.12.022.

[44] G. Horvat, M. Pantić, Ž. Knez, Z. Novak, Encapsulation and drug release of poorly water soluble nifedipine from bio-carriers, Journal of Non-Crystalline Solids. 481 (2018) 486–493. https://doi.org/10.1016/j.jnoncrysol.2017.11.037.

[45] M. Salgado, F. Santos, S. Rodríguez-Rojo, R.L. Reis, A.R.C. Duarte, M.J. Cocero, Development of barley and yeast β-glucan aerogels for drug delivery by supercritical fluids, Journal of CO2 Utilization. 22 (2017) 262–269. https://doi.org/10.1016/j.jcou.2017.10.006.

[46] M. Martins, A.A. Barros, S. Quraishi, P. Gurikov, S.P. Raman, I. Smirnova, A.R.C. Duarte, R.L. Reis, Preparation of macroporous alginate-based aerogels for biomedical applications, The Journal of Supercritical Fluids. 106 (2015) 152–159. https://doi.org/10.1016/j.supflu.2015.05.010.

[47] S. Quraishi, M. Martins, A.A. Barros, P. Gurikov, S.P. Raman, I. Smirnova, A.R.C. Duarte, R.L. Reis, Novel non-cytotoxic alginate–lignin hybrid aerogels as scaffolds for tissue engineering, The Journal of Supercritical Fluids. 105 (2015) 1–8. https://doi.org/10.1016/j.supflu.2014.12.026.

[48] G. Santos-López, W. Argüelles-Monal, E. Carvajal-Millan, Y. López-Franco, M. Recillas-Mota, J. Lizardi-Mendoza, Aerogels from Chitosan Solutions in Ionic Liquids, Polymers. 9 (2017) 722. https://doi.org/10.3390/polym9120722.

## 6. Proanthocyanidins load in GO-G aerogels

Once the GO-G aerogel properties were evaluated on their synthesis conditions, the proanthocyanidins (PAs) were loaded into the aerogels to evaluate their influence on the main properties to further applications. Thereby, elastic modulus, surface charge, and PBS absorption were evaluated in loaded GO-G aerogels.

### 6.1 Synthesis of loaded GO-G aerogels

The extraction of PAs from seeds of *Pais* grape was performed in an Erlenmeyer flask with 250 mL of 33% v/v of acetone in water using a New Brunswick G24 gyratory shaker (New Brunswick Scientific Co., Edison, NJ, USA) for 15 hours at room temperature and in the dark to avoid oxidation. The acetone was eliminated at reduced pressure and temperature, under 35°C, in a rotary evaporator (Bibby Sterlin Ltd, RE-100B, Stone Staffordshire, England) until 50 mL of the grape seed extract solution remained. The liposoluble compounds of the grape extracts were removed using three 50 mL washing steps with n-hexane.

For the aerogel synthesis, previous to the cross-linking process on the original methodology described in section 5.3.1, the GO-G suspension is mixed with a 50 mL solution at known PAs concentration for final 5% and 10% w/w on the loaded GO-G aerogels. Then, follow the cross-linking and the lyophilization processes as were described in the original synthesis method.

The analyses of the loaded GO-G aerogel properties were performed with the same methodology described before in the section 5.3.2 for stiffness, surface charge, and PBS absorption evaluation.

### 6.2 Functional properties of loaded GO-G aerogels

GO-G aerogels loaded with PAs at 5% and 10% w/w were evaluated on their stiffness through the measurement of their elastic modulus, these results are shown in Figure 6.1.

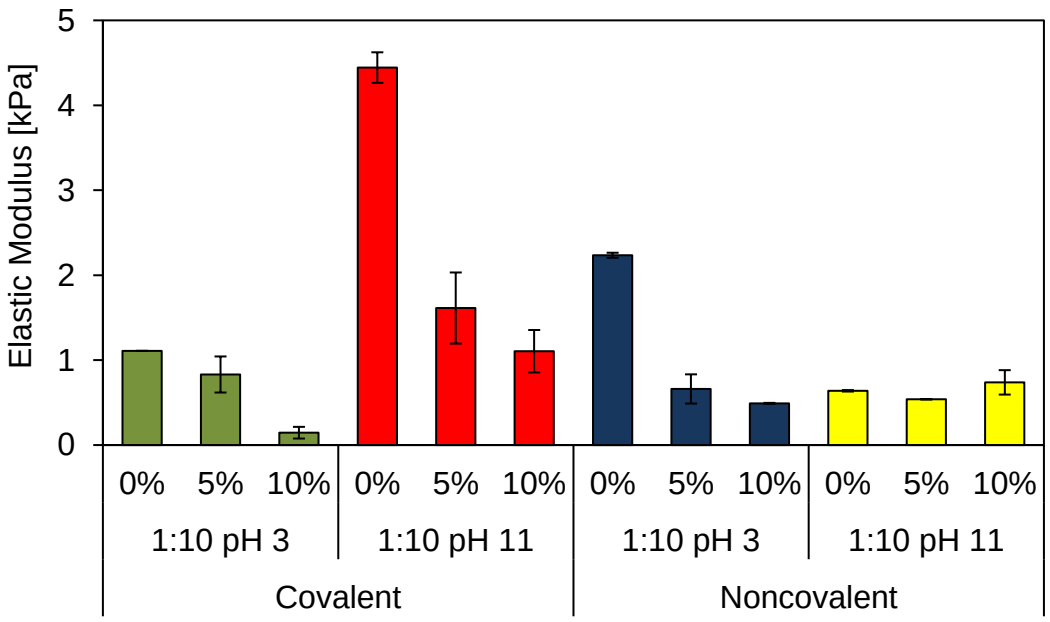


Figure 6.1: Elastic modulus of GO-G aerogels with different PA concentrations.

GO-G aerogels present a reduction in their stiffness when are loaded with PAs. The main reductions were presented at synthesis conditions that promote the main interaction, pH 11 and pH 3 for covalent and noncovalent aerogels, respectively. Covalent aerogels at alkali condition showed a reduction of the elastic modulus from 4.44±0.18 kPa to 1.10±0.25 kPa while noncovalent aerogels at acidic conditions showed a reduction from 2.23±0.03 kPa to 0.49±0.01 kPa. However, noncovalent aerogels at alkali conditions remain their stiffness with 0.74±0.14 kPa at 10% w/w of PAs loaded. This decrease in the aerogel stiffness is possibly due to the enhancement of the structural heterogenicity induced by the addition of the PAs. The same behavior was reported for PVA-Tannic acid hydrogels loaded over 6% w/w.[1] However, under this concentration, this material reports significant improvements in their mechanical properties. This enhancement on the structure on materials with low percent of PAs loaded is widely reported such as in PVA-rGO nanocomposites coated with tannic acid or gelatin-sodium alginate edible films loaded with tea polyphenols.[2,3]

Regard to the surface charge (Figure 6.2), estimated by the measurement of the ʒ-potentials, the addition of PAs does not induce significative differences in aerogels

synthesized with acidic GO suspensions with ʒ-potential values of 15.77±2.51 mV and 17.81±2.71 mV at 5% and 10% w/w of PAs loaded, respectively. In the case of alkali GO suspensions, GO-G aerogels presented a decrease in their surface charge which showed non-significative differences between 5% and 10% w/w of PAs loaded with ʒ-potentials of -15.71±2.26 mV and -16.97±2.30 mV, respectively.

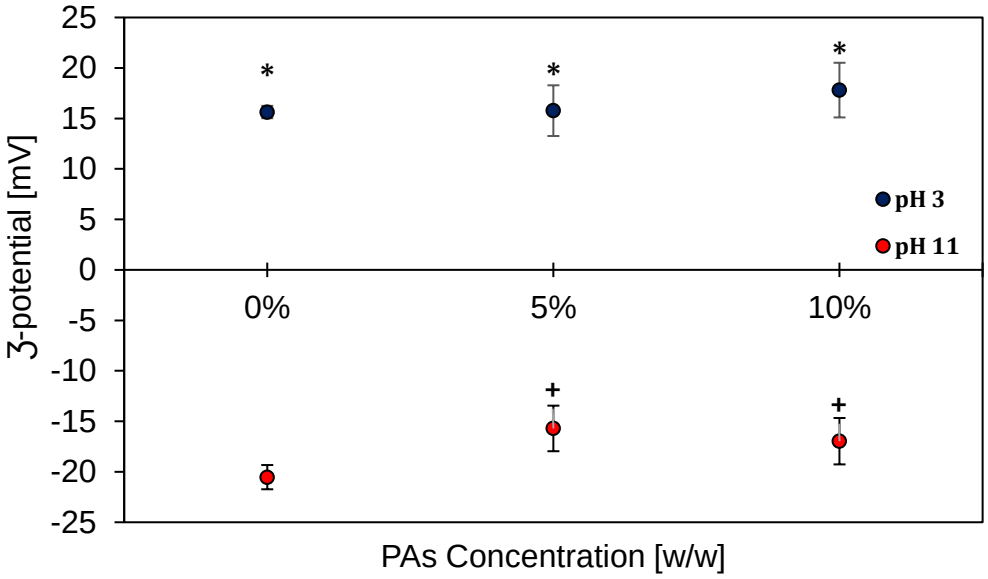


Figure 6.2: ʒ-potential of GO-G aerogels with different PAs concentrations

These results suggest that a load of PAs does not affect significantly the surface charge of the GO-G aerogels, probably due to the interaction of the gelatin chains with the molecules of the loaded tannins that could inhibit the activity of their oxygenated groups. This behavior was also reported in epigallocatechin gallate solutions impeding the access to reactive oxygenated groups depleting their interactions with diammonium salt.[4] Moreover, had been reported that Oxisol soil loaded with tea polyphenols at pH over 5.0 do not present substantial differences on its surface charge.[5]

In terms of the PBS absorption (Figure 6.3), GO-G aerogels with PAs loaded shows non-significative differences on their absorption rates between 5% and 10% w/w (p-value > 0.05). GO-G aerogels with alkali GO suspensions at synthesis showed non-significative differences in PBS absorption to both aerogels after a load of PAs with rates of 37.48±5.12 $g_{PBS}/g_{aerogel}$ and 41.99±3.24 $g_{PBS}/g_{aerogel}$ for covalent and noncovalent aerogels, respectively. Regard to acidic GO suspensions at synthesis,

covalent aerogels enhance their PBS absorption from 35.78±3.07 $g_{PBS}/g_{aerogel}$ to 43.92±4.33 $g_{PBS}/g_{aerogel}$. On the other hand, noncovalent aerogels had a decrease in their PBS absorption from 49.58±3.78 $g_{PBS}/g_{aerogel}$ to 38.11±3.63 $g_{PBS}/g_{aerogel}$.

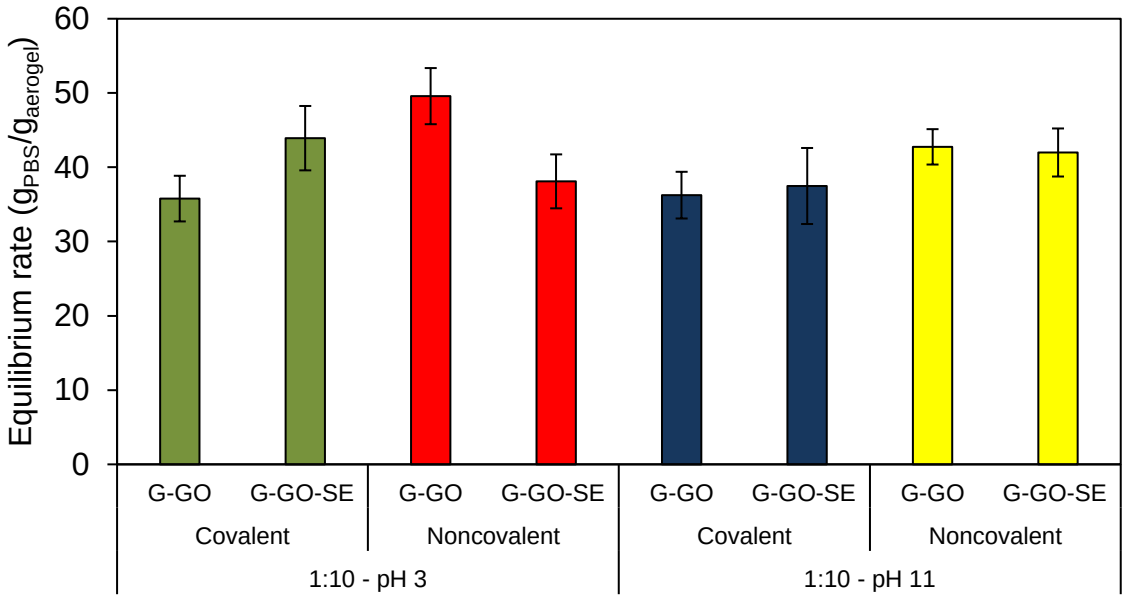


Figure 6.3: PBS absorption capacity of GO-G aerogels loaded with PAs (G-GO-SE: Graphene Oxide-Gelatin aerogels with Pais grape seed extract).

As was discussed previously, the interaction of the gelatin with the PAs loaded could inhibit the activity of their oxygenated groups that might remain the hydrophilicity and the PBS uptake of the GO-G aerogels synthesized at alkali conditions. However, at acidic conditions, PAs showed an influence on PBS absorption. Intermolecular complexation between polyphenols and some proteins involves hydrophobic interactions and hydrogen bonding.[6] These hydrophobic interactions could be promoted on covalent GO-G aerogels due to the presence of the reduced GO sheets and the hydrophobic sites in the gelatin chain which can provide free hydroxyl groups from the PAs enhancing their hydrophilicity. On the other hand, these interactions enhance the structural stability of the matrix which prevents its distention that could produce a reduction in the PBS uptake. Similar behavior was reported to collagen scaffolds where the addition of tannic acid produce a reduction of the water uptake.[7]

## 6.3 Conclusions

Regard to the previous results, GO-G aerogels do not show the expected improvements on their main conditions for hemostatic applications remaining the same surface charge and enhancing their absorption capacity only in covalent aerogels. However, this improvement is still under the absorption rates showed by noncovalent aerogels without PAs loaded. Thus, the load of proanthocyanidins was rejected for further analysis and noncovalent GO-G aerogels were evaluated for potential hemostatic applications.

## 6.4 References

(1) Chen, Y.-N.; Peng, L.; Liu, T.; Wang, Y.; Shi, S.; Wang, H. Poly(Vinyl Alcohol)–Tannic Acid Hydrogels with Excellent Mechanical Properties and Shape Memory Behaviors. *ACS Applied Materials & Interfaces* **2016**, *8* (40), 27199–27206. https://doi.org/10.1021/acsami.6b08374.

(2) Lim, M.-Y.; Shin, H.; Shin, D. M.; Lee, S.-S.; Lee, J.-C. Poly(Vinyl Alcohol) Nanocomposites Containing Reduced Graphene Oxide Coated with Tannic Acid for Humidity Sensor. *Polymer* **2016**, *84*, 89–98. https://doi.org/10.1016/j.polymer.2015.12.048.

(3) Dou, L.; Li, B.; Zhang, K.; Chu, X.; Hou, H. Physical Properties and Antioxidant Activity of Gelatin-Sodium Alginate Edible Films with Tea Polyphenols. *International Journal of Biological Macromolecules* **2018**, *118*, 1377–1383. https://doi.org/10.1016/j.ijbiomac.2018.06.121.

(4) Reitzer, F.; Allais, M.; Ball, V.; Meyer, F. Polyphenols at Interfaces. *Advances in Colloid and Interface Science* **2018**, *257*, 31–41. https://doi.org/10.1016/j.cis.2018.06.001.

(5) Wang, R.; Zhu, X.; Qian, W.; Tang, H.; Jiang, J.; Yu, Y.; Xu, R.-K. Effect of Tea Polyphenols on Copper Adsorption and Manganese Release in Two Variable-Charge Soils. *Journal of Geochemical Exploration* **2018**, *190*, 374–380. https://doi.org/10.1016/j.gexplo.2018.04.006.

(6) Poncet-Legrand, C.; Gautier, C.; Cheynier, V.; Imberty, A. Interactions between Flavan-3-Ols and Poly( L -Proline) Studied by Isothermal Titration Calorimetry: Effect of the Tannin Structure. *Journal of Agricultural and Food Chemistry* **2007**, *55* (22), 9235–9240. https://doi.org/10.1021/jf071297o.

(7) Natarajan, V.; Krithica, N.; Madhan, B.; Sehgal, P. K. Preparation and Properties of Tannic Acid Cross-Linked Collagen Scaffold and Its Application in Wound Healing. *J. Biomed. Mater. Res.* **2013**, *101B* (4), 560–567. https://doi.org/10.1002/jbm.b.32856.

## 7. In-Vitro Blood Clotting Performance for Graphene Oxide-Gelatin Aerogels as Potential Wound Dressings

*Sebastián Guajardo[a], Toribio Figueroa[a], Jessica Borges[a], Claudio Aguayo[b], Katherina Fernández[a,*]*



[a] Laboratorio de Biomateriales, Departamento de Ingeniería Química, Facultad de Ingeniería, Universidad de Concepción, P.O. Box 160-C, Concepción 4030000, Chile.

[b] Departamento de Biomquímica Clínica e Inmunología, Facultad de Química y Farmacia, Universidad de Concepción, Concepción 4030000, Chile.

The research was done in the Laboratory of Biomaterials, Department of Chemical Engineering, Faculty of Engineering, University of Concepcion, P.O. Box 160-C, Concepcion 4030000, Chile.

**Corresponding author:** Tel: +56 41 220 4534. E-mail: kfernandeze@udec.cl

## 7.1 Abstract

Graphene oxide (GO)-gelatin (G) aerogels were synthesized via the physical interactions between GO-oxygenated groups and gelatin amine groups to obtain potential hemostatic devices. The influence of the aerogel synthesis conditions -acid and basic GO suspensions- were used to evaluate their clotting performance. These materials were also characterized by FTIR, XRD, Raman, and TGA, and their properties of absorption, stiffness, porosity, surface charge and pore size were measured and compared. The clotting activity of the materials was evaluated by PT, aPTT, sP-selectin, and *in vitro* dynamic clotting assays; as well as, their cytotoxicity. GO-G aerogels presented heterogeneous microporous structures with porosities over 90% and a high PBS absorption capacity, 49.6±3.8 $g_{PBS}/g_{aerogel}$ for positive aerogels (15.63±0.5 mV) and 42.75±2.38 $g_{PBS}/g_{aerogel}$ for negative aerogels (-20.53±1.07 mV). Comparatively, positive aerogels had superior structural properties than negative aerogels, such as stiffness, porosities, and pore sizes, because they promote H-bonding. In regard to hemostatic activity, negative aerogels had higher clotting performance, reaching 95.6% clotted blood, and therefore provide a suitable structure for the coagulation process and promote clot formation without using common mechanisms. Also, negative aerogels were not cytotoxic and promoted fibroblast proliferation. Therefore, negative GO-G aerogels may be a potential hemostatic device that can be used as a wound dressing.

**Keywords:** aerogel synthesis; wound dressing; hemostatic device; graphene oxide; gelatin

## 7.2 Introduction

Stopping bleeding is a crucial step in emergency treatment, especially in cases of uncontrolled hemorrhage, one of the main causes of trauma deaths worldwide, and over half of these deaths occur before emergency care can be reached.[1] Moreover, reduced circulating volumes after severe hemorrhage leads to insufficient oxygen delivery to tissues and complications, such as hypothermia, coagulopathy, and acidosis, which are associated with increased morbidity and mortality.[2] Normally, massive blood loss cannot be controlled by the natural hemostatic mechanism. Therefore, a hemostatic intervention is necessary to minimize loss of blood, thus driving the development of more effective hemostatic dressings beyond standard gauze.[3]

The first natural response to an injury is hemostasis, which includes the formation of a platelet plug and an enzymatic cascade resulting in fibrin formation. The blood clotting mechanism involves a series of coagulation factors interacting with each other in a cascade that is activated via two pathways: intrinsic and extrinsic pathways, which are related to the presence or absence of these factors in the bloodstream.[4]

Polymeric biomaterials can facilitate the activation of coagulation, and blood-material interactions are determined by the surface properties of the materials, which promote protein adsorption and subsequent coagulatory enzyme catalysis and blood cell adhesion.[5] In comparison with synthetic polymers and inorganic materials, such as cyanoacrylates and zeolite, natural materials, including fibrin glue, gelatin, and chitosan, have been particularly appealing in the development of hemostatic materials due to their bioactive and biochemical functions in the human body.[6] In particular, gelatin has gained attention as a source for hemostatic materials due to its excellent characteristics, such as its low antigenicity, biocompatibility, biodegradability, and relatively low cost. These gelatin materials have a composition similar to the extracellular matrix, which can activate platelet aggregation and provide a structure for the adsorption of hemostatic agents.[7,8]

Another interesting material that has recently gained attention in biomedicine is graphene oxide (GO) because of its prominent properties relevant to biological applications, including its good water dispersal, pH sensitivity, unique optical and surface properties, and large surface area, among others.[9,10] Furthermore, GO can interact with G through the formation of physical bonds between the oxygenated groups of GO and polymer amine groups.[11,12] Furthermore, since GO is pH-sensitive, modifying the pH of the GO suspension during GO-G aerogel synthesis can modulate GO-G interactions and their properties through the ionization of oxygenated functional groups.[9,13,14]

Despite gelatin-based materials have been developed previously for hemostatic applications, including gelatin-chitosan sponges and mats[7,15], two-layer gelatin sponges[16], among others, the interaction of GO-G with blood has not been reported to improve clotting.

In the study of hemostatic biomaterials, some tests are commonly used to measure their clotting capacity and hemostatic activity. A dynamic *in vitro* clotting assay is commonly used to estimate the clotting behavior of whole blood by measuring hemoglobin in suspension.[6,17] Furthermore, blood coagulation can be principally activated either through intrinsic (FXII activation) or extrinsic (FVII activation) pathways and is supported by the activation of FIX through previous platelet activation. These mechanisms are measured by *in vitro* assays, such as measurement of the prothrombin time (PT), partially activated thromboplastin time (aPTT), and quantification of soluble P-selectin (sP-selectin).[7,18,19]

Therefore, the aim of this study was to evaluate the influence of the pH of the GO suspension on the GO-G aerogels physicochemical properties; as well as, its influence on the clotting performance of aerogels to assess their use as hemostatic devices.

## 7.3 Experimental section

### 7.3.1 Materials

Graphite powders (Flake, mesh 325) were purchased from Asbury Online (Asbury Carbons, NJ). Gelatin Type B was purchased from Sigma-Aldrich Company (SKU: 48723) (St. Louis, MO). All other chemicals and solvents, such as sulfuric acid ($H_2SO_4$, 98%), potassium permanganate powder ($KMnO_4$, 99.9%), sodium nitrate ($NaNO_3$), hydrochloric acid (HCl, 37%), and calcium chloride ($CaCl_2$), were purchased from Merck (Darmstadt, Germany) and were used as received without further purification. Milli-Q water was used throughout the work, and gauze sponges (sterile, aseptic, and hydrophilic, 100% cotton) were purchased from a commercial pharmacy.

### 7.3.2 GO-G aerogel synthesis

A GO precursor was synthesized from natural graphite powder using a modified Hummers' method.[20] GO-G aerogels were prepared using a noncovalent synthesis method reported by Piao & Chen with some modifications.[21] In the typical synthesis of GO-G aerogels, 1.0 g of G was dissolved in 150 mL of Milli-Q water at 60°C with constant stirring for 1 h. Additionally, a 2 mg $mL^{-1}$ GO suspension was prepared and sonicated for 30 min. Then, 50 mL of the GO suspension was dropwise added to the G solution with constant stirring. The suspension was stirred for 2 min at 37°C to promote physical interactions. The final suspension was stored at 4°C for 12 h to obtain a three-dimensional network and was frozen at -86°C (BIOBASE Ultra Freezer, China). Finally, the samples were freeze-dried (LABCONCO Freeze Dryers, USA) to obtain the final aerogels. To study the effect of surface charge on the hemostatic performance, the pH of the GO suspension during synthesis was modified to pH 3 or pH 11 to obtain positive and negative surfaces on the GO-G aerogel, respectively. These properties were confirmed by a ʒ-potential measurement.

### 7.3.3 GO-G aerogel characterization

The X-ray diffraction (XRD) patterns of GO and the powdered aerogel samples were obtained using an X-ray diffractometer (Bruker AXS, D4 Endeavor, USA) with Cu Kα radiation (λ=1.541841 Å; 2.2 kW) as the reference target, a voltage of 40 kV, and a current of 20 mA. The samples were measured from 2° to 50° (2θ) with steps of 0.02° and a measuring time of 141 seconds per step.

Fourier transform infrared (FT-IR) spectroscopy (Perkin Elmer UATR Two FT-IR Spectrometer, USA) was used to characterize GO and the powdered aerogel samples at wavenumbers ranging from 500 $cm^{-1}$ to 4000 $cm^{-1}$.

Raman spectroscopy was used to characterize and compare the GO and GO-G aerogels. The vibrational analysis was performed using a high-resolution confocal microscope (Horiba LabRam HR Evolution, Japan) with a 633 nm excitation laser line, a power of 13.3 mW, and 1.96 eV. The laser spot was centered on the sample using a lens (Olympus 100x VIS and a NUV camera B/S UV 50/50 + Lens F125 D25). The intensity of the laser remained constant to minimize any damage to the sample. The samples were measured using an object holder at room temperature (~22°C); none of the samples were characterized in solution.

Thermogravimetric analysis (TGA) was used to study the thermal stability of the samples. TGA was performed with a simultaneous thermal analysis instrument (NETZSCH STA 409 PC/PG, Germany) at a heating ratio of 10°C $min^{-1}$ from room temperature to 800°C under a nitrogen atmosphere (100 mL $min^{-1}$).

Scanning electron microscopy (SEM) was performed using a (JEOL JSM-6380LV, Japan) microscope at 10 kV. The samples were coated using a gold sputter coater, and the surfaces were observed at different resolutions for comparison. Additionally, the images were processed with Digital Gatan Microscopy 3.0 software to analyze the pore size distribution.

Aerogel porosity was measured by submerging an approximately 10 mm x 10 mm x 7 mm aerogel sample on a pycnometer that had a total volume ($V_m$) of 50 mL and was filled with absolute ethanol at a density ($\rho_e$) of approximately 0.789 g $cm^{-3}$. The

mass of the pycnometer ($W_0$), the pycnometer with the sample ($W_m$), the full ethanol pycnometer ($W_e$), and the pycnometer with the submerged sample ($W_w$) was measured, and the porosity of the sample was calculated as follows:

$$Porosity\ (\%) = 100 \times \left(1 - \frac{(W_e - W_0) - (W_w - W_m)}{\rho_e \times V_m}\right) . \quad (1)$$

Dynamic light scattering (DLS) analysis was used to determine the response contour of the surface charge (ℨ-potential) using a nanoparticle analyzer (SZ-100 Horiba Scientific, Japan), in which the samples (approximately 1 $cm^3$) were suspended in 30 mL of Milli-Q water, vigorously shaken and then sonicated for 30 min before being measured.

The elastic modulus (E) was measured with a uniaxial compression test in which a cylindrical sample (diameter ~ 4.5 cm, height ~ 1 cm) was compressed until reaching constant compressive stress of 480 kN in a universal testing system (Instron Model 4468, USA) with a loading capacity of 0.001 ~ 500 kN and constant loading speed of 1 mm $min^{-1}$. The samples were freeze-dried in a Petri dish (90 mm diameter) to obtain a regular cylindrical form. The compressive modulus was calculated in the first linear region, 10% - 40%, of the strain axis.

The absorption of phosphate-buffered saline (PBS) at equilibrium was measured by submerging a 10 mm x 10 mm x 7 mm aerogel sample in 3 mL of PBS (pH 7.4) in a Petri dish. Then, excess PBS was extracted from the dish at different times (15, 30, and 45 min). The mass of the sample before ($S_0$) and after ($S_{PBS}$) every immersion was measured, and the ratio was calculated as follows:

$$PBS\ Absorption\ Ratio = \frac{(S_{PBS} - S_0)}{S_0} . \quad (2)$$

### 7.3.4 Hemostatic assays

To evaluate the clotting performance of the aerogels, a dynamic *in vitro* coagulation assay was performed using human whole blood via previously reported methodologies.[17] A total volume of 50 µL of fresh human blood was dropped directly into the material samples, all of which had equal size (10 mm x 10 mm x 7 mm), in a 12-well plate. Each group was allowed to interact for 30, 60, 120, and 240

seconds at room temperature; this procedure was repeated three times with the same blood under the same conditions. After each repetition, 3 mL of Milli-Q water was added slowly to the sample to remove unclotted hemoglobin and quantify it from the supernatant. The hemoglobin content was quantified by measuring the absorption at 540 nm with a UV-vis double spectrophotometer (Techcomp, UV2300, China). The absorption of 50 µL fresh blood in 3 mL Milli-Q water was measured as a reference. The blood-clotting index was estimated using the following equation, where $I_s$ is the absorbance of the resulting sample and $I_r$ is the absorbance of the reference value.

$$\text{Hemoglobin Content}\ (\%) = \frac{\mathrm{I_s}}{\mathrm{I_r}} \times 100\ \% \qquad (3)$$

In regard to the clotting activity, assays to determine the prothrombin time (PT), activated partial thromboplastin time (aPTT), and soluble human P-selectin (sP-selectin) were performed to identify the pathway that these materials used to promote coagulation. First, Platelet-poor Plasma (PPP) was prepared by centrifuging fresh human blood for 15 min. Then, 2 mL of PPP was added to each material sample and incubated at 37°C for 10 min under static conditions. For measurement of the aPTT, 200 µL of the supernatant of PPP was mixed with 100 µL of aPTT reagent and incubated at 37°C for 3 min. Following the incubation, 100 µL of aqueous $CaCl_2$ (0.03 M) was added to the mixture, and the clotting time was recorded by an automated blood coagulation analyzer (Rayto RT-2204C, China). The PT measurements were carried out by adding 100 µL of PT reagent to 200 µL of the supernatant of PPP, followed by incubation and evaluation using the same instrument used for the aPTT measurement. Each experiment was repeated in triplicate.

The activation of platelets was determined by measuring the soluble P-selectin (sP-selectin) level in plasma.[22] Gauze and GO-G samples were incubated with 200 µL of Platelet-rich Plasma for 30 min at 37°C under static conditions. The supernatant was subsequently centrifuged at 2000 g for 10 min to obtain PPP. The concentration

of sP-selectin in plasma was determined using a P-selectin (soluble) (CD62) Human ELISA Kit (Thermo Fisher, USA). Each experiment was repeated in triplicate.

### 7.3.5 Cell viability

To evaluate the cell-viability of the material, an MTT assay was performed. Human Dermal Fibroblast (HDF) cells (Sigma-Aldrich, Germany) were used at a density of $10^4$ cells/mL. First, 100 µL of DMEM was added to 10 mg of the material (G, GO, and GO-G aerogel) to achieve full contact. After a 24 h incubation at 37°C, the culture media was recovered and used as a complete medium after mixing with 2% v/v fetal bovine serum (FBS), 1% v/v antibiotics (100 units/mL of penicillin and 100 units/mL of streptomycin), and 1% of amphotericin to avoid a proliferation of fungi in cells, which served as test groups. Pure DMEM culture medium was used as a positive control, and DMEM culture medium with 5 µL of hydrogen peroxide was used as a negative control. The supernatant of each sample was added to cells and incubated for 48 h at 37°C under a humidified air condition with 5% v/v of $CO_2$. Then, the supernatant was removed, and the cells were washed with PBS (pH 7.4). Next, 100 µL of fresh DMEM medium was added to the cells, and a 5 mg $mL^{-1}$ MTT solution was used to measure the HDF cell viability. The samples with MTT solution were incubated for 4 h at 37°C with $CO_2$, and then, 85 µL of the medium was removed and 50 µL of dimethyl sulfoxide (DMSO) was added for 10 min. Then, the supernatant was removed, and the formazan crystals were dissolved in 100 µL of DMSO, followed by shaking for 5 min. The absorbance at 570 nm was measured using a microplate reader (Spectra Plus, USA). The relative growth rate was estimated by the following equation.

$$Relative\ growth\ (\%) = \frac{absorbance\ of\ sample}{absorbance\ of\ positive\ control} \times 100\ \% \qquad (4)$$

### 7.3.6 Statistics

All the numeric results are expressed as the arithmetic mean with the standard deviation. Paired and ANOVA tests were performed using Statgraphics Centurion XVI software with significance defined by a p-value ≤ 0.05. Additionally, OriginPro8 software was used to plot the results.

## 7.4 Results and discussion

### 7.4.1 Chemical characterization of GO-G aerogels

To study the chemical environment of the GO-G aerogels, FTIR was performed, and their spectra are shown in Figure 7.1.

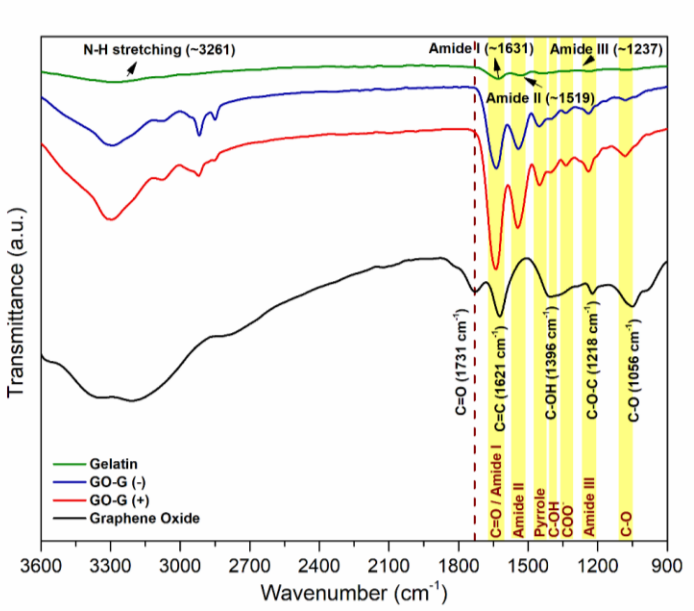


Figure 7.1: FTIR spectra of gelatin, graphene oxide, and GO-G aerogels with positive (+) and negative (-) surfaces.

The gelatin spectrum showed the characteristic stretching of the N-H bond at 3261 $cm^{-1}$ from the amine groups on the gelatin chains and vibrations related to amide groups: the amide I bond vibrations at 1631 $cm^{-1}$ was related to the stretching of the C=O bond, the amide II at 1519 $cm^{-1}$ was from the bending of N-H, and the amide III at 1237 $cm^{-1}$ was related to the stretching of the C-N bond. On the other hand, the GO spectrum showed different oxygenated functional groups: O-H stretching bonds at 3200-3400 $cm^{-1}$, C-O alkoxy groups at 1056 $cm^{-1}$, C-O-C epoxy groups at 1218 $cm^{-1}$, C-OH stretching vibration at 1396 $cm^{-1}$, C=C vibrations from aromatic structures at 1621 $cm^{-1}$, and C=O stretching at 1731 $cm^{-1}$ from carboxylic groups.[23,24]

The spectrum of the GO-G aerogel presented the same characteristic bands as the gelatin and GO spectra but with complete reduction of the C=O peak at 1731 $cm^{-1}$ as a consequence of forming a physical complex, which produced a shift in the C=O

peak close to the wavenumber related to amide I at 1631 $cm^{-1}$.[25] Furthermore, comparing the synthesis conditions of the GO-G aerogels, the deconvolution of the spectra in the 1000-1800 $cm^{-1}$ range showed the main differences in the peaks related to the amine groups associated with the effects of the pH being under the isoelectric point of gelatin. Thus, in general, the GO-G aerogels showed the same chemical behavior, with the main differences being in their amine groups due to their chemical activation. These interactions have been previously reported for different GO-G hydrogels[21,23,24] and other polymers forming similar physical complexes.[26,27]

Therefore, positive and negative GO-G aerogels had similar FT-IR spectra with slight differences in their amine peaks, with the chemical behavior expected to be the same for both types of aerogel. To complement this chemical characterization, XRD, TGA, and Raman spectroscopy were performed, and the results are shown in Figure 7.2.

The XRD patterns of the gelatin, GO, and GO-G aerogels are shown in Figure 7.2A. The GO spectrum showed a peak at 10° related to the agglomeration of its sheets. The spectrum of gelatin presented a broad peak at 21°, which is related to its crystalline structure originates from an α-helix and its triple-helical structure. The GO peak tended to disappear in the synthesized aerogels, suggesting the good dispersion of the GO sheets on the matrix due to the formation of physical complexes with the gelatin chains.[24,28]

A)

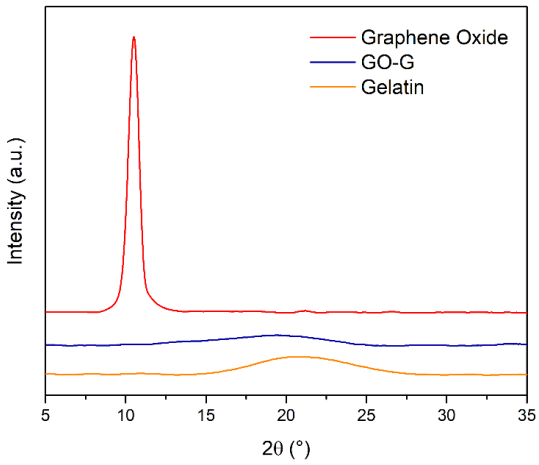

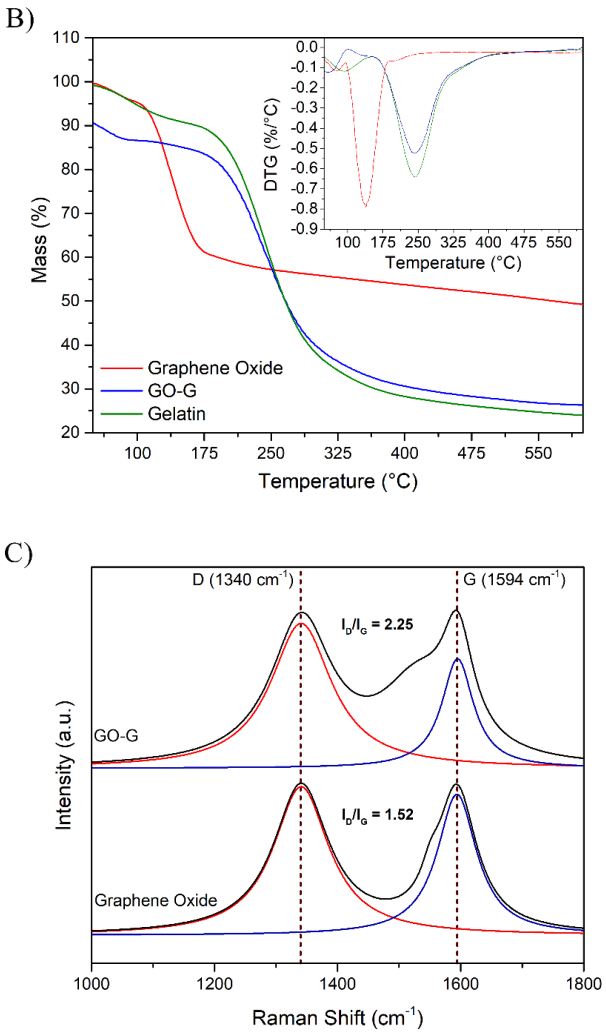


Figure 7.2: Chemical characterization of gelatin, GO, and GO-G aerogels through XRD (A), TGA, and DTG analyses (B), and Raman spectroscopy (C).

All the samples evaluated by TGA (Figure 7.2B) showed a mass loss before 100°C, which corresponded to the evaporation of moisture present in the material. The GO samples and GO-G aerogels started to lose mass at approximately 105°C, and gelatin started to lose mass at 160°C. At 600°C, GO-G aerogels lost approximately 61% of their mass, whereas gelatin samples lost approximately 66% of their mass, and GO samples lost approximately 32% of their mass.

According to these results, DTG analysis suggests that the decomposition of GO-G aerogels occurred in two main steps. Initially, the GO-G aerogels suffered a mass

loss at 105°C due to the decomposition of the oxygenated groups and then exhibited a mass loss related to the pyrolysis of the gelatin chains.

The above results agree with the thermal stability previously reported for similar GO-G materials, for which authors reported mass losses of less than 70% of their total mass [29,30], while a total mass loss value close to 61% was obtained with our GO-G aerogels in the same steps.

The Raman spectra of GO and GO-G aerogels are shown in Figure 7.2C. In the figure, the spectra show that the G band at 1594 $cm^{-1}$ was related to the in-phase vibration of the graphitic lattice and the D band at 1340 $cm^{-1}$ was induced by structural disorder and defects on the GO sheets. The comparable intensity between these bands is the result of the high content of defects present in the crystal, which can be associated with oxygenated groups.[23,31] The G band of the GO-G aerogels showed the same Raman shift as the GO sample, as was expected for physical interactions. Furthermore, the $I_D/I_G$ ratio was evaluated as a comparative index of $sp^2$ over $sp^3$ hybridization. The GO-G aerogels had an $I_D/I_G$ ratio of 2.25, higher than that of the GO sample, which had an $I_D/I_G$ ratio of 1.52. The $I_D/I_G$ ratio of the GO-G aerogels, without a shift on the G band, suggests partial disorder on the GO crystal structure due to the formation of physical complexes without a reduction of their oxygenated groups.[32–34]

Therefore, GO-G aerogels were synthesized by forming physical complexes between their GO oxygenated groups and the amine groups from the gelatin chains. The different types of GO-G aerogels had a similar chemical environment, with the main differences being in their amine groups due to their chemical activation, with good dispersion of their GO sheets on the gelatin matrix and high thermal stability.

### 7.4.2 GO-G aerogels properties and structure

The GO-G aerogels were synthesized under acid and basic conditions of the GO suspension to obtain positive and negative surface charges, respectively. Since changing pH activates the oxygenated groups on GO, differences in the structure

and properties can be produced. Therefore, some aerogel properties were measured and are summarized in Table 7.1.

Table 7.1: Aerogel properties

| Properties | GO-G (+) | GO-G (-) |
|---|---|---|
| Surface Charge (mV) | 15.63 ± 0.55 | -20.53 ± 1.07 |
| Absorption ($g_{PBS}/g_{Aerogel}$) | 49.58 ± 3.78 | 42.75 ± 2.38 |
| Elastic modulus (E) (kPa) | 2.23 ± 0.03 | 0.64 ± 0.01 |
| Pore Size (µm) | 42.17 ± 12.54 | 25.30 ± 10.38 |
| Apparent Porosity (%) | 96.69 ± 1.33 | 94.09 ± 2.54 |

When the pH went from acidic to alkali, aerogels presented ʒ-potential values of 15.63±0.55 mV and -20.53±1.07 mV. GO has negative ʒ-potential in a water suspension at pH values above its isoelectric point (IP ~ 2.0).[13,14,35] Therefore, GO was less activated when the suspension was near pH 3, and the GO-G aerogel had a similar surface charge to that of pure gelatin, as was reported for gelatin nanoparticles.[36] At high pH, the GO-G samples were more negative due to the chemical activation of the oxygenated groups present on GO. Thus, the activation of the GO sheets by modifying the pH to alkali conditions enhanced the influence of the GO sheets on the surface charge of the GO-G aerogel.

Focusing on potential hemostatic applications, PBS (pH 7.4) was employed to measure the absorption capacity of aerogels because of their similarity with mammalian extracellular fluids. The PBS absorption at the equilibrium of GO-G aerogels was 42.75±2.38 $g_{PBS}/g_{aerogel}$ for negative aerogels and 49.6±3.8 $g_{PBS}/g_{aerogel}$ for positive ones. GO-G aerogels form H-bonds on their physical complexes, which are promoted by acidic pH in the GO suspension, and H-bonds help to increase the hydrophilicity and structural stability of GO-G aerogels when they are in an aqueous medium. Likewise, hydrophilicity due to H-bond interactions has been widely reported for several materials, including G-based ones; in the above scenario, a pH

decrease might lead to an increase in the interactions of the hydrophilic segments of the chain and thus make the hydration network more extensive and stronger.[36,37]

The elastic modulus (E) of GO-G aerogels was measured as an indicator of material stiffness. GO-G aerogels were stiffer under an acidic pH in the GO suspension, with an E value of 2.23±0.03. In contrast, an alkali pH in the GO suspension showed an E value of 0.64±0.01 kPa. These results were due to the ionization of the oxygenated groups in the GO sheets, which led to a decrease in the number of free chemical groups that could form H-bonds. Comparatively, this result suggests that GO sheets could hinder network formation in GO-G aerogels at basic pH values in the GO suspension. The E values found were comparable in order of magnitude with other materials based on GO (or their reduced form) and gelatin methacryloyl or peroxide-reactive gelatin.[38–40]

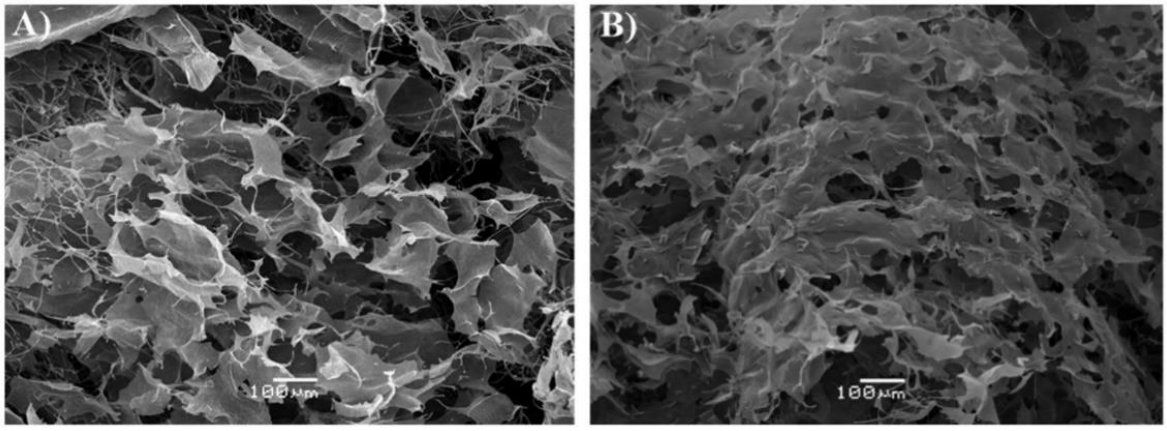


Figure 7.3: SEM images of positive surfaces (A) and negative surfaces (B) of GO-G aerogels.

With respect to the morphology of GO-G aerogels, SEM images (Figure 7.3) showed a highly heterogeneous microporous structure, with larger pore sizes in basic aerogels (42.17±12.54 µm, Figure 7.3A) than in acid aerogels (25.30±10.38 µm, Figure 7.3B). As with stiffness, these pore size results are related to the capability of aerogels to form physical complexes through H-bonding. Therefore, an acidic pH in the GO suspension leads to the formation of smaller pores than alkali conditions in the GO suspension through the promotion of the formation of physical complexes.

Furthermore, heterogeneous structures are expected for protein-based materials[41–43] with a microporous nature, as has been reported for similar GO-G materials with comparable pore-size scales. For example, gelatin aerogels with reduced GO presented pore sizes of approximately several and tens of micrometers[23], GO-G covalent hydrogels presented sizes between 2.3±1.1 μm and 7.7±5.4 μm,[24] and GO-G hydrogels with polyacrylic acid presented sizes between 70 μm and 300 μm.[44]

GO-G aerogels presented high apparent porosities, over 90%, as expected for this material type.[45] No significant differences were obtained (p-value<0.05) between acid and basic aerogels, whose porosities were 96.69±1.33% and 94.09±2.54%, respectively. These results suggest that despite the chemical activation of GO and the pH dependence of the capacity to form physical complexes with gelatin chains, the structure remains highly porous, possibly due to the low amount of GO in the gelatin matrix. GO-G aerogels had better porosities than similar previously reported materials, such as hydrogels based on reduced GO and methacryloyl gelatin or lyophilized G-GO activated with KOH, which presented porosities between 72% and 95%.[40,46]

### 7.4.3 Hemostatic performance of the aerogels

The high PBS absorption capacity and the charged surface of GO-G aerogels make them potential materials for hemostatic applications. Therefore, *in vitro* dynamic clotting assays were performed, and the results are shown in Figure 7.4.

As a result, positive aerogels had a poor clotting capability, with 8.1% of whole blood clotted after four minutes. Negative aerogels presented a whole blood clotted rate of 85.5% at one minute and 95.6% at two minutes of contact exposure, with no further changes after that time. Additionally, gauze had a similar clotting behavior to whole blood, with 41.6% of blood clotted after four minutes. In comparison, negative GO-G aerogels performed more than two times better than clinical gauze at equilibrium. Moreover, these aerogels presented high whole-blood clotting rates during the first minute of contact exposure, making them potential wound dressings with improved hemostatic properties.

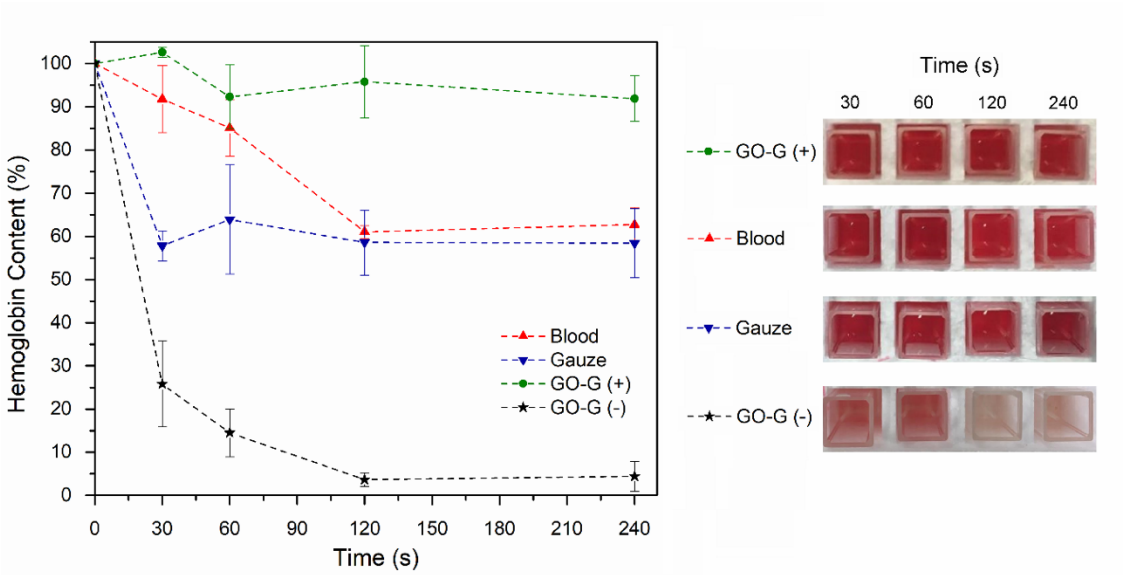


Figure 7.4: In vitro dynamic clotting assay of whole blood on positive aerogels (GO-G(+)), negative aerogels (GO-G(-)), and gauze (measured by UV-Vis at 540 nm), and images of their supernatants.

Similar clotting rates to those other biomaterials have been reported, such as hydrophilic gel microcapsules or metal-oxide composites, where the negatively charged surfaces showed stronger interactions with erythrocytes and other blood cells than positive surfaces.[47,48] Different collagen sponges, reinforced with chitosan and calcium pyrophosphate, have been tested for hemostatic applications, showing under 70% clotted whole blood at one minute, reaching 80-90% in the five minutes.[7,8] Moreover, similar performances of GO-based hemostatic materials, such as cross-linked graphene sponges and PVA-graphene oxide aerogels loaded with flavan-3-ols, have been reported, with 70-90% clotted whole blood at one minute of contact exposure.[17,49]

The enhanced clotting activity of biomaterials with a negative surface is commonly related to the promotion of procoagulant protein adhesion and the affinity of erythrocytes and other blood cells on the surface due to the presence of oxygenated functional groups on the GO sheets and their chemical activation triggering the coagulation cascade.[48] As soon as the blood contacts negative materials, a quick deposition of proteins on the surface takes place.[50] These proteins can be displaced by other proteins, including factor XII (FXII), fibrinogen, and albumin,

among others. Activation of these proteins, especially FXII, leads to the initiation of the coagulation cascade. Even though the protein deposition is nonspecific, some components of the contact system particularly react with negative surfaces, thus explaining the promotion of the intrinsic clotting pathway by negative materials.[50,51]

To confirm the clotting support mechanism, PT, aPTT, and sP-selectin were measured. These results are shown in Table 7.2.

Table 7.2: Clotting activity assays

| Sample | PT (s) | aPTT (s) | sP-Selectin (µg/mL) * |
|---|---|---|---|
| Control | 12.00 ± 0.53 | 30.60 ± 0.35 | 56.67 ± 2.52 |
| Gauze | 11.91 ± 0.21 | 29.46 ± 0.52 | 60.89 ± 2.34 |
| GO-G (+) | 11.54 ± 0.26 | 63.40 ± 3.14 | 55.61 ± 4.17 |
| GO-G (-) | 11.06 ± 0.11 | 32.44 ± 2.07 | 58.61 ± 1.39 |

*nonsignificant differences (p-value > 0.05). PT: prothrombin time, aPTT: activated partial thromboplastin time, and sP-Selectin: soluble human P-selectin.

Platelet-poor plasma was used to measure PT and aPTT, and Platelet-rich plasma for sP-selectin, as control values. The measurements show a PT of 12.00 ± 0.53 s, aPTT of 30.60 ± 0.35 s, and sP-selectin level of 56.67 ± 2.52 µg/mL as indicators of normal clotting activity. Similar values were measured for gauze and GO-G aerogels using the PT and sP-Selectin assays; a difference was only found for aPTT on positive GO-G aerogels. These results suggest that contact with these materials does not activate either tissue factors or platelets on the surface, thus retaining the same activity as whole blood for the support clotting mechanisms. Similar results have been reported in polystyrene nanoparticles, in which the activation of platelets is independent of the surface charge, even when stronger effects on cationic nanoparticles than anionic nanoparticles are expected, as was reported for amine-terminated polystyrene nanoparticles.[52,53] However, while gauze and negative GO-G aerogels showed the same activated partial thromboplastin time as the

control, positive GO-G aerogels showed a higher activated partial thromboplastin time, 63.40±3.14 seconds, which is twice the time showed by whole blood without material contact. These results suggest that contact with positive GO-G aerogels depletes clotting factors in plasma, which inhibits coagulation activity by inhibiting the intrinsic pathway. This behavior explains the reduced clotting performance of positive GO-G aerogels on the dynamic *in vitro* clotting assay. The same results have been reported for different positive materials, such as amine-modified polystyrene nanoparticles or modified nonwoven chitosan dressings.[53,54]

In contrast, even though the promotion of the intrinsic pathway by a negative surface has been widely reported [53,55,56], compared with the control, negative GO-G aerogels did not have a significantly different aPTT, suggesting that had the same intrinsic clotting activity as plasma without material contact. These results suggest that negative GO-G aerogels do not trigger the coagulation cascade through the common activation of the intrinsic pathway. Therefore, these aerogels probably promote clotting activity through an alternative mechanism. It has been reported that gelatin-based matrices used as hemostats are commonly related to physical surface effects providing a proper structure for endogenous coagulation than any action on the blood clotting mechanisms.[57,58] Moreover, negative carbon-based materials, such as carboxylated carbon nanotubes or GO sheets, had shown the acceleration of the clotting cascade by providing a platform for the enzymatic activity of factor IXa, and the activation of the complement system.[59–61]

Therefore, negatively charged GO-G aerogels showed accelerated clot formation and high hemostatic performance, independent of the common support mechanisms. These results were probably achieved by negatively charged GO-G aerogels providing an appropriate structure for the coagulation process or interacting with different clotting factors in alternative support mechanisms triggered by negative carbon-based materials, such as the complement system or the enzymatic activity of factor IXa.

### 7.4.4 Cell viability

To evaluate the cell-viability of GO-G aerogels as a wound dressing, human dermal fibroblast (HDF) cells were used, and the results of the MTT assay are shown in Figure 7.5.

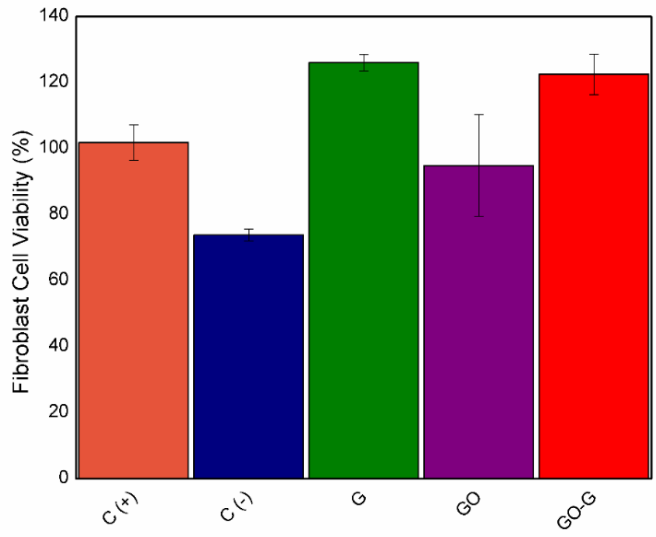


Figure 7.5: HDF viability in G, GO, and negative GO-G aerogels after a 1-day incubation. C(+): Positive control, pure DMEM culture medium. C(-): Negative control DMEM culture medium with 5 µL of hydrogen peroxide.

Compared to the controls, GO, gelatin, and GO-G aerogels were noncytotoxic after 1-day incubation. Moreover, gelatin and GO-G aerogels promoted the proliferation of HDF cells according to the MTT assay. These results could be explained by the amino acid content in the matrix and the structural properties of the material. Polymer matrices with a high amino acid content lead to major fibroblast cytocompatibility. Furthermore, macroporous structures with high porosity are optimal matrices for fibroblast proliferation and the regeneration of adult mammalian skin.[62–64] Additionally, despite the widely reported GO cytotoxicity, the low concentration of GO and the hydrophilicity of their oxygenated functional groups support cell viability results regardless of GO cytotoxicity.[11] Similar results have been reported for other gelatin-based matrices, such as gelatin-poly(hydroxybutyrate-co-hydroxyvalerate) nanofibrous mats and gelatin-carboxymethyl chitosan hybrid hydrogels, where high content of gelatin enhances fibroblast proliferation.[64,65]

Therefore, due to their high clotting performance, the capability to accelerate the coagulation process, and high gelatin content allowing fibroblast proliferation, negatively charged GO-G aerogels could be a potential external hemostatic device.

### 7.5 Conclusions

Aerogels based on gelatin and GO were successfully synthesized with positive and negative surface charges. Chemical characterization confirmed the dispersion of the GO sheets over the matrix, forming physical complexes between the oxygenated groups of GO and the amine groups of the gelatin chains. Both types of aerogel presented high PBS absorption, porosities over 90%, and were stable in aqueous media. However, compared to negative GO-G aerogels, positive GO-G aerogels showed superior mechanical properties and had a better structure due to the promotion of H-bond formation by the acidic GO suspension.

In terms of hemostatic activity, negative GO-G aerogels had an outstanding clotting performance, with a principal difference in plasma protein adsorption, which promotes the activation of the intrinsic coagulation pathway. This aerogel showed high hemostatic performance, independent of the common support mechanism pathways, probably providing an appropriate structure for the coagulation process or promoting alternative support mechanisms, such as activation of the complement system or provision of a platform for the enzymatic activity of factor IXa. Moreover, negative GO-G aerogels were not cytotoxic and promoted fibroblast proliferation over the matrix, thus making this material a potential hemostatic device to use in trauma treatments as a wound dressing.

## 7.6 References


[1] D.S. Kauvar, R. Lefering, C.E. Wade, Impact of Hemorrhage on Trauma Outcome: An Overview of Epidemiology, Clinical Presentations, and Therapeutic Considerations, Journal of Trauma and Acute Care Surgery. 60 (2006) S3. https://doi.org/10.1097/01.ta.0000199961.02677.19.

[2] L.W. Chan, C.H. Kim, X. Wang, S.H. Pun, N.J. White, T.H. Kim, PolySTAT-modified chitosan gauzes for improved hemostasis in external hemorrhage, Acta Biomaterialia. 31 (2016) 178–185. https://doi.org/10.1016/j.actbio.2015.11.017.

[3] A.M. Behrens, M.J. Sikorski, T. Li, Z.J. Wu, B.P. Griffith, P. Kofinas, Blood-aggregating hydrogel particles for use as a hemostatic agent, Acta Biomaterialia. 10 (2014) 701–708. https://doi.org/10.1016/j.actbio.2013.10.029.

[4] F. di Lena, Hemostatic polymers: the concept, state of the art and perspectives, J. Mater. Chem. B. 2 (2014) 3567–3577. https://doi.org/10.1039/C3TB21739F.

[5] R. Simon-Walker, J. Cavicchia, D.A. Prawel, L.P. Dasi, S.P. James, K.C. Popat, Hemocompatibility of hyaluronan enhanced linear low density polyethylene for blood contacting applications: Hemocompatibility of Hyaluronan Enhanced LLDPE, Journal of Biomedical Materials Research Part B: Applied Biomaterials. 106 (2018) 1964–1975. https://doi.org/10.1002/jbm.b.34010.

[6] J.-Y. Liu, Y. Li, Y. Hu, G. Cheng, E. Ye, C. Shen, F.-J. Xu, Hemostatic porous sponges of cross-linked hyaluronic acid/cationized dextran by one self-foaming process, Materials Science and Engineering: C. 83 (2018) 160–168. https://doi.org/10.1016/j.msec.2017.10.007.

[7] G. Lan, B. Lu, T. Wang, L. Wang, J. Chen, K. Yu, J. Liu, F. Dai, D. Wu, Chitosan/gelatin composite sponge is an absorbable surgical hemostatic agent, Colloids and Surfaces B: Biointerfaces. 136 (2015) 1026–1034. https://doi.org/10.1016/j.colsurfb.2015.10.039.

[8] T. Yan, F. Cheng, X. Wei, Y. Huang, J. He, Biodegradable collagen sponge reinforced with chitosan/calcium pyrophosphate nanoflowers for rapid

hemostasis, Carbohydrate Polymers. 170 (2017) 271–280. https://doi.org/10.1016/j.carbpol.2017.04.080.

[9] S.F. Kiew, L.V. Kiew, H.B. Lee, T. Imae, L.Y. Chung, Assessing biocompatibility of graphene oxide-based nanocarriers: A review, Journal of Controlled Release. 226 (2016) 217–228. https://doi.org/10.1016/j.jconrel.2016.02.015.

[10] C. McCallion, J. Burthem, K. Rees-Unwin, A. Golovanov, A. Pluen, Graphene in therapeutics delivery: Problems, solutions and future opportunities, European Journal of Pharmaceutics and Biopharmaceutics. 104 (2016) 235–250. https://doi.org/10.1016/j.ejpb.2016.04.015.

[11] B. Zhang, Y. Wang, G. Zhai, Biomedical applications of the graphene-based materials, Materials Science and Engineering: C. 61 (2016) 953–964. https://doi.org/10.1016/j.msec.2015.12.073.

[12] D.R. Dreyer, S. Park, C.W. Bielawski, R.S. Ruoff, The chemistry of graphene oxide, Chem. Soc. Rev. 39 (2010) 228–240. https://doi.org/10.1039/B917103G.

[13] Z. Lei, N. Christov, X.S. Zhao, Intercalation of mesoporous carbon spheres between reduced graphene oxide sheets for preparing high-rate supercapacitor electrodes, Energy & Environmental Science. 4 (2011) 1866. https://doi.org/10.1039/c1ee01094h.

[14] K. Min, T.H. Han, J. Kim, J. Jung, C. Jung, S.M. Hong, C.M. Koo, A facile route to fabricate stable reduced graphene oxide dispersions in various media and their transparent conductive thin films, Journal of Colloid and Interface Science. 383 (2012) 36–42. https://doi.org/10.1016/j.jcis.2012.06.021.

[15] B.K. Gu, S.J. Park, M.S. Kim, Y.J. Lee, J.-I. Kim, C.-H. Kim, Gelatin blending and sonication of chitosan nanofiber mats produce synergistic effects on hemostatic functions, International Journal of Biological Macromolecules. 82 (2016) 89–96. https://doi.org/10.1016/j.ijbiomac.2015.10.009.

[16] T. Takagi, H. Tsujimoto, H. Torii, Y. Ozamoto, A. Hagiwara, Two-layer sheet of gelatin: A new topical hemostatic agent, Asian Journal of Surgery. 41 (2018) 124–130. https://doi.org/10.1016/j.asjsur.2016.09.007.

[17] K. Quan, G. Li, D. Luan, Q. Yuan, L. Tao, X. Wang, Black hemostatic sponge based on facile prepared cross-linked graphene, Colloids and Surfaces B: Biointerfaces. 132 (2015) 27–33. https://doi.org/10.1016/j.colsurfb.2015.04.067.

[18] Q. Zhu, Y. Wang, M. Zhou, C. Mao, X. Huang, J. Bao, J. Shen, Preparation of Anionic Polyurethane Nanoparticles and Blood Compatible Behaviors, Journal of Nanoscience and Nanotechnology. 12 (2012) 4051–4056. https://doi.org/10.1166/jnn.2012.5858.

[19] H.M. Amin, S. Ahmad, J.M. Walenga, D.A. Hoppensteadt, H. Leitz, J. Fareed, Soluble P-Selectin in Human Plasma: Effect of Anticoagulant Matrix and its Levels in Patients With Cardiovascular Disorders, Clin Appl Thromb Hemost. 6 (2000) 71–76. https://doi.org/10.1177/107602960000600204.

[20] D.C. Marcano, D.V. Kosynkin, J.M. Berlin, A. Sinitskii, Z. Sun, A. Slesarev, L.B. Alemany, W. Lu, J.M. Tour, Improved Synthesis of Graphene Oxide, ACS Nano. 4 (2010) 4806–4814. https://doi.org/10.1021/nn1006368.

[21] Y. Piao, B. Chen, Self-assembled graphene oxide-gelatin nanocomposite hydrogels: Characterization, formation mechanisms, and pH-sensitive drug release behavior, Journal of Polymer Science Part B: Polymer Physics. 53 (2015) 356–367. https://doi.org/10.1002/polb.23636.

[22] H. Liu, X. Li, X. Niu, G. Zhou, P. Li, Y. Fan, Improved Hemocompatibility and Endothelialization of Vascular Grafts by Covalent Immobilization of Sulfated Silk Fibroin on Poly(lactic- *co* -glycolic acid) Scaffolds, Biomacromolecules. 12 (2011) 2914–2924. https://doi.org/10.1021/bm200479f.

[23] C. Liu, H. Liu, A. Xu, K. Tang, Y. Huang, C. Lu, In situ reduced and assembled three-dimensional graphene aerogel for efficient dye removal, Journal of Alloys and Compounds. 714 (2017) 522–529. https://doi.org/10.1016/j.jallcom.2017.04.245.

[24] Y. Piao, B. Chen, One-pot synthesis and characterization of reduced graphene oxide–gelatin nanocomposite hydrogels, RSC Advances. 6 (2016) 6171–6181. https://doi.org/10.1039/C5RA20674J.

[25] Y. Piao, B. Chen, Synthesis and mechanical properties of double cross-linked gelatin-graphene oxide hydrogels, International Journal of Biological Macromolecules. 101 (2017) 791–798. https://doi.org/10.1016/j.ijbiomac.2017.03.155.

[26] B. Boeckx, G. Maes, Experimental and Theoretical Observation of Different Intramolecular H-bonds in Lysine Conformations, J. Phys. Chem. B. 116 (2012) 12441–12449. https://doi.org/10.1021/jp306916e.

[27] E. Garand, M.Z. Kamrath, P.A. Jordan, A.B. Wolk, C.M. Leavitt, A.B. McCoy, S.J. Miller, M.A. Johnson, Determination of Noncovalent Docking by Infrared Spectroscopy of Cold Gas-Phase Complexes, Science. 335 (2012) 694–698. https://doi.org/10.1126/science.1214948.

[28] J. An, Y. Gou, C. Yang, F. Hu, C. Wang, Synthesis of a biocompatible gelatin functionalized graphene nanosheets and its application for drug delivery, Materials Science and Engineering: C. 33 (2013) 2827–2837. https://doi.org/10.1016/j.msec.2013.03.008.

[29] W. Wang, Z. Wang, Y. Liu, N. Li, W. Wang, J. Gao, Preparation of reduced graphene oxide/gelatin composite films with reinforced mechanical strength, Materials Research Bulletin. 47 (2012) 2245–2251. https://doi.org/10.1016/j.materresbull.2012.05.060.

[30] E.M. Zadeh, A. Yu, L. Fu, M. Dehghan, I. Sbarski, I. Harding, Physical and thermal characterization of graphene oxide modified gelatin-based thin films, Polymer Composites. 35 (2014) 2043–2049. https://doi.org/10.1002/pc.22865.

[31] N.A. Kumar, H.-J. Choi, Y.R. Shin, D.W. Chang, L. Dai, J.-B. Baek, Polyaniline-Grafted Reduced Graphene Oxide for Efficient Electrochemical Supercapacitors, ACS Nano. 6 (2012) 1715–1723. https://doi.org/10.1021/nn204688c.

[32] S. Bose, T. Kuila, Md.E. Uddin, N.H. Kim, A.K.T. Lau, J.H. Lee, In-situ synthesis and characterization of electrically conductive polypyrrole/graphene

nanocomposites, Polymer. 51 (2010) 5921–5928. https://doi.org/10.1016/j.polymer.2010.10.014.

[33] K.N. Kudin, B. Ozbas, H.C. Schniepp, R.K. Prud'homme, I.A. Aksay, R. Car, Raman Spectra of Graphite Oxide and Functionalized Graphene Sheets, Nano Letters. 8 (2008) 36–41. https://doi.org/10.1021/nl071822y.

[34] V.K. Rana, M.-C. Choi, J.-Y. Kong, G.Y. Kim, M.J. Kim, S.-H. Kim, S. Mishra, R.P. Singh, C.-S. Ha, Synthesis and Drug-Delivery Behavior of Chitosan-Functionalized Graphene Oxide Hybrid Nanosheets, Macromolecular Materials and Engineering. 296 (2011) 131–140. https://doi.org/10.1002/mame.201000307.

[35] K. Krishnamoorthy, M. Veerapandian, K. Yun, S.-J. Kim, The chemical and structural analysis of graphene oxide with different degrees of oxidation, Carbon. 53 (2013) 38–49. https://doi.org/10.1016/j.carbon.2012.10.013.

[36] S.M. Ahsan, C.M. Rao, The role of surface charge in the desolvation process of gelatin: implications in nanoparticle synthesis and modulation of drug release, International Journal of Nanomedicine. Volume 12 (2017) 795–808. https://doi.org/10.2147/IJN.S124938.

[37] E.-P. Ng, S. Mintova, Nanoporous materials with enhanced hydrophilicity and high water sorption capacity, Microporous and Mesoporous Materials. 114 (2008) 1–26. https://doi.org/10.1016/j.micromeso.2007.12.022.

[38] C. Cha, S.R. Shin, X. Gao, N. Annabi, M.R. Dokmeci, X.S. Tang, A. Khademhosseini, Controlling Mechanical Properties of Cell-Laden Hydrogels by Covalent Incorporation of Graphene Oxide, Small. 10 (2014) 514–523. https://doi.org/10.1002/smll.201302182.

[39] J.H. Lee, Y. Lee, Y.C. Shin, M.J. Kim, J.H. Park, S.W. Hong, B. Kim, J.-W. Oh, K.D. Park, D.-W. Han, *In situ* forming gelatin/graphene oxide hydrogels for facilitated C2C12 myoblast differentiation, Applied Spectroscopy Reviews. 51 (2016) 527–539. https://doi.org/10.1080/05704928.2016.1165686.

[40] S.R. Shin, C. Zihlmann, M. Akbari, P. Assawes, L. Cheung, K. Zhang, V. Manoharan, Y.S. Zhang, M. Yüksekkaya, K. Wan, M. Nikkhah, M.R. Dokmeci, X.S. Tang, A. Khademhosseini, Reduced Graphene Oxide-GelMA Hybrid Hydrogels as Scaffolds for Cardiac Tissue Engineering, Small. 12 (2016) 3677–3689. https://doi.org/10.1002/smll.201600178.

[41] S.-H. Lee, M. Kotal, J.-H. Oh, P. Sennu, S.-H. Park, Y.-S. Lee, I.-K. Oh, Nanohole-structured, iron oxide-decorated and gelatin-functionalized graphene for high rate and high capacity Li-Ion anode, Carbon. 119 (2017) 355–364. https://doi.org/10.1016/j.carbon.2017.04.031.

[42] C. Bastioli, Rapra Technology Limited, eds., Handbook of biodegradable polymers, Rapra Technology, Shrewsbury, 2005.

[43] M. Ramos, A. Valdés, A. Beltrán, M. Garrigós, Gelatin-Based Films and Coatings for Food Packaging Applications, Coatings. 6 (2016) 41. https://doi.org/10.3390/coatings6040041.

[44] S. Mohammadi, H. Keshvari, M. Eskandari, S. Faghihi, Graphene oxide–enriched double network hydrogel with tunable physico-mechanical properties and performance, Reactive and Functional Polymers. 106 (2016) 120–131. https://doi.org/10.1016/j.reactfunctpolym.2016.07.015.

[45] N. Hsing, U. Schubert, Aerogels-Airy Materials: Chemistry, Structure, and Properties, Angew. Chem. Int. Ed. (1998) 24.

[46] H. Fan, W. Shen, Gelatin-Based Microporous Carbon Nanosheets as High Performance Supercapacitor Electrodes, ACS Sustainable Chem. Eng. 4 (2016) 1328–1337. https://doi.org/10.1021/acssuschemeng.5b01354.

[47] K. Makino, M. Umetsu, Y. Goto, A. Nakayama, T. Suhara, J. Tsujii, A. Kikuchi, H. Ohshima, Y. Sakurai, T. Okano, Interaction between charged soft microcapsules and red blood cells: effects of PEGylation of microcapsule membranes upon their surface properties, Colloids and Surfaces B: Biointerfaces. 13 (1999) 287–297. https://doi.org/10.1016/S0927-7765(99)00041-7.

[48] T.A. Ostomel, Q. Shi, P.K. Stoimenov, G.D. Stucky, Metal Oxide Surface Charge Mediated Hemostasis, Langmuir. 23 (2007) 11233–11238. https://doi.org/10.1021/la701281t.

[49] C. Mellado, T. Figueroa, R. Báez, R. Castillo, M. Melendrez, B. Schulz, K. Fernández, Development of Graphene Oxide Composite Aerogel with Proanthocyanidins with Hemostatic Properties As a Delivery System, ACS Appl. Mater. Interfaces. 10 (2018) 7717–7729. https://doi.org/10.1021/acsami.7b16084.

[50] P. Vadgama, Surfaces and Interfaces for Biomaterials, CRC Press, 2005.

[51] I.H. Jaffer, J.I. Weitz, The blood compatibility challenge. Part 1: Blood-contacting medical devices: The scope of the problem, Acta Biomaterialia. 94 (2019) 2–10. https://doi.org/10.1016/j.actbio.2019.06.021.

[52] A. Mayer, M. Vadon, B. Rinner, A. Novak, R. Wintersteiger, E. Fröhlich, The role of nanoparticle size in hemocompatibility, Toxicology. 258 (2009) 139–147. https://doi.org/10.1016/j.tox.2009.01.015.

[53] C. Oslakovic, T. Cedervall, S. Linse, B. Dahlbäck, Polystyrene nanoparticles affecting blood coagulation, Nanomedicine: Nanotechnology, Biology and Medicine. 8 (2012) 981–986. https://doi.org/10.1016/j.nano.2011.12.001.

[54] D. Yan, S. Hu, Z. Zhou, S. Zeenat, F. Cheng, Y. Li, C. Feng, X. Cheng, X. Chen, Different chemical groups modification on the surface of chitosan nonwoven dressing and the hemostatic properties, International Journal of Biological Macromolecules. 107 (2018) 463–469. https://doi.org/10.1016/j.ijbiomac.2017.09.008.

[55] C. Sperling, M. Fischer, M.F. Maitz, C. Werner, Blood coagulation on biomaterials requires the combination of distinct activation processes, Biomaterials. 30 (2009) 4447–4456. https://doi.org/10.1016/j.biomaterials.2009.05.044.

[56] J.L. Brash, T.A. Horbett, R.A. Latour, P. Tengvall, The blood compatibility challenge. Part 2: Protein adsorption phenomena governing blood reactivity,

Acta Biomaterialia. 94 (2019) 11–24. https://doi.org/10.1016/j.actbio.2019.06.022.

[57] H. Seyednejad, M. Imani, T. Jamieson, A.M. Seifalian, Topical haemostatic agents, British Journal of Surgery. 95 (2008) 1197–1225. https://doi.org/10.1002/bjs.6357.

[58] E.A. Boonstra, I.Q. Molenaar, R.J. Porte, M.T. De Boer, Topical haemostatic agents in liver surgery: do we need them?, HPB. 11 (2009) 306–310. https://doi.org/10.1111/j.1477-2574.2009.00065.x.

[59] P.P. Wibroe, S.V. Petersen, N. Bovet, B.W. Laursen, S.M. Moghimi, Soluble and immobilized graphene oxide activates complement system differently dependent on surface oxidation state, Biomaterials. 78 (2016) 20–26. https://doi.org/10.1016/j.biomaterials.2015.11.028.

[60] M. Fedel, Hemocompatibility of Carbon Nanostructures, C. 6 (2020) 12. https://doi.org/10.3390/c6010012.

[61] A.R. Burke, R.N. Singh, D.L. Carroll, J.D. Owen, N.D. Kock, R. D'Agostino, F.M. Torti, S.V. Torti, Determinants of the thrombogenic potential of multiwalled carbon nanotubes, Biomaterials. 32 (2011) 5970–5978. https://doi.org/10.1016/j.biomaterials.2011.04.059.

[62] F. Dehghani, N. Annabi, Engineering porous scaffolds using gas-based techniques, Current Opinion in Biotechnology. 22 (2011) 661–666. https://doi.org/10.1016/j.copbio.2011.04.005.

[63] P. Iyer, K.J. Walker, S.V. Madihally, Increased matrix synthesis by fibroblasts with decreased proliferation on synthetic chitosan-gelatin porous structures, Biotechnol. Bioeng. 109 (2012) 1314–1325. https://doi.org/10.1002/bit.24396.

[64] C. Wang, Y. Lan, W. Yu, X. Li, Y. Qian, H. Liu, Preparation of amino-functionalized graphene oxide/polyimide composite films with improved mechanical, thermal and hydrophobic properties, Applied Surface Science. 362 (2016) 11–19. https://doi.org/10.1016/j.apsusc.2015.11.201.

[65] C. Yang, L. Xu, Y. Zhou, X. Zhang, X. Huang, M. Wang, Y. Han, M. Zhai, S. Wei, J. Li, A green fabrication approach of gelatin/CM-chitosan hybrid hydrogel for wound healing, Carbohydrate Polymers. 82 (2010) 1297–1305. https://doi.org/10.1016/j.carbpol.2010.07.013.

## 8. Conclusiones

Se sintetizaron aerogeles OG-G cuya naturaleza, covalente o no covalente, pudo ser confirmada mediante análisis de FTIR y XPS, donde las principales interacciones fueron la formación de amidas y de complejos físicos mediante puentes de hidrógeno, respectivamente.

Comparativamente, bajas proporciones OG:G en condiciones alcalinas de la suspensión de OG, promovieron las interacciones covalentes en los aerogeles OG-G. Por el contrario, altas proporciones OG:G bajo condiciones acidas de la suspensión de OG promovieron las interacciones la formación de complejos físicos. Estas condiciones mejoraron la morfología de los aerogeles en cada caso, presentando una estructura microporosa heterogénea, con una alta porosidad y rigidez.

Estos materiales presentaron el mismo comportamiento en su carga superficial independiente de la naturaleza covalente o no covalente de su interacción,. Sin embargo, los aerogeles no covalentes mostraron mayor capacidad de absorción de PBS y estabilidad en medios acuosos que los aerogeles covalentes, debido principalmente a su capacidad de formación de puentes de hidrógeno.

Además, se sintetizaron aerogeles OG-G con carga de PAs, los cuales mantuvieron el comportamiento de la carga superficial mostrado por aerogeles OG-G sin carga de extractos. La incorporación de PAs mejoró la capacidad de absorción de PBS sólo en los aerogeles covalentes. Esta mejora se mantuvo por debajo de las razones de absorción presentadas por aerogeles no covalentes sin carga de extracto.

Se evaluó el desempeño hemostático *in-vitro* sólo en aerogeles OG-G no covalentes, donde los aerogeles sintetizados en condiciones alcalinas de la suspensión de OG mostraron un alto rendimiento hemostático en comparación a la gasa y al aerogel OG-G sintetizado en condiciones ácidas. Este rendimiento no depende de los mecanismos comunes de apoyo a la coagulación, debiéndose probablemente a una estructura apropiada para el proceso de coagulación o a la promoción de mecanismos de apoyo alternativos. Además, este aerogel mostró la

capacidad de promover la proliferación de fibroblastos en su matriz, debido a la estructura generada en el material y al alto contenido de aminoácidos en la estructura, otorgando mayor cito-compatibilidad.

De este modo, se concluye que el aerogel OG-G no covalente de carga superficial negativa podria ser un potencial material hemostático, para uso como apósito en el tratamiento del sangramiento profuso.